

CONTROL OF SHUNT ACTIVE POWER FILTER UNDER ADVERSE GRID CONDITIONS

DISSERTATION / THESIS

SUBMITTED IN PARTIAL FULFILLMENT OF THE REQUIREMENTS
FOR THE AWARD OF THE DEGREE
OF

MASTER OF TECHNOLOGY
IN
POWER SYSTEMS

Submitted by:

Simar Preet Kaur

Roll No. 2K17 / PSY / 017

Under the supervision of

PROFESSOR (DR.) ALKA SINGH



**DEPARTMENT OF ELECTRICAL ENGINEERING
DELHI TECHNOLOGICAL UNIVERSITY**

(Formerly Delhi College of Engineering)
Bawana Road, Delhi - 110042

2020

CONTROL OF SHUNT ACTIVE POWER FILTER UNDER ADVERSE GRID CONDITIONS

DISSERTATION / THESIS

SUBMITTED IN PARTIAL FULFILLMENT OF THE REQUIREMENTS
FOR THE AWARD OF THE DEGREE
OF

MASTER OF TECHNOLOGY
IN
POWER SYSTEMS

Submitted by:

Simar Preet Kaur
Roll No. 2K17 / PSY / 017

Under the supervision of
PROFESSOR (DR.) ALKA SINGH



DEPARTMENT OF ELECTRICAL ENGINEERING
DELHI TECHNOLOGICAL UNIVERSITY

(Formerly Delhi College of Engineering)
Bawana Road, Delhi - 110042

2020



DELHI TECHNOLOGICAL UNIVERSITY
(Formerly Delhi College of Engineering)
Bawana Road, Delhi - 110042

CANDIDATE'S DECLARATION

I, Simar Preet Kaur, Roll No (s). 2K17 / PSY / 017 student of M. Tech. (Power Systems), hereby declare that the project Dissertation titled "Control of Shunt Active Power Filter under Adverse Grid Conditions" which is submitted by me to the Department of Electrical Engineering, Delhi Technological University, Delhi in partial fulfillment of the requirement for the award of the degree of Master of Technology, is original and not copied from any source without proper citation. This work has not previously formed the basis for the award of any Degree, Diploma Associateship, Fellowship or other similar title or recognition.

A handwritten signature in blue ink that reads 'Simar' with a horizontal line underneath.

Place: Delhi

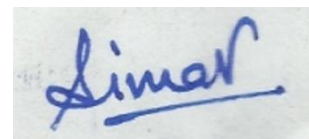
SIMAR PREET KAUR

Date: 30th June 2020

DEPARTMENT OF ELECTRICAL ENGINEERING
DELHI TECHNOLOGICAL UNIVERSITY
(Formerly Delhi College of Engineering)
Bawana Road, Delhi - 110042

CERTIFICATE

I, Simar Preet Kaur, Roll No. 2K17 / PSY / 017 student of M. Tech., hereby declare that the dissertation / project titled “Control of Shunt Active Power Filter under Adverse Grid Conditions” under the supervision of Professor (Dr.) Alka Singh of Electrical Engineering Department Delhi Technological University in partial fulfillment of the requirement for the award of the degree of Master of Technology has not been submitted elsewhere for the award of any Degree.



SIMAR PREET KAUR

Place: Delhi

Date: 30.06.2020



Prof. (Dr.) ALKA SINGH

Professor

ACKNOWLEDGEMENT

I have taken efforts in this project. However, it would not have been possible without the kind support and help of many individuals and organizations. I would like to extend my sincere thanks to all of them. I am highly indebted to Professor (Dr.) Alka Singh for her guidance and constant supervision as well as for providing necessary information regarding the project & also for her support in completing the project.

I would like to express my gratitude towards my parents and members of Delhi Technological University for their kind co – operation and encouragement which helped me in completion of this project. I would like to thank Mr. Hemant Saxena for his moral support and help in completing the project. My thanks and appreciations also go to my colleagues in developing the project and people who have willingly helped me out with their abilities.

ABSTRACT

This report discusses the design together with the application of a Double Second Order Generalized Integrator (DSOGI) for grid integration. A moderately distorted supply (having a THD equal to 8.49 %) feeds a non – linear load and a Shunt Active Power Filter (SAPF) is used as a compensator.

In this report, two different control approaches have been used to derive reference currents for the SAPF. These algorithms are the Unit Template (UT) based controller and Synchronous Reference Frame (SRF) theory – based approach. Both the algorithms fail to achieve less than 5 % distortion in supply currents when used under distorted / polluting grid conditions.

Hence a DSOGI based controller has been realized to generate perfectly sinusoidal reference currents even under adverse grid conditions. With the proposed modification in the controller design using the DSOGI block, perfectly sinusoidal grid currents can be generated. System has been simulated in the MATLAB environment using SIMULINK and PSB toolboxes. Performance results demonstrate the effectiveness of DSOGI based non – phase locked loop approach for grid synchronization.

CONTENTS

Candidate's Declaration	i
Certificate	ii
Acknowledgement	iii
Abstract	iv
Contents	v – vii
List of Figures	viii – xi
List of Tables	xii
List of Symbols / Abbreviations	xiii – xix
CHAPTER 1 INTRODUCTION	1
1.1 General	1 – 2
1.2 Distributed Generation systems	2 – 5
1.3 Repercussions of DG on electric power system	5
1.3.1 Controlling & operating	5 – 6
1.3.2 Modification in the Capacity for Short Circuit (SSC)	6
1.3.3 Stability of network	6
1.3.3.1 Voltage level of integration	7
1.3.3.2 Harmonics / deviations in voltage waveform	7
1.3.4 Power quality issues	8
1.3.5 Unbalancing of the system network	8
1.3.6 Protection scheme & security specifications	8 – 9
1.4 SAPF system	9 – 10
1.5 Literature Review	10 – 12
CHAPTER 2 CONTROL & PRINCIPLE OF SAPFs	13 – 14
2.1 SAPF Operating Principle	14 – 16
2.2 SAPF controlling techniques	16 – 18
2.3 Unit Template – (UT -) based controller with results	18 – 19
2.3.1 SAPF Controlling technique in UPF Method	19 – 21

2.3.1.1 With normal/distorted source	22
2.3.1.1.1 Voltage and current outputs	22 – 23
2.3.1.1.2 v_g , i_g and i_L THD values	23 – 24
2.3.1.1.3 DQ current outputs	24
2.3.1.2 With distorted source	25
2.3.1.2.1 Voltage and current outputs	25 – 26
2.3.1.2.2 v_g , i_g and i_L THD values	26 – 27
2.3.1.2.3 DQ current outputs	27
2.3.2 SAPF Controlling technique in ZVR Operating Method	27 – 31
2.3.2.1 With normal/distorted source	32
2.3.2.1.1 Voltage and current outputs	32 – 33
2.3.2.1.2 v_g , i_g and i_L THD values	33 – 34
2.3.2.1.3 Quadrature – axis current (i_q) output	34
2.3.2.2 With distorted source	35
2.4 Synchronous Reference Frame control algorithm of SAPF	35 – 37
2.4.1 With normal source	38
2.4.1.1 Voltage and current outputs	38 – 39
2.4.1.2 v_g , i_g and i_L THD values	40
2.4.1.3 DQ current outputs	40 – 41
2.4.2 With distorted source	41
2.4.2.1 Voltage and current outputs	42
2.4.2.2 v_g , i_g and i_L THD values	43
2.4.2.3 DQ current outputs	43 – 44
CHAPTER 3 DESIGN OF DUAL SOGI ALGORITHM	45
3.1 Introduction	45 – 49
3.2 Algorithm Employed for Reference Current Generation	49 – 51
3.3 Design Guidelines	51 – 53
3.4 Configuration and control algorithm	54 – 56
3.5 UPF Method with DSOGI	56
3.5.1 Voltage and current outputs	57

3.5.2 v_g , i_g and i_L THD values	57 – 58
3.5.3 Quadrature – axis current (i_q) output	58
3.6 SRFT control with DSOGI	59
3.6.1 Voltage and current outputs	59 – 60
3.6.2 v_g , i_g and i_L THD values	60 – 61
3.6.3 DQ current outputs	61 – 62
3.7 Conclusion	62 – 63
CHAPTER 4 SRF BASED CONTROL OF GRID-TIED PV	64 – 65
4.1 Introduction	65 – 67
4.2 Grid tied Photovoltaic system	68
4.2.1 PV array	68 – 69
4.2.2 Maximum Power Point Tracker	69 – 70
4.2.3 Implementation of 3 - ϕ Grid connected PV Network	70 – 71
4.2.4 Phase Locked Loop grid synchronization algorithm	72
4.3 Employing of Synchronous Reference Frame PLL Algorithm	73 – 74
4.4 Results & Discussions	74 – 83
4.5 Conclusion	83 – 84
CONCLUSION OF THE THESIS	85
FUTURE SCOPE OF WORK	86
REFERENCES	87 – 93

LIST OF FIGURES

1. A one – directional centrally delivered system for power generation (left) and a 2 – directional system with distributed generation (right). [16]
2. Basic circuit diagram of the SAPF system.
3. A three – leg VSC – based three – phase three – wire SAPF.
4. A 3 wire, 3 ϕ and midpoint capacitor based SAPF and a Voltage Source Converter which is H – bridge type.
5. A 3 wire and 3 ϕ SAPF based on Voltage Source Converters (3 in number) which are single ϕ .
6. UT – based control technique of SAPFs (without DSOGI technique).
7. UT – based control technique of SAPFs with normal source.
8. UT – based control algorithm outcome (without DSOGI technique).
9. THD values for UT – based control algorithm (without DSOGI technique).
10. Direct – axis current ($I_{d(\text{new})}$) and quadrature – axis current (i_q) output for the UPF mode of operation without the use of DSOGI technique.
11. UT – based control technique of SAPFs with distorted source.
12. UT – based control algorithm outcome (without DSOGI technique).
13. THD values for UT – based control algorithm (without DSOGI technique).
14. Phasor diagrams for ZVR mode of operation:
 - a. Without a SAPF and
 - b. With a SAPF.
15. SAPF control technique based on UT in Zero Voltage Regulation operating method.
16. UT – based control technique of SAPFs (ZVR) with normal source.
17. UT – based control algorithm (ZVR) outcome (without DSOGI technique).
18. THD values for UT – based control algorithm (ZVR) without DSOGI technique.

19. Quadrature – axis current (i_q) output for the ZVR mode of operation without the use of DSOGI technique.
20. UT – based control technique (ZVR) of SAPFs with distorted source.
21. SRFT – based control algorithm (without DSOGI technique).
22. SRFT – based control technique of SAPFs with normal source.
23. SRFT – based control algorithm outcome (without DSOGI technique) using normal source.
24. THD values for SRFT – based control algorithm (without DSOGI technique) using normal source.
25. Direct – axis current ($i_{d(new)}$) and quadrature – axis current (i_q) output for the SRFT – based scheme without the use of DSOGI technique (normal source).
26. SRFT – based control technique of SAPFs with distorted source.
27. SRFT – based control algorithm outcome (without DSOGI technique) in adverse grid conditions.
28. THD values for SRFT – based control algorithm (without DSOGI technique) in adverse grid conditions.
29. Direct – axis current ($i_{d(new)}$) and quadrature – axis current (i_q) output for the SRFT – based scheme without the use of DSOGI technique (distorted source).
30. SAPF connected in parallel with nonlinear load.
31. Multi – SOGI structure. [45]
32. Algorithm employed for Reference Current Generation:
 - (i) general technique and
 - (ii) inside the Second Order Generalized Integrator subsystem block.
33. QSG based on SOGI.
34. Basic scheme of suggested Reference Current Generation (RCG) technique ($3 - \phi$).
35. UT – based control technique of SAPFs (with DSOGI technique).

36. UT – based control algorithm outcome (with DSOGI technique).
37. THD values for UT – based control algorithm (with DSOGI technique).
38. Quadrature – axis current (i_q) output for the UPF mode of operation with the use of DSOGI technique.
39. SRFT – based control algorithm (with DSOGI technique).
40. SRFT – based control algorithm outcome (with DSOGI technique).
41. THD values for SRFT – based control algorithm (with DSOGI technique).
42. Direct ($i_{d(new)}$) and quadrature – axis current (i_q) output for the SRFT mode of operation with the use of DSOGI technique.
43. PV cell, module, panel and array.
44. Layout of grid connected PV system.
45. Grid connected Photovoltaic system layout.
46. (a) Power Voltage plot of Photovoltaic array and
(b) Flowchart for Maximum Power Point Tracker technique based on Perturb and Observe algorithm.
47. Basic block diagram for a Phase Locked Loop technique.
48. (a) Power – Voltage Characteristics and
(b) Current – Voltage characteristics of each Photovoltaic cell of the concerned PV array at various values of solar irradiance.
49. Voltage and current waveforms at inverter output.
50. Voltage and current waveforms at grid, converter current, load current and dc current.
51. Total Harmonic Distortion at o/p grid current and voltage and load current using FFT.
52. Capacitor at DC – link.
53. Voltage across capacitor at DC – link.
54. SRF based closed loop model with PV.
55. PV current generation.

56. PV current, grid power signals, PLL outputs and analog filter signals.
57. Controlled load current, input current, unfiltered and filtered voltage signals.
58. Single phase PLL system.

LIST OF TABLES

1. Typical available size per module for DG. [16, 22]
2. Comparison of all schemes used in this chapter.
3. Comparison of resulting Total Harmonic Distortion (THD) values.
4. Functions of PLL components.
5. System Specification of The GRID – Tied PV System.

LIST OF SYMBOLS / ABBREVIATIONS

SAPF (s)	-	Shunt Active Power Filter (s)
No. (s)	-	Number (s)
Prof.	-	Professor
M. Tech.	-	Master of Technology
THD	-	Total Harmonic Distortion
%	-	Percent
DSOGI	-	Double Second Order Generalized Integrator
MATLAB	-	Matrix Laboratory
SRFT	-	Synchronous Reference Frame Theory
UT -	-	Unit Template -
QSGs	-	Quadrature Signal Generators
PLL (s)	-	Phase Locked Loop (s)
Φ	-	Phase
DQ / d – q / dq	-	Direct Quadrature / direct – quadrature / direct quadrature
L	-	Inductance
Z_s	-	Source side branch impedance
Z_L	-	Load side branch impedance
V_s	-	Source Voltage
V_{dc}	-	DC Voltage
i_L	-	Load current
i_s	-	Source current
RC	-	Resistive Capacitive
g	-	Gating pulse
DC / dc	-	Direct Current
C_{dc}	-	DC link Capacitance
Fig. (s)	-	Figure (s)
RCG	-	Reference Current Generation
DFT	-	Digital / Discrete Fourier Transform
Viz.	-	Namely
PCC	-	Point of Common Coupling
CC - VSC	-	Current – Controlled Voltage Source Converter

AC	-	Alternating Current
V_{ga}	-	Phase a conditioned grid – Voltage signal
V_{gb}	-	Phase b conditioned grid – Voltage signal
V_{gc}	-	Phase c conditioned grid – Voltage signal
PI	-	Proportional Integral
I_{ga}^*	-	A ϕ of in – phase current reference component at grid
I_{gb}^*	-	B ϕ of in – phase current reference component at grid
I_{gc}^*	-	C ϕ of in – phase current reference component at grid
R_{ga}	-	Phase a unit current template
R_{gb}	-	Phase b unit current template
R_{gc}	-	Phase c unit current template
UPF	-	Unity Power Factor
V_{*D}	-	DC link Voltage reference value
V_{*Da}	-	DC link Voltage average value
LPF	-	Low Pass Filter
I_{spp}^*	-	Discrete PI controller output
L	-	Sample instant
K_1	-	Integral gain
K_2	-	Proportional gain
V_{gp}	-	Voltage magnitude at PCC
V_a	-	Phase a voltage
V_b	-	Phase b voltage
V_c	-	Phase c voltage
i_{La}	-	Phase a Load current
i_{Lb}	-	Phase b Load current
i_{Lc}	-	Phase c Load current
i_d	-	Direct current
i_q	-	Quadrature – axis current
i_{ga}	-	Phase a grid current
i_{gb}	-	Phase b grid current
i_{gc}	-	Phase c grid current
$\alpha - \beta / \alpha \beta$	-	Alpha – beta / alpha beta
cos	-	Cosine
θ	-	Transformation angle
sin	-	Sine

Mux	-	Multiplexer
K	-	Gain
V_{gABCpu}	-	Three phase grid Voltage in per unit
Sum	-	Summation
$I_{D,DC} / i_{d,dc} / i_{d,DC}$	-	DC Direct current / dc direct current / DC direct current
ω	-	Angular frequency
V_{abc}	-	Three phase voltage
V'_{sa}	-	Phase a reference source Voltage
V'_{sb}	-	Phase b reference source Voltage
V'_{sc}	-	Phase c reference source Voltage
$I_{q,dc} / i_{q,DC}$	-	DC quadrature current
$V'_{\alpha} / q v'_{\alpha}$	-	α axis Voltages
$V'_{\beta} / q v'_{\beta}$	-	β axis Voltages
V_{sABC}	-	Three phase source Voltage
I_{sABC}	-	Three phase source current
I_{cABC}	-	Three phase controller current
I_{LABC}	-	Three Phase Load current
V_{DC}	-	DC Voltage
$V_{g,abc}$	-	Three phase grid Voltage
$I_{g,abc}$	-	Three phase grid current
$I_{c,abc}$	-	Three phase controller current
$I_{L,abc}$	-	Three Phase Load current
V_g / v_g	-	Voltage at the supply
I_g	-	Current at the supply
I_L	-	Current at the load
IEEE	-	Institute of Electrical and Electronics Engineers
Mag.	-	Magnitude
FFT	-	Fast Fourier Transform
Hz	-	Hertz
I_s	-	Source current / Cell Saturation current (Ampere (s))
I	-	First / Output current (Ampere (s))
Oct.	-	October
U. K.	-	United Kingdom
Trans.	-	Transaction
Vol.	-	Volume

Jan.	-	January
Jul.	-	July
Feb.	-	February
Conf.	-	Conference
Apr.	-	April
Sep.	-	September
ZVR	-	Zero Voltage Regulation
L_S	-	Finite (non – zero) internal inductance of the utility
R_S	-	Finite (non – zero) internal resistance of the utility
V_M	-	Supply voltage
$I_{sp d}^*$	-	Amplitude of in – phase reference supply currents
V_{sp}	-	Amplitude of supply voltage
$u_{sad}, u_{sbd}, u_{scd}$	-	In-phase unit current vectors
$I_{sp q}^*$	-	Amplitude of quadrature reference supply currents
$i_{saq}^*, i_{sbq}^*, i_{scq}^*$	-	Quadrature components of reference supply currents
$i_{sa}^*, i_{sb}^*, i_{sc}^*$	-	Three – phase reference supply currents
V_{sp}^*	-	Voltage reference value at the Point of Common Coupling
$V_{sp e}$	-	Error voltage
$I_{sp q}^*(n)$	-	Output of the PI voltage controller at the nth sampling instant
K_{pt}	-	Proportional gain constant of the AC bus voltage PI controller
K_{it}	-	Integral gain constant of the AC bus voltage PI controller
$v_{spe}(n)$	-	Voltage error at the n th instant
$v_{spe}(n - 1)$	-	Voltage error at the (n – 1) th instant
$I_{spq}^*(n - 1)$	-	Q (Reactive power) needed at the (n – 1) th instant
$u_{saq}, u_{sbq}, u_{scq}$	-	Quadrature unit current templates
DG	-	Distributed Generation
SCC	-	Short Circuit Capacity
HVDC	-	High Voltage Direct Current
e.g.	-	Example
HV	-	High Voltage
LV	-	Low Voltage
SCADA	-	Supervisory Control and Data Acquisition
PWM	-	Pulse – Width Modulation
IGBT (s)	-	Insulated Gate Bipolar Thyristor (s)
BPT	-	Power Balance Theory

CSD	-	Current Synchronous Detection
IRPT	-	Instantaneous Reactive Power Theory
ISCT	-	Instantaneous Symmetrical Components Theory
EPLL	-	Enhanced Phase Locked Loop
S	-	Stockwell
EMD	-	Empirical Decomposition
Aug.	-	August
Mar.	-	March
Jun.	-	June
Dec.	-	December
Etc.	-	Etcetera
i_c	-	Compensating current
SDFT	-	Sliding Digital Fourier Transform
RDFT	-	Recursive Digital Fourier Transform
v'_{ga}	-	In – phase version of the voltage at supply
$v'_{g\beta}$	-	q phase version of the voltage at supply
i'_{La}	-	In – phase version of the load current
$i'_{L\beta}$	-	Quadrature – phase version of the load current
k	-	Damping factor
τ	-	Time constant
t_s	-	Settling time
PV	-	Photovoltaic
MPPT	-	Maximum Power Point Tracker
PCU	-	Power Conditioning Unit
I_{ph}	-	Pure current source / current generated by incident light
I_o	-	Dark – saturation current
R_{sh}	-	Shunt resistance
P & O	-	Perturb and Observe
KCL	-	Kirchhoff's Current Law
v_{pv}	-	Capacitor voltage
i_{dc}	-	Input current of the inverter
VCO	-	Voltage Controlled Oscillator
P_{in}	-	Maximum possible PV array power
P_{out}	-	Output power from the capacitor
$I_{d, ref}$	-	Reference current

$V_{d, ref}, V_{q, ref}$	-	Reference voltage signals
Eq	-	Equation
V	-	Output voltage (Volt (s))
G	-	Operating solar irradiation (KW (s) m^{-2})
T	-	Operating temperature (C)
k	-	Boltzmann's constant (J (s) / K)
q	-	Electron charge (C (s))
n	-	Ideal factor dependent of the PV characteristics
k_i	-	Short – circuit current temperature coefficient (A (s) / K)
E_g	-	Band gap energy of semiconductor used in a cell (eV (s))
N_s	-	Number of cell (s) in series
N_p	-	Number of cell (s) in parallel
T_r	-	Reference temperature at STC (K)
V_{OC}	-	Open circuit voltage (Volt (s))
I_{SC}	-	Short circuit current (Ampere (s))
I_r	-	Cell Reverse saturation current (Ampere (s))
$I_{s s}$	-	Photo current at operating temperature
KW (s)	-	Kilowatt (s)
m (s)	-	Meter (s)
C	-	Celsius
J (s)	-	Joule (s)
K	-	Kelvin
Kg (s)	-	Kilograms (s)
s (s)	-	Second (s)
A (s)	-	Ampere (s)
eV (s)	-	ElectronVolt (s)
STC	-	Standard Temperature Conditions
inf	-	Infinity
Si	-	Silicon
P – V	-	Power – Voltage
VSI	-	Voltage Source Inverter
$i_{d(new)}$	-	Direct – axis current
PE	-	Power Electronic
HCC	-	Hysteresis Current Control
ANN	-	Artificial Neural Network

AICT	-	Adaptive Interference Canceling Theory
AD	-	Adaptive Detecting
CB	-	Circuit Breaker
WECS	-	Wind Energy Conversion System
CS	-	Control System

CHAPTER 1

INTRODUCTION

1.1 General

In order to meet the growing power demands, Distributed Generation (DG) systems which are based on renewable energy sources such as biofuels, Photovoltaic (PV) power, Wind Energy Conversion System, hydro power etc. are getting quite popular. These resources mentioned, need to be connected in proper synchronization, for a grid connected system. These synchronization techniques help to estimate and track the magnitude, frequency as well as phase angle of the input voltage signals. Today, non – Phase Locked Loop (PLL) and PLL both techniques are in use. Researchers have focused on a no. of 1 ϕ and 3 ϕ PLLs, which is evident in literature review.

Active Power Filter is used in order to reduce the power quality issues which are induced by loads, specifically non – linear and is defined as a converter – based PE equipment.

A number of strategies for active power filter action have been recommended, with the most extensively used being the shunt APFs [1] – [3]. A Shunt Active Power Filter (SAPF) is meant for compensation of reactive power as well as to improve the supply current power factor, voltage regulation, load balancing, harmonic reduction etc. [4]

For this purpose, multiple control strategies have been documented, for instance, strategy using neural network techniques, Power Balance Theory (PBT) – based control technique, computation based on per phase basis, $I \cos \phi$ – based control technique, current compensation with the help of dc bus regulation, Synchronous Reference Frame Theory (SRFT), Current Synchronous Detection (CSD) control technique, Instantaneous Symmetrical Components Theory (ISCT) – based control technique, Instantaneous Reactive Power (IRP) theory, single – ϕ PQ technique – based control technique, single – ϕ DQ theory – based control technique. [5] – [13]

Phase Locked Loops (PLLs) are well established techniques aimed at grid synchronization besides tracking the phase angle. Single – ϕ PLL based on Transport delay, adaptive transport delay, power – PLL, inverse Park PLL etc. are popular and commonly employed. [57]

A popular non – PLL based synchronization technique is Second Order Generalized Integrator (SOGI) and can be realized easily in single – phase systems. An extension of two SOGI circuits can be realized for three – phase systems and is termed as DSOGI based synchronization.

1.2 Distributed Generation systems

“Distributed generation” (DG) pertains to the generation of electrical energy near the consumption place. The DG resources are co – generative and renewable. This means that there is the simultaneous occurrence of generation of electrical energy as well as heat energy. [17]

The impact, on electric power system networks, of DG is explained in section 1.2. DG is called the generation of power very near or in the proximity of the place where it will be consumed. Impacts of DG are listed below. They are:

1. System protection schemes might get hampered,
2. May affect reliability and power quality of the network,
3. Network branches might experience congestion,
4. Voltage transients may initiate,
5. Alteration in voltage profiles is seen along the system,
6. Losses at the load terminals alter and
7. Rise in SC levels.

The effects of distributed nature of generation on electric power systems and analyzing the typical characteristics of distributed generation are focused upon in this section.

Forms of energy, which either directly or indirectly depend on the Sun, such as biomass, heat from within the Earth (Geothermal), movement of ocean currents, tidal movement, Solar radiation and wind energy [17] those from natural resources are called renewable forms of energy.

DG is highlighted by various characteristics which are absent in traditional centralized systems:

1. Relative freedom of location in the area under the network,
2. Relatively lower amount of power produced and
3. Variation in power generated due on the readiness of availability and variance in primary energy. [23]

Higher vicinity to loads at the customer end is the primary benefit of Distributed Generation. Distributed Generation helps in the following:

1. Increases in the quality of the power generated,
2. Increased voltage support,
3. Mitigation of losses during transmission,
4. Increase grid durability.

There is one environmental factor too. DG acts as a source of clean energy, as it helps to reduce pollutant concerns by reducing emission of greenhouse gases. [19]

In Table 1 [16, 22] are presented the widely popular Distributed Generation technologies and the typical size of their module.

Table I. Typical available size per module for DG. [16, 22]

Technology	Typical available size per power module
Small Hydro	1 – 100 MW
Micro Hydro	25 kW – 1 MW
Wind Turbine	200 W – 3 MW
Photovoltaic Arrays (PV Arrays)	20 W – 100 kW
Biomass Gasification	100 kW – 20 MW
Geothermal	5 – 100 MW
Ocean Energy	100 kW – 5 MW

Various characteristics of distribution system operation, implementation and design have been revolutionized by Distributed Energy Resources (DER). Losses within the networks of power distributing infrastructure have been lowered. This is because of power distribution now being in close proximity to the areas in demand for the consumption. This comes with a rise in the number of more Distributed Generation systems which are formed by power generation from units of a smaller size than usual and then connecting them straight to the preexisting networks for power distribution. [21]

A distribution system with a higher incidence in the spread of distribution of the generated power gives rise to numerous problems [16]:

- Voltage profiles change along the network, depending on how much power is produced and consumed at that system level, leading to a behavior different from that of a typical unidirectional network;
- Voltage transients will appear as a result of connection and disconnection of generators or even as a result of their operation;
- Power flow is bidirectional (Fig. 1);
- Short circuit levels are increased;
- Load losses change as a function of the production and load levels;
- Power quality and reliability may be affected;
- Utility protection and DG protection measures must be coordinated.

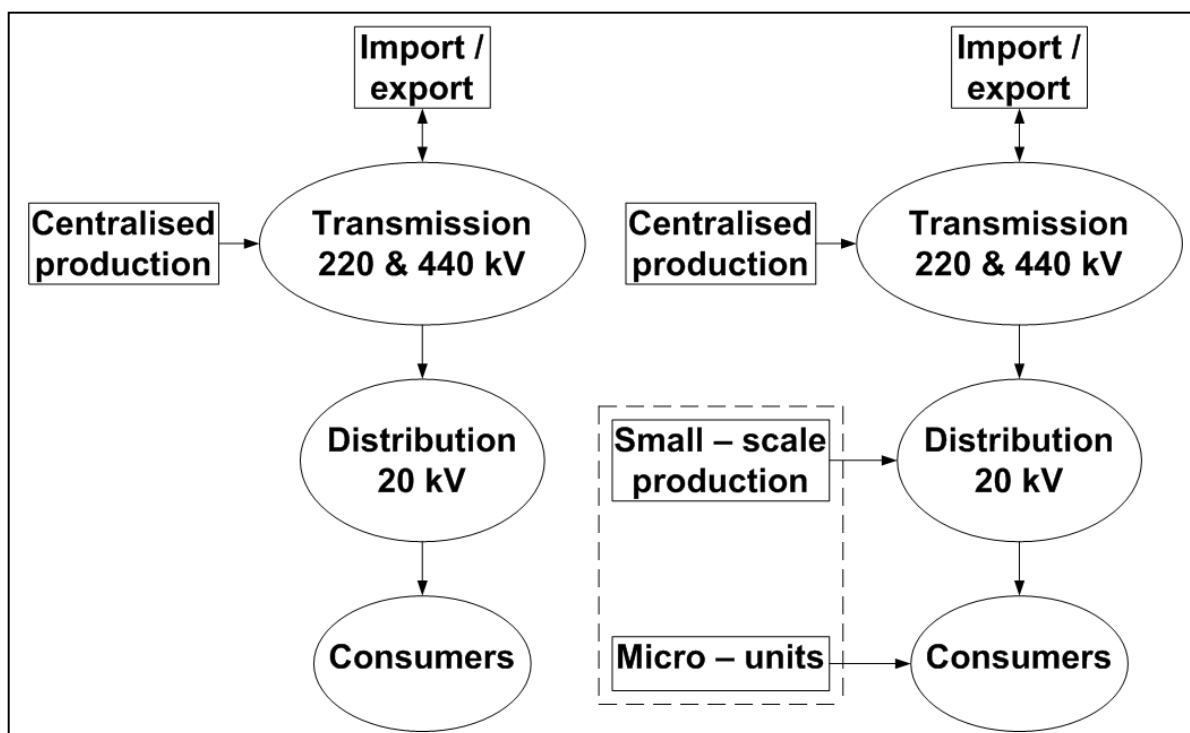


Fig. 1. A one – directional centrally delivered system for power generation (left) and a 2-directional system with distributed generation (right). [16]

1.3 Repercussions of DG on electric power system

There are several important effects of Distributed Generation on electric power systems that are presented further.

1.3.1 Controlling and operating

Variation in the local load demand is the parameter according to which Distributed Generation power production is varied. However, without dependence on the loading in the concerned area, also, can production by Distributed Generation be altered.

When there is a huge amount of penetration of Distributed Generation, it can lead to risks such as control and stability complications. If a CB in a distribution unit is open circuited, this can land the Distributed Generation system into an islanding situation. Like in situations when the value of fault current is still less than the limit, it may happen that the

Distribution Generation continues to work because it does not detect the loss of mains power. In an isolated system, at the load terminal, when the Distribution System is accurately able to match values of P (active power) and Q (reactive power), it will continue its operation in the islanded condition also, without facing any difficulties. It is, though, very unlikely that Distribution Generation will precisely match the load requirement in the system, at the instant when the CB is open circuited. Therefore, actual frequency / voltage fluctuations in huge amounts will take place when the Distribution Generation system tries to supply load. A detection system in place that is able to detect a loss of main power is, therefore, needed in almost all interconnection modes. In a situation where there is loss – of – main power, till the supply is restored, the detection system should be able to automatically disconnect the Distribution Generation system and also remain in that disconnected manner. [22]

1.3.2 Modification in the Capacity for Short Circuit (SSC)

The introduction of distributed generators in the distribution networks has the potential to increase the capacity for short circuit (SCC). In some cases, though, it is favorable to have a large SCC, for e.g., in case of existence of large loads with suddenly varying demands or at a spot at which there is connection of the inverter in a line commuted High Voltage Direct Current station, the increase of the Short Circuit Capacity, in usual terms, potentially indicates trouble. [22]

1.3.3 Stability of network

Provided the transmission system was itself stable, in almost all situations, the network also remained stable. Stability problems were not needed to be considered by the distribution system earlier. It was due to the radial and passive nature of the network. This situation, however, is changing due to the increasing contribution of new systems to network security and the coming up of new systems is on a rise. First swing stability (transient stability), dynamic stability (long term) and collapse of voltage, all three areas need to be taken into consideration. [22]

1.3.3.1 Voltage level of integration and interconnection

Value of the voltage is decreased as the distance from the generator / the transformer increases. It would be right to say that the distance from the generator / the transformer and value of the voltage are inversely proportional. The unidirectional design of the traditional distribution system is the reason behind this occurrence. When designing the system, the above said voltage drops can be predicted and they can further be taken into consideration for optimum system design. By doing this, it can be assured that the value of voltage is within the set tolerance range, under all normal operating conditions. The major difficulty comes into picture and the situation changes when a Distributed Generation is connected in the network. With this, the flow of current is reversed / changed in general and the voltage value will normally rise in such a way which is very difficult to predict. Now, the capacity of Distributed Generation that can be connected to the network is restricted by the need to meet statutory voltage limit values, especially at the low voltage value. [16]

1.3.3.2 Harmonics / deviations in voltage waveform signals

Depending on the fact that whether it is a rotating machine / an electronic converter, the connection of a Distribution unit to the system influences the amount of distortion in the voltage value. PE interfaces have been employed for advanced network support possibilities but harmonic currents are injected into the network which is a disadvantage. Viz., topology of the network and impedance value at the connection point are two factors upon which it depends if excessive harmonic voltage values will take place. These excessive harmonic voltage values can take place locally or at some other point in the grid. Due to non – linearities in core and design of the winding generators with rotation also have the ability to introduce harmonics. The relevance of this phenomenon is dependent upon 2 factors: one being the grid layout and second being specific Distributed Generation details. [16]

1.3.4 Power quality issues

Different types of power quality problems are created by different Distribution Generations. They having varying characteristics is the reason behind it. For increasing the system fault level, adding generation, often results in improved power quality. There however is a notable exception which comprises a huge single Distributed Generation. It is that there may arise power quality issues, specifically, at the time of commencing and stopping a weak system which contains a WECS turbine. Power quality issues are brought in by modern day PE devices and controls.

1.3.5 Unbalancing of the system network

Various DGs, which supply to the network in single – phase, are available. If DG exists in supply, the unbalancing of the system that occurs should not increase beyond the permissible limit. Moreover, with the unbalancing of loads in the phases, operation of DGs suffers. Unbalancing leads to deterioration in their performance. [22]

1.3.6 Protection scheme & security specifications

Depending on the characteristics of DG (its rated power, mode of operation, technology used), the location of DG and network configuration, the impact of DG on the over current protection may vary, so DG will have an impact on the protection scheme of the distribution grid. DG does not interfere with the normal operation of the protection system if the protection system of DG units is able to rapidly disconnect from the network after the fault is detected. If a fault occurs, the DG unit will have to be disconnected. [22]

Though some solutions may obviously be adopted from the high voltage (HV) systems, there is a need for totally new solutions. Traditionally based on fuses, the protection of low voltage (LV) networks is an interesting topic. Suppose that a low voltage branch is being supplied energy by a low power DG unit and also supplied by a LV transformer. If a fault develops far from the DG unit the fault current from the transformer will cause the

transformer protection to operate. This leaves the DG unit supplying a fault current which may be insufficient to operate the DG protection due to the relatively high impedance of the system. [16]

However, these days, networks in place of distribution are self – sustaining and feature SCADA systems, so the protection system in place must be correctly designed and synchronized. [22]

1.4 SAPF system

A Shunt Active Power Filter is shown in Fig. 2 shows which is linked in parallel with the nonlinear load. It is further controlled using a control algorithm to inject or draw i_c , compensating current, to or from the supply so that at the Point of Common Coupling (PCC) i_g , the grid current, is a sinusoidal wave in $-\phi$ with the grid voltage, v_g . The non – linear load is connected in the form of diode rectifier. An Insulated Gate Bipolar Thyristor (IGBT) three – ϕ , 3 leg – based bridge is modelled as a SAPF.

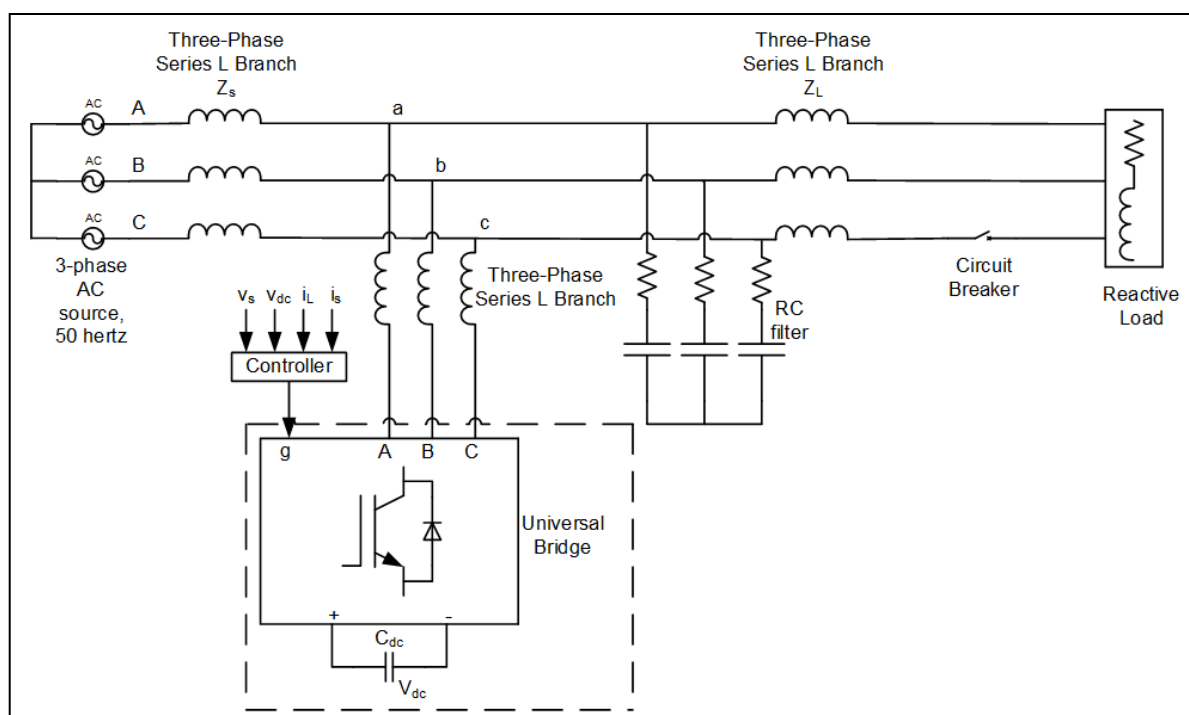


Fig. 2. Basic circuit diagram of the SAPF system.

The reference compensating current generation step in the control process of an APF is undoubtedly the most significant step. Many algorithms for Reference Current Generation (RCG) have been cited in literature. Time and frequency domain algorithms are 2 broad categories for the RCG techniques. Digital Fourier Transform (DFT), Fast Fourier Transform (FFT), Sliding DFT (SDFT) or Recursive Digital Fourier Transform (RDFT) techniques are the most commonly used techniques in the case of frequency domain.

For the control of SAPF 2 control algorithms viz. unit template – based theory and SRFT are described in detail. The performance is studied under the normal / undistorted as well as distorted grid conditions.

1.5 Literature Review

Power utility corporations as well as consumers are becoming increasingly vulnerable to the susceptibility of electronic consumer devices, other electronic instrumentation devices and other high-tech facilities to the quality of power. Today, such devices need high quality power with a great measure of reliability in greater volumes and increasingly smaller time scales. [1]

The total distorted currents on the electrical network has been amplified by the spread of nonlinear loads in the industry in addition to in electronic equipment these days. Growing worry has been shown as towards the effect of the level of harmonic currents being produced and injected into the ac power lines and the pf, henceforth. As a resolution in the direction of compensating distortion caused by constant nonlinear loads, passive inductance – capacitance (LC) filters tuned on the fundamental harmonics have been used, conventionally. These filters are intended to offer a low impedance path meant for the changing harmonics, accomplishing decent power quality (PQ) by means of little price and an easy strategy. Nevertheless, passive filters have some disadvantages for example

- Huge passive component values that lead toward massive implementations,
- Dependence on the conditions of the power source system,
- Reverberation and
- Mistuning.

Quite a lot of topologies functioning with power semiconductor switches have been established, intended for high – quality requirements. These topologies are designed to refine the PQ, by cancelling the original current in addition to voltage harmonic distortion by means of injecting the equal sensed distortion, but then with the reverse polarity. With the objective of improving current / voltage distortion, active filters can be linked in parallel (SAFs) otherwise in series to the nonlinear loads, universally. SFs proficiently eradicate the Q produced through nonlinear loads and current distortion and therefore remain the most commonly used resolution. In 3 – phase structures where a hefty capacity is required, SFs are generally used. But, in conditions where the user can have access only to a single – phase network, which occurs in inhabited, light industrial and countryside expanses / in variable speed motor – powered drives fed by a single – phase utility power, single – phase AF can be applied.

Towards controlling SAPFs, quite a few switching procedures have been described. These can be clustered into frequency – domain techniques and time – domain systems. Since CC – VSC are recurrently used as SFs, the utmost regularly employed control methods used for time – domain controllers are CC systems, for example

- Linear CC,
- Digital deadbeat control,
- HC in addition to
- One – cycle control.

Frequency – domain techniques, on the other hand, suffer from the associated effects of time delay produced by means of algorithm calculations and sampling because they are based on the periodicity of the current harmonics and Fourier analysis. Additionally, the well – identified shortcoming of providing a nonlinear portrayal of the closed – loop structure dynamics is found in both frequency – domain and time – domain control systems. Generally, tedious trial – and – error approaches are carried out for the design of these closed – loop schemes.

Additional advanced control procedures have as well been described, for example the

- NN,
- Optimization,
- Adaptive estimation systems and

- Sliding mode control.

The sliding mode control, amongst the aforementioned techniques, is a natural technique in the direction of controlling time – varying topologies and therefore has remained extensively used towards powering converters. It as well stands out for its essential features such as

- Simple control operation,
- Insensitivity toward system parameter variation in addition to
- toughness.

For some power converter structures, nonlinear control procedures based on feedback linearization scheme have been used lately. Systematic linear strategy can be applied to these methods because they often let one towards finding a control rule that input – output linearizes the nonlinear structure. Also, this approach makes available an efficient technique in the direction of deriving the control laws meant for nonlinear arrangements, whose applicability may well be checked in advance by means of some geometric conditions that the system model essentially satisfies. This promising control technique in APFs has still been exploited by very minute former work. [2 – 6]

CHAPTER 2

CONTROLLING TECHNIQUES AND OPERATING PRINCIPLE OF SAPFs FOR 3 - ϕ SYSTEM

The basic function of SAPFs is to mitigate almost all of the power quality problems which are based on current for example:

1. To provide balanced and sinusoidal grid currents with the automated DC bus of the Voltage Source Converter which is employed as a SAPF,
2. Any harmonics that might be present and neutral current,
3. Currents that are unbalanced and
4. Q (Reactive power).

Fig. 4 demonstrates a basic circuit diagram of the SAPF for a 3 ϕ and 3 wire AC system and loads that can be unbalanced or balanced. The SAPF which is used here is an Insulated Gate Bipolar Transistor based Current Controlled Voltage Source Converter (CC VSC) and it also contains a capacitor at the DC link. Reference current values of the SAPF can be controlled with the help of a controlling technique which estimates the SAPF reference currents for the direct Voltage Source Converter current control. On the same scale when the reference current at the grid is estimated, in place of SAPF reference currents, Indirect Voltage Source Converter current control, on the other hand, can be achieved. Without carrier pulse – width modulation / the pulse – width modulation in which the frequency is fixed which is also called as hysteresis is employed for the latter technique that is the indirect Voltage Source Converter current control. The SAPF is supplied with the gating pulses that are produced by the technique discussed above. The compensation of Q (reactive power), with the use of the SAPF and also the compensation of the currents that are unbalanced, are achieved, in all the current control techniques used. Also, ZVR is successfully achieved when at the Point of Common Coupling the current control technique is adequately changed or modified from UPF mode.

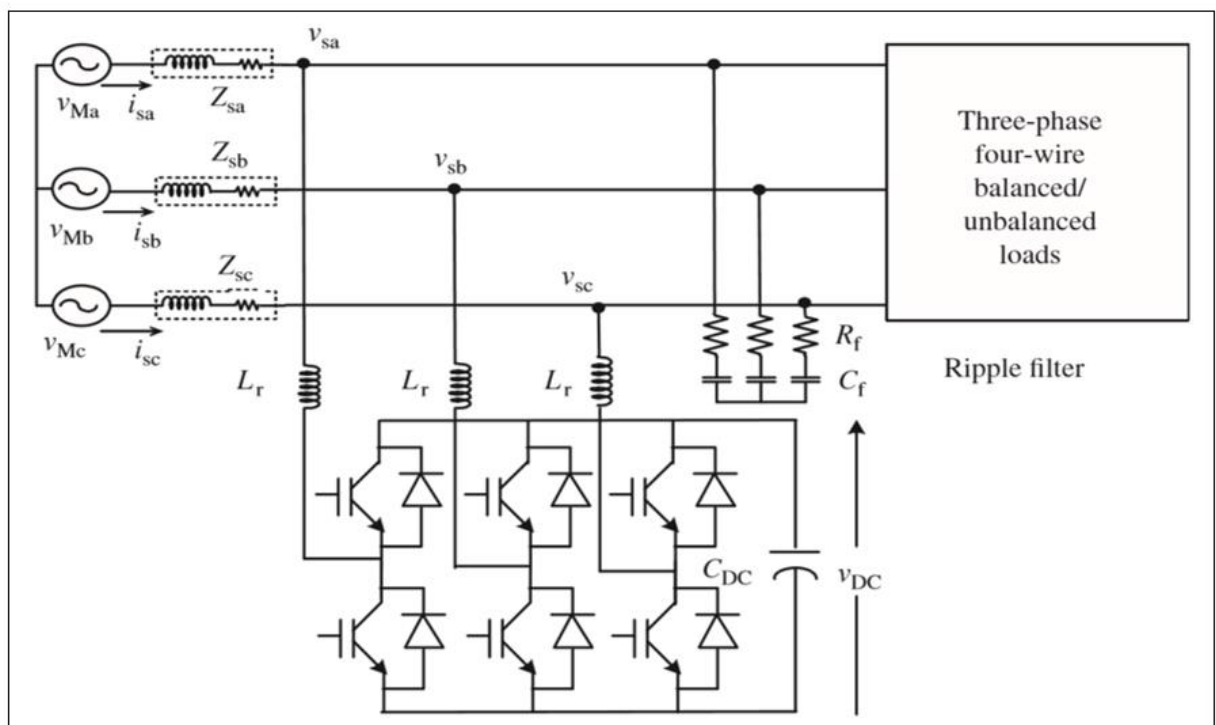


Fig. 3. A three – leg VSC – based three – phase three – wire SAPF.

2.1 SAPF Operating Principle

On the distribution end of a system the power quality issues based on current are suppressed by the SAPFs which also is the principal aim of the SAPFs. Most of the current power quality issues are suppressed by an SAPF, for example:

1. Its DC link VR helps to provide balanced grid currents that are sinusoidal in nature,
2. Any system / consumer load fluctuations and harmonics that might be present,
3. Current at the neutral phase,
4. Unbalance and
5. Balance of Q (reactive power).

The connections of a SAPF at the DC and AC sides is demonstrated in Figs 3 – 5. Commonly, at the consumer end across the loads / across the Point of Common Coupling the AC side of the SAPF is connected in parallel. Moreover, a Voltage Source Converter is connected at the DC bus of the SAPF. Voltage Source Converter uses hysteresis current

control technique; hence, it requires small ripple filters in order to suppress the ripples caused due to switching. In order to implement the above said SAPF controlling technique, generally a Digital Signal Processing is used, in order to produce gating pulses for the solid – state devices of the Voltage Source Converter of the SAPF. Hall effect voltage value and current sensors are needed for the feedback loop signals by the Hysteresis current control. For the control of the Voltage Source Converter, HCC method is generally used as a control technique in order to inject proper currents in the system. A number of passive devices are required by the SAPF as well, for example:

1. Small filters that passive in nature,
2. Transformers that are required for isolation and injection,
3. Inductances that interact at the AC and
4. A capacitor at the DC bus of the SAPF.

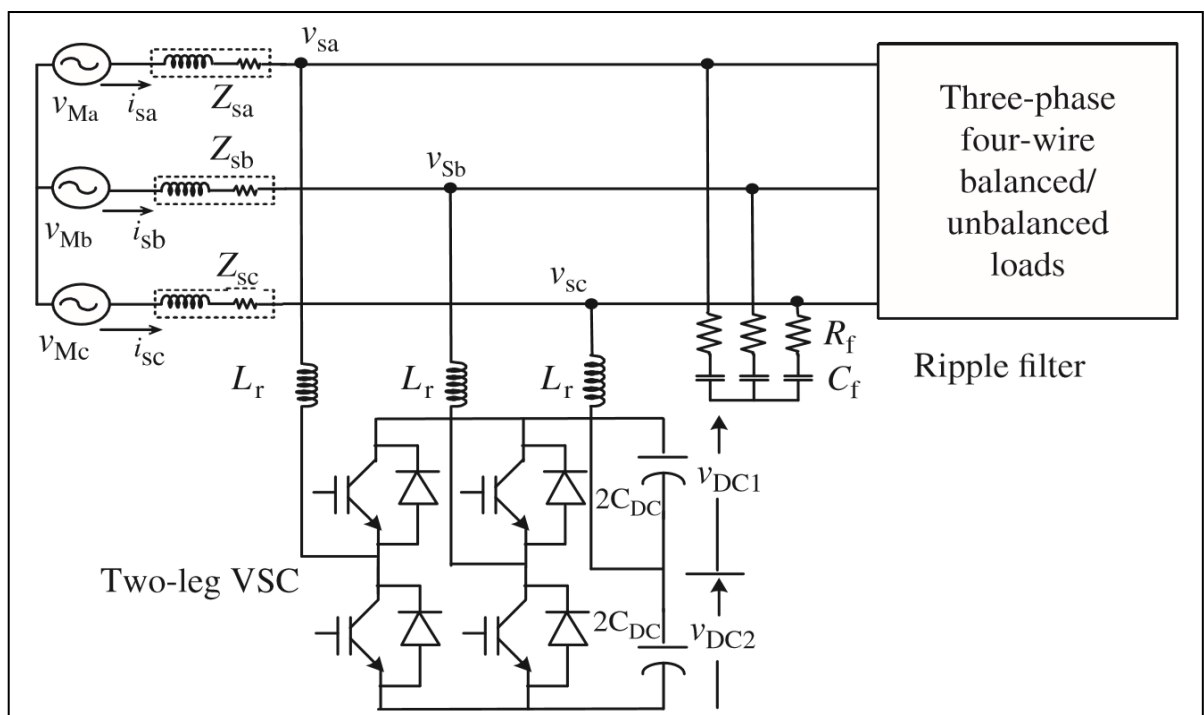


Fig. 4. A 3 wire, 3 ϕ and midpoint capacitor based SAPF and a Voltage Source Converter which is H – bridge type.

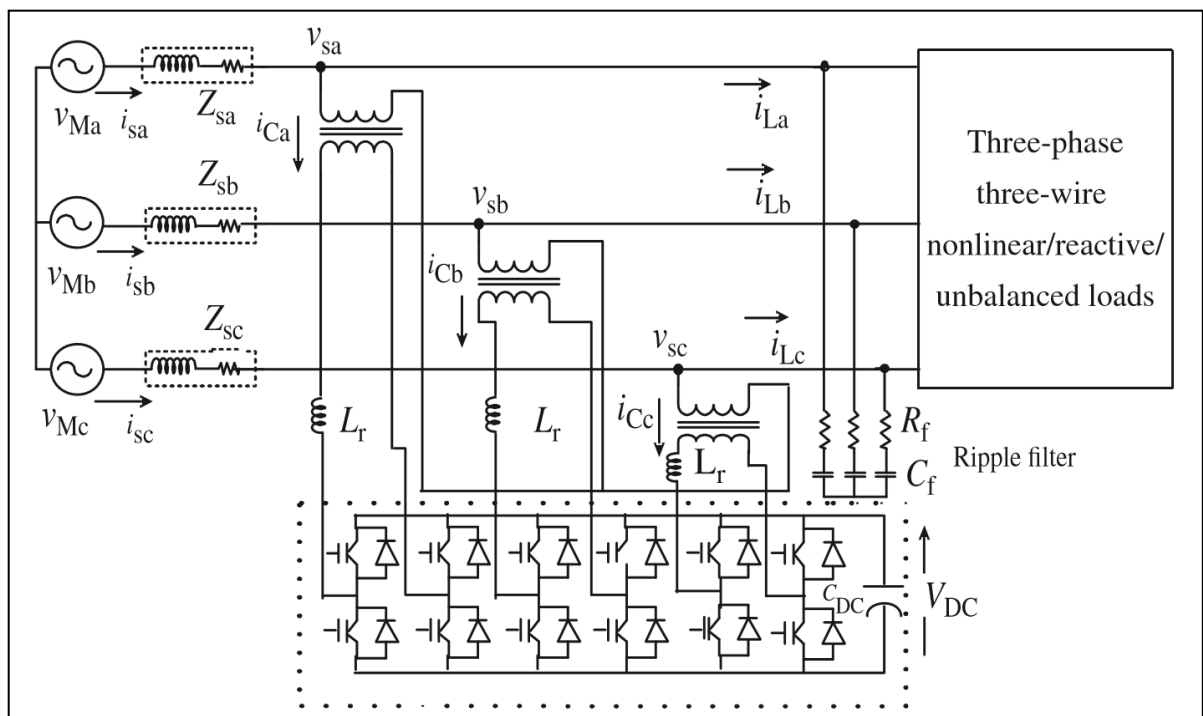


Fig. 5. A 3 wire and 3 ϕ SAPF based on Voltage Source Converters (3 in number) which are single ϕ .

2.2 SAPF controlling techniques

Signals at the feedback loop are used for the reference current value estimation. This is the principal aim of the SAPF CC technique. HCC is implemented, for Insulated Gate Bipolar Transistors (switching devices) of the Voltage Source Converter which is used as a SAPF, in order to produce the Hysteresis gating pulses. Further, the sensed current values along with the corresponding reference current values are required for the HCC technique. For the control of SAPFs, there is an availability of many CC techniques for the estimation of the reference current values as the value for these signals have to be calculated accordingly. Many CC techniques of the time domain type can be brought to use, in order to control the SAPFs. Following are some of those current control techniques that are being used:

- AICT which is also called as AD CC theory,
- Model based on Conductance,
- Technique for CC based on EPLL,
- Adaline technique based on Widrow's LMS (ANN algorithm),

- Direct Quadrature technique (1ϕ),
- PQ technique (1ϕ),
- ISC Theory,
- Direct Quadrature model which is also called as SRFT,
- Technique based on $\alpha \beta$ which is also called as PQ algorithm / IRP Theory,
- Algorithm based on CSD model,
- Current control technique of $I \cos \Phi$,
- BPT and
- Theory that is based on Proportional Integral / UT algorithm.

Techniques mentioned in the above list are CC theories in the time domain. Almost all of the above – mentioned algorithms are taken into consideration, for the CC and compensation of devices such as SAPFs and other devices.

Just like the CC theories that are time domain – based, around a dozen CC techniques based on frequency domain are also available. Following is a list of a few of the frequency domain – based CC models:

- Algorithm based on Hilbert Huang transformation,
- Technique based on EMD transformation,
- Method based on S transform,
- Algorithm based on Wavelet transformation,
- CC technique based on Kalman filter,
- Analysis / theory based on Recursive DFT,
- Analysis / theory based on FFT,
- Analysis / theory based on DFT and
- Algorithm based on Fourier series.

The 9 techniques mentioned above are the techniques for CC in the frequency domain. Wherein monitoring of the power quality is required, almost all of these above – mentioned techniques find applications. For example, in power analyzers and PQ instruments among others. Moreover, a few of these techniques have also been used for the CC of SAPFs. Although, these CC algorithms are not given preference, as far as real time

CC technique requirements are concerned. It is because of the disadvantages that come with these techniques which are that these techniques are sluggish, slow and also require a very heavy computation burden.

For the control of SAPFs, all these control algorithms may be used.

2.3 Unit Template - (UT -) based controller with results

In applications such as AC VR at load terminals / Point of Common Coupling and balancing of the loads that are unbalanced the technique based on Proportional Integral controller also known as UT finds role. It is a basic CC technique which can be used for SAPFs or other active compensating devices. This CC technique is flexible and also balances the unbalanced loads and can be easily changed accordingly, with the help of compensation of Q (reactive power), for either of the two applications: 1st being UPF at the Point of Common Coupling by correcting the value of the PF to unity / 2nd one is control of the voltage which is also known as ZVR at the Point of Common Coupling. A self – supporting DC bus of the Voltage Source Converter which is being used as a SAPF is inherently present in this CC technique. When a calculation is executed in order to estimate compensator reference current values, it is known as the direct method of CC of Voltage Source Converter current values of the SAPF. Whereas, indirect method of CC of the current values at the grid for generating Hysteresis switching pulses is used for the devices that are used in the Current Controlled Voltage Source Converter used as a SAPF. The indirect CC method of the SAPF provides quite a few advantages. These include speedy CC, decreased processor burden by use of Digital Signal Processing for implementation, the inherent suppression of sharp notches in current values and many more features. Values of voltage at DC bus of the SAPF act / are used as feedback pulses. These pulses along with sensed AC values of voltage at the Point of Common Coupling are then processed to generate grid reference current values (3 ϕ) which is beneficial due to the pros / advantages mentioned above. Now, using two Proportional Integral controllers of voltage, the magnitudes of in phase and quadrature components of grid reference currents are approximated.

Function of one of the 2 Proportional Integral controllers is the regulation of the DC bus of the Voltage Source Converter which is used as a SAPF and the other / 2nd

Proportional Integral controller regulates the voltage amplitude at the Point of Common Coupling.

2.3.1 SAPF Controlling technique in Unity Power Factor Operating

Method

The UT based controlling system is a basic technique which is meant for load compensation. Besides this, it can also be used for equalization and balancing of unbalanced loads. For the control of SAPF, the above – mentioned algorithm can be adapted / modified / changed according to the need either for the control of voltage for achieving ZVR by employing compensation of Q (reactive power) at the PCC / for the improvement of the power factor to maintain a Unity Power Factor (UPF).

In this control process, a self – sufficient DC bus of the Voltage Source Converter (VSC) is used as a SAPF. This technique can be employed for direct mode of CC of Voltage Source Converter current values of SAPF and in addition to this, this technique also generates the reference grid currents.

However, an indirect grid CC is favored; in order to get Pulse Width Modulated switching pulses which will be used by the devices employed for Current Controlled – Voltage Source Converter employed like a SAPF. Some of the benefits / advantages / pros associated with the indirect current control of the SAPF are fast switching, decreased computational load on the Digital Signal Processor and the characteristic removal of sharp peaks in currents. 3 – ϕ supply reference current values are generated with the help of 3 – ϕ AC voltages which are sensed at PCC, for the purpose of pulse generation. In addition to this, for the control algorithm, the DC bus voltage (V_D) of the SAPF is taken as an input.

Fig. 7 demonstrates the UT – based control logic of SAPF developed for Power Factor Correction (PFC) of the grid currents at PCC. The Fig. 7 shows three – ϕ distorted grid voltage signals as inputs and three – ϕ conditioned voltage signals (v_{ga} , v_{gb} , v_{gc}) are outputs after processing by the DSOGI block.

In order to control the DC link voltage (V_{Da}) to its reference value (V^*_D), a discrete PI controller is put in work. The output from the discrete PI controller on the DC bus voltage of the SAPF is assumed to be the magnitude denoted as I^*_{spp} . Using 3 – ϕ unit current templates that is r_{ga} , r_{gb} and r_{gc} that are in $-\phi$ with the conditioned grid voltages that is v_{ga} , v_{gb} and v_{gc} , the in – phase reference grid current components that is i^*_{ga} , i^*_{gb} and i^*_{gc} are obtained.

The product of the generated in – phase unit templates and the in – phase magnitude gives the three – ϕ reference grid currents i.e. i^*_{ga} , i^*_{gb} and i^*_{gc} . Therefore, for fundamental UPF grid current values, the in – phase reference grid current values, that can be seen calculated by the use of the way that is explained above, actually turn out to be the supply reference current values that are needed.

It can be seen that, for calculating what is called as magnitude of reference grid currents by using average value V^*_{Da} and V^*_D of the SAPF, discrete controller of the Proportional Integral type has been employed. The difference in V^*_{Da} and V^*_D voltage values of the SAPF results in a voltage error (V_{De}), which is further fed into a discrete PI regulator as shown in the equation below:

$$V_{De}(l) = V^*_D(l) - V_{Da}(l) \quad (2.1)$$

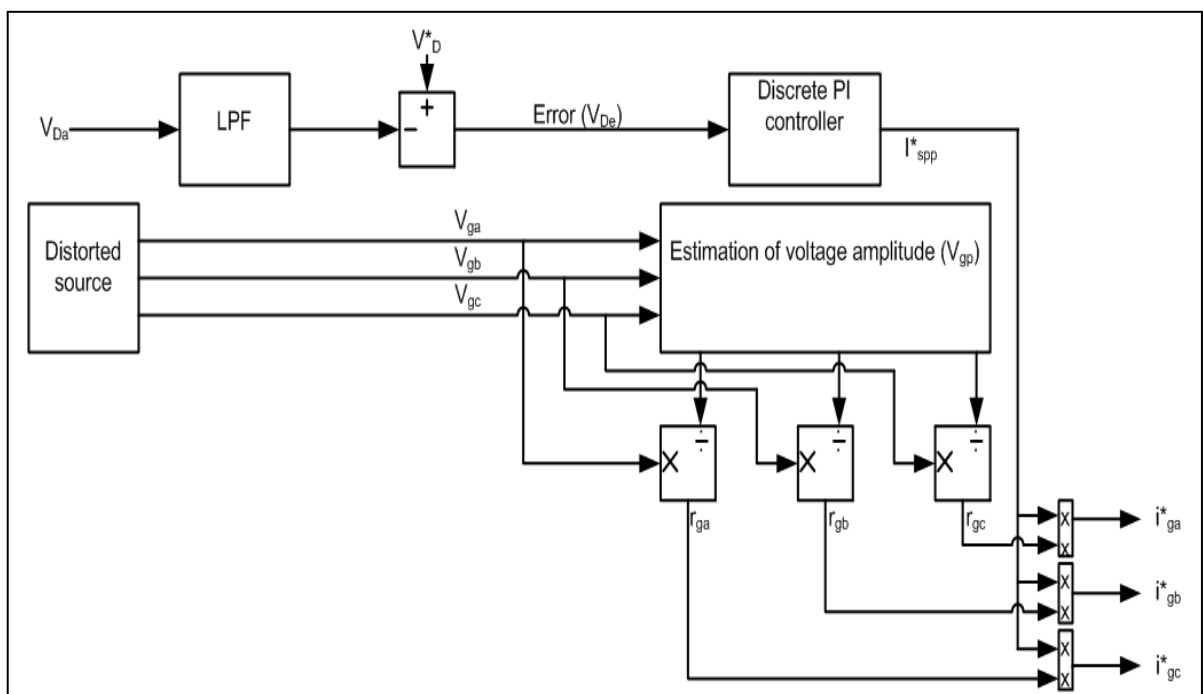


Fig. 6. UT – based control technique of SAPFs (without DSOGI technique).

In order to eliminate the ripple produced in the voltage magnitude across the DC link, in general, an LPF is used. Further, erroneous value of voltage that has been generated in the above steps is given as an input to the discrete PI regulator, further the discrete PI regulator output is shown in the equation below:

$$I_{spp}(l) = I_{spp}(l-1) + K_1 \{V_{De}(l) - V_{De}(l-1)\} + K_2 V_{De}(l) \quad (2.2)$$

in which K_1 denotes the integral gain constant and K_2 being the proportional gain constant of the DC voltage discrete PI regulator, respectively and $V_{De}(l) = V^*_D(l) - V_{Da}(l)$ is the difference or the error between V^*_D and V_{Da} DC voltages at the l^{th} sample instant.

The magnitude of the voltage denoted by V_{gp} at the PCC can be calculated as per the following equation:

$$V_{gp} = \sqrt{\frac{2}{3} (v_{ga}^2 + v_{gb}^2 + v_{gc}^2)} \quad (2.3)$$

The in $-\phi$ unit templates r_{ga} , r_{gb} and r_{gc} can be derived as per the following equation:

$$r_{ga} = \frac{v_{ga}}{V_{gp}}, r_{gb} = \frac{v_{gb}}{V_{gp}}, r_{gc} = \frac{v_{gc}}{V_{gp}} \quad (2.4)$$

Now, in order to attain a desired DC voltage output, proportional gain constant (K_2) and integral gain constant (K_1) is selected accordingly. Finally, the three $-\phi$ reference grid current in $-\phi$ phase components are calculated by the in $-\phi$ unit templates which are derived in phase with the PCC voltages in addition to the above mentioned magnitude:

$$i^*_{ga} = I^*_{spp} r_{ga}, i^*_{gb} = I^*_{spp} r_{gb}, i^*_{gc} = I^*_{spp} r_{gc} \quad (2.5)$$

In this chapter we will see that this technique fails to generate reference grid currents that are perfectly sinusoidal, in case of distorted grid conditions. Hence, a DSOGI based UT controller is developed in the next chapter.

2.3.1.1 Control of SAPF with the use of Unit Template – based theory with use of normal / undistorted source

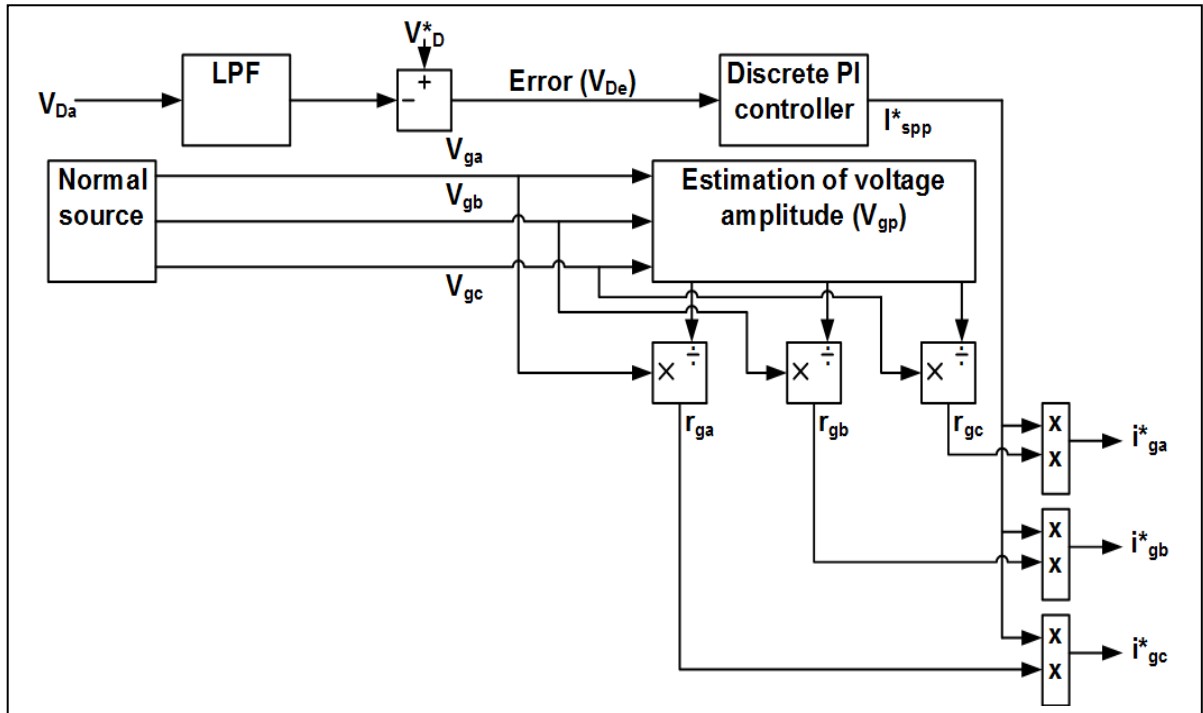


Fig. 7. UT – based control technique of SAPFs with normal source.

2.3.1.1.1 Voltage and current outputs

Fig. 8 demonstrates the dynamic performance of a SAPF with the unit template theory – based current extractor without using DSOGI technique.

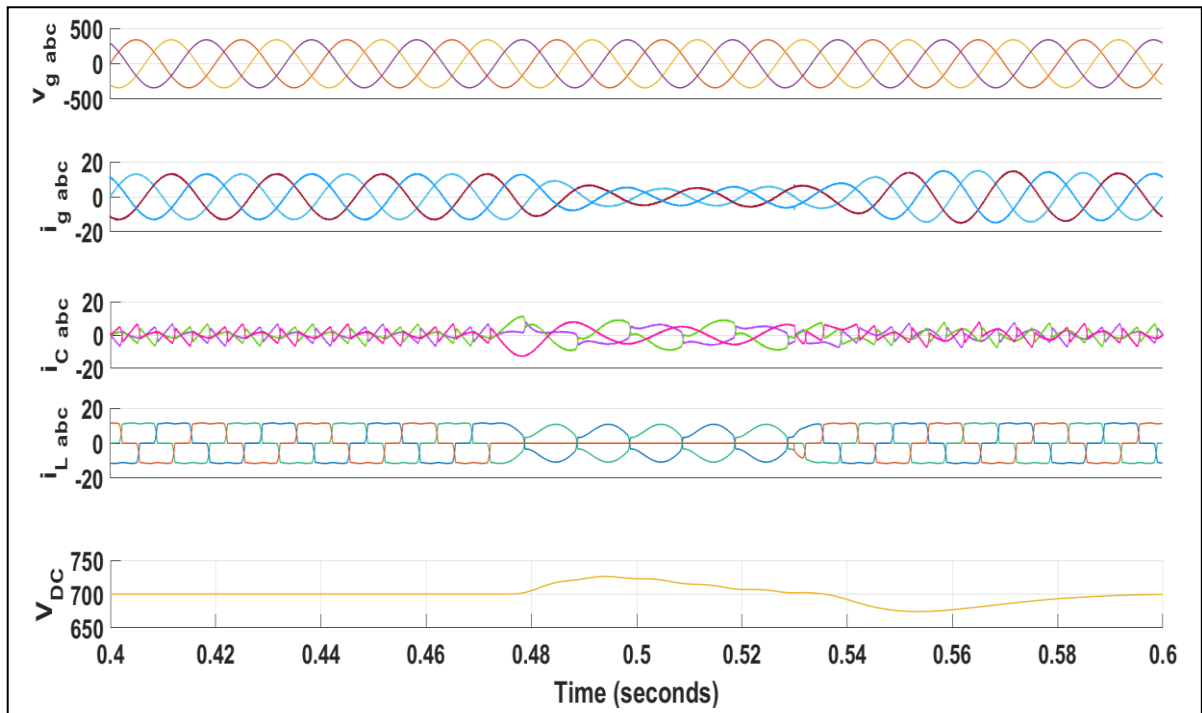


Fig. 8. UT – based control algorithm outcome (without DSOGI technique).

Fig. 8 shows the plots of grid voltage $v_{g,abc}$, grid current $i_{g,abc}$, compensator current $i_{C,abc}$, load current $i_{L,abc}$, and DC link voltage V_{DC} without DSOGI technique. Voltage and current inputs are undistorted/normal. An unbalance, in system, is created at 0.47 seconds by open circuiting one of the three phases at the load terminal. This leads to an unbalance in waveforms as shown in figure 8 above. Then, at 0.53 seconds all the three phases are connected normally, the effect of which can be seen through waveforms above. It is seen that V_{DC} settles to the 700 V value at 0.59 seconds. During model simulation, the reference value is taken as 700 V.

2.3.1.1.2 v_g , i_g and i_L THD values

Fig. 9 shows the corresponding THD values for v_g , i_g , and i_L . The THD value for i_g is 2.96 % which meets the IEEE 519 standard. Hence, this technique works with undistorted/normal sources.

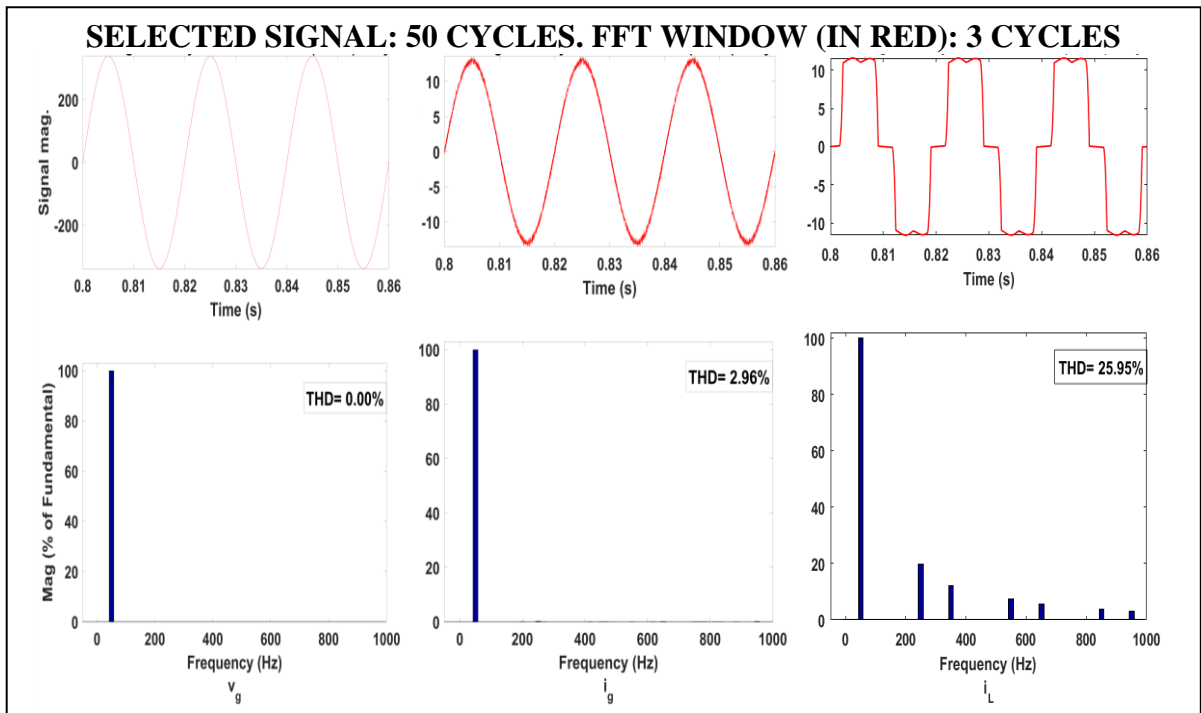


Fig. 9. THD values for UT – based control algorithm (without DSOGI technique).

2.3.1.1.3 Direct – axis current ($I_{d(new)}$) and quadrature – axis current (I_q) outputs

Fig. 10 shows the corresponding direct – axis current ($I_{d(new)}$) and quadrature – axis current (I_q) output values of the control of SAPF in UPF mode of operation without the use of DSOGI technique.

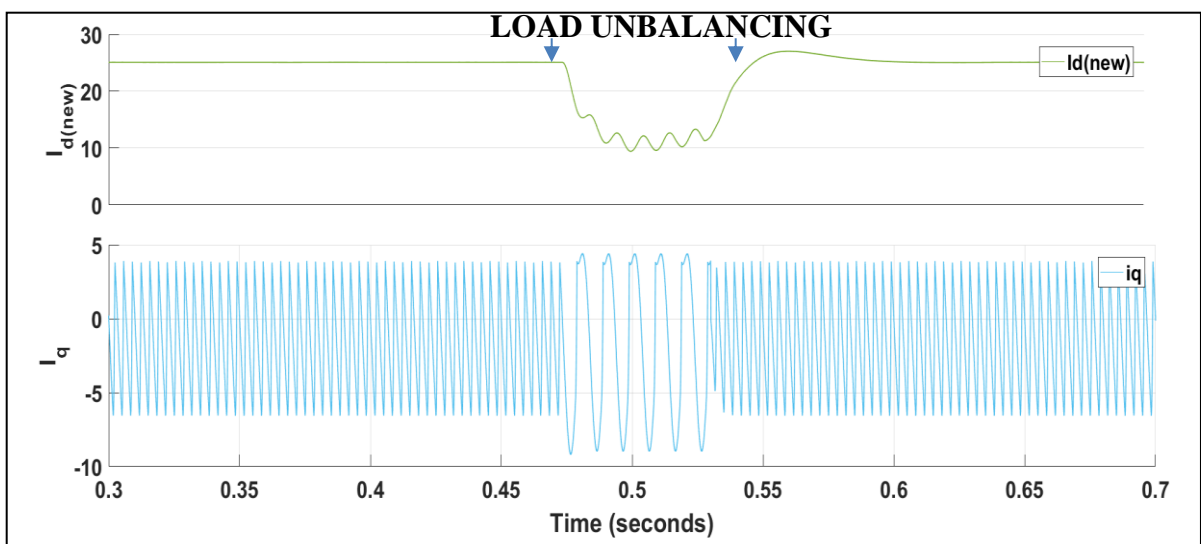


Fig. 10. Direct – axis current ($I_{d(new)}$) and quadrature – axis current (i_q) output for the UPF mode of operation without the use of DSOGI technique.

2.3.1.2 Control of SAPF with the use of Unit Template – based theory with use of distorted source

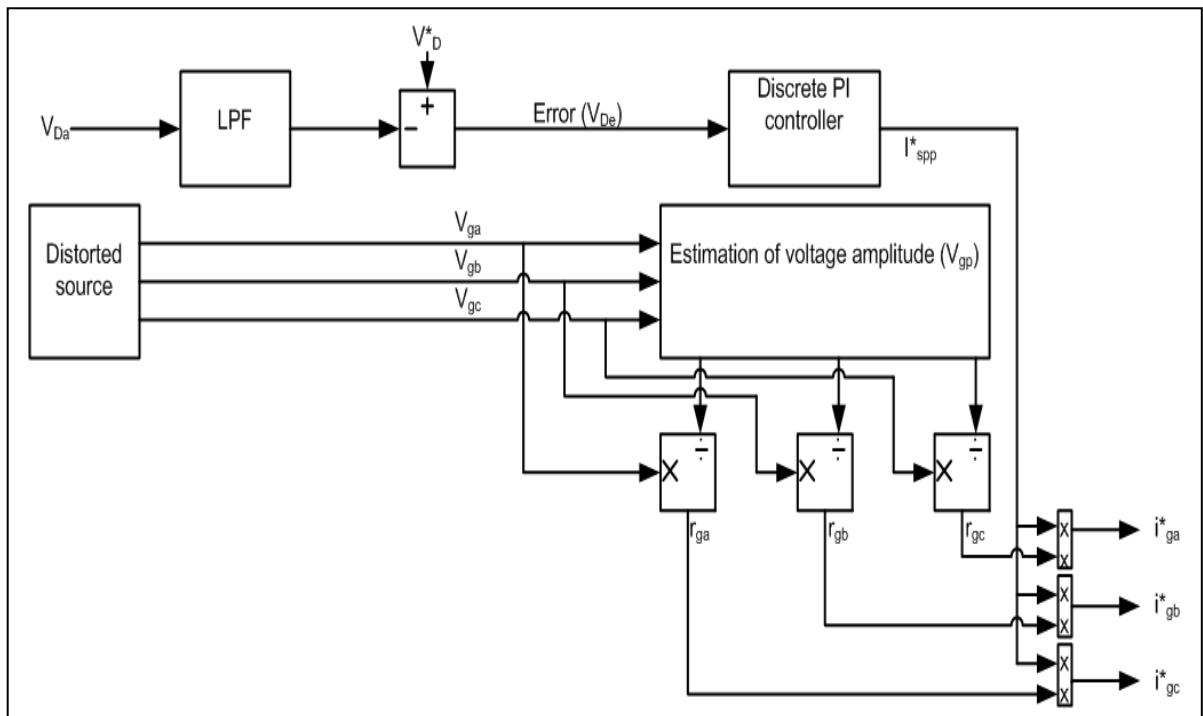


Fig. 11. UT – based control technique of SAPFs with distorted source.

2.3.1.2.1 Voltage and current outputs

Fig. 12 demonstrates the dynamic performance of a SAPF with the unit template theory – based current extractor without using DSOGI technique.

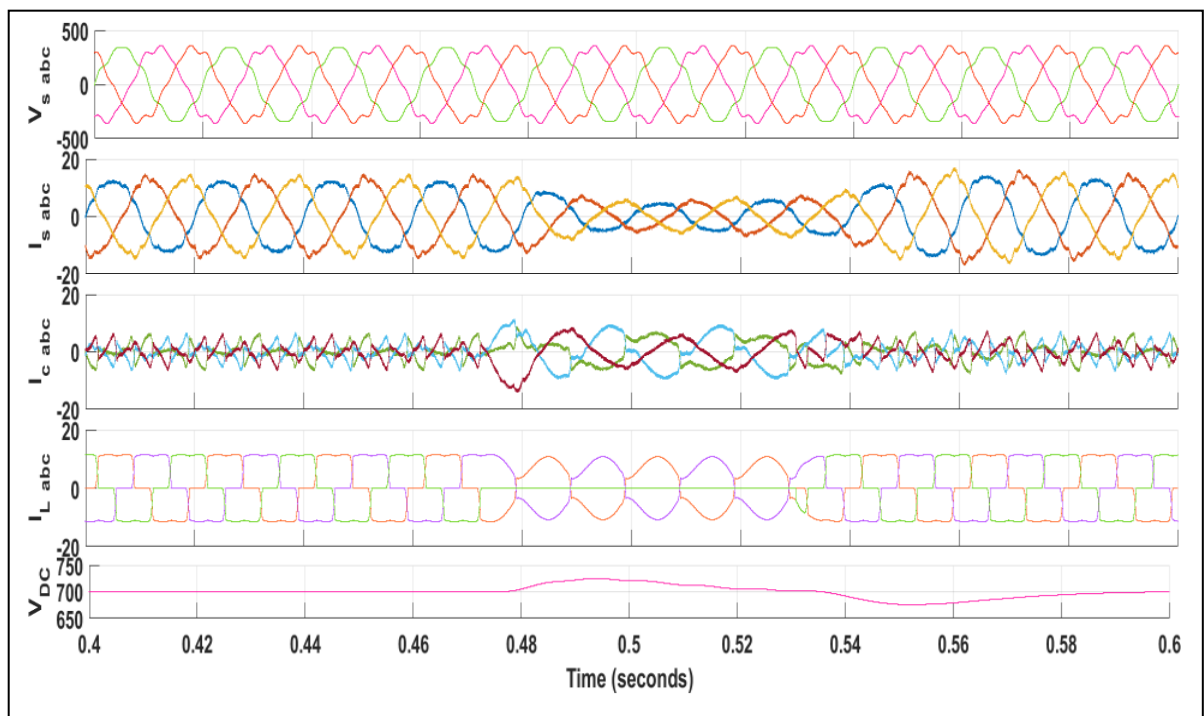


Fig. 12. UT – based control algorithm outcome (without DSOGI technique).

Fig. 12 shows the plots of grid voltage $v_{s, abc}$, grid current $i_{s, abc}$, compensator current $i_{c, abc}$, load current $i_{L, abc}$, and DC link voltage V_{DC} without DSOGI technique. In this case, current and voltage input waveforms are distorted. An unbalance, in system, is created at 0.47 seconds by open circuiting one of the three phases at the load terminal. This leads to an unbalance in waveforms as shown in figure 12 above. Then, at 0.53 seconds all the three phases are connected normally, the effect of which can be seen through waveforms above. It is seen that V_{DC} settles to the 700 V value at 0.59 seconds. During model simulation, the reference value is taken as 700 V.

2.3.1.2.2 v_s , i_s and i_L THD values

Fig. 13 shows the corresponding THD values for v_s , i_s , and i_L . The THD value for i_s is 8.74 % which does not meet the IEEE 519 standard. Hence, we can see from results that this technique fails when supplied with a distorted source.

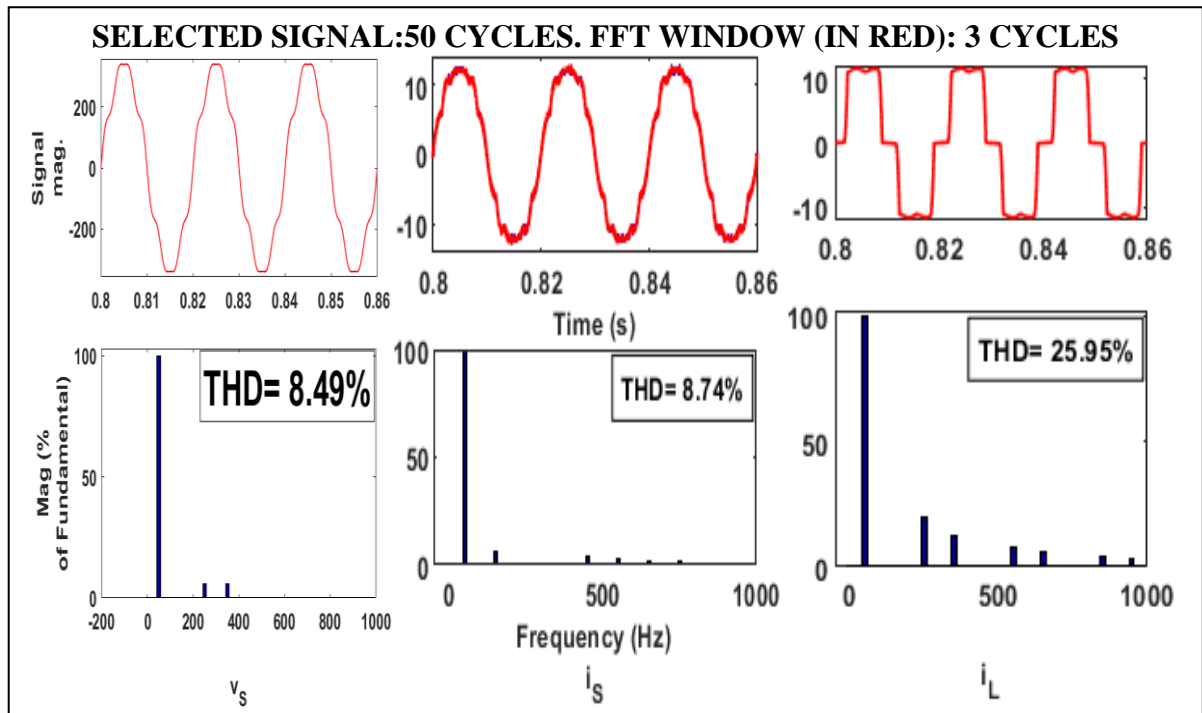


Fig. 13. THD values for UT – based control algorithm (without DSOGI technique).

2.3.1.2.3 Direct – axis current ($i_{d(new)}$) and quadrature – axis current (i_q) outputs

The corresponding direct – axis current ($i_{d(new)}$) and quadrature – axis current (i_q) output values of the control of SAPF in UPF mode of operation without the use of DSOGI technique when supplied with distorted source is similar to Fig. 10 wherein identical system is supplied with undistorted/normal source.

2.3.2 SAPF Controlling technique in Zero Voltage Regulation (ZVR) Operating Method

It is seen that the Q (reactive power) compensation and the current values (negative sequence) of the loads can be successfully achieved by the SAPF. Still, the outcome of the non – regulated waveforms of voltage present at Point of Common Coupling going towards other loads is that a drop in voltage magnitude is observed. Reason behind this is the finite (non – zero) internal Z_S of the system, its components are shown as Z_S (L_S, R_S). Its outcome is that other loads that are connected at the Point of Common Coupling get affected by this drop in the voltage magnitude. In order to avoid, SAPF should be used for this

regulation of the voltage values at the Point of Common Coupling. It is well known that direct on line starting of motors with a huge number of loads leads to inrush currents being generated. This results in / is the reason behind drop in the voltage magnitude. Solution to this problem is VR mode of operation of the SAPF, which is hence compulsorily required to be switched to.

A SAPF can be brought to use, for balancing of the load which has been mentioned before and also in order to maintain the same voltage value at Point of Common Coupling. Fig. 14 demonstrates phasor diagrams which details the fact that (normally) because of lagging PF loads, a leading current component is taken by the SAPF for the application of maintaining constant voltage. Fig. 14 (a) shows that because of the decrease in the grid impedance $Z_S (L_S, R_S)$, V_M has a high magnitude as compared to V_S . This happens when, without the use of a SAPF, the system is operated. The current at the supply and therefore the drop across the impedance at the grid can be controlled, now that the SAPF is operating in the model and drawing a leading current component. This leads to the magnitudes of voltage at the Point of Common Coupling and voltage at grid becoming equivalent, it is demonstrated as can be seen in Fig. 14 (b). ϕ and the magnitude of current value at the grid can be altered, in order to maintain the voltage value at load as per the requirement. This can be achieved by SAPF CC. Therefore, it is understood that both Unity Power Factor and Zero Voltage Regulation techniques cannot work at the same instance.

Fig. 15 demonstrates the SAPF for Zero Voltage Regulation mode at Point of Common Coupling. In order to maintain voltage at Point of Common Coupling at the required value, this is the CC technique used. With the use of this above – mentioned technique, AC VR at load end / Point of Common Coupling and balancing of unbalanced loads can be achieved. i_{sa}^* , i_{sb}^* , i_{sc}^* have 2 different components that are employed for VR at Point of Common Coupling. One of the components being (i_{sad}^* , i_{sbd}^* , i_{scd}^*) is in phase with the voltages at PCC to feed active power to the loads and the losses of the SAPF. The second component (i_{saq}^* , i_{sbq}^* , i_{scq}^*) is in quadrature with the voltage values at Point of Common Coupling to feed Q (reactive power) to the loads and to compensate the line voltage drop by Q (reactive power) injection at Point of Common Coupling. For the purpose of bringing the value of PF to unity and load balancing of unbalanced loads, the quadrature component of grid reference current values is nullified. Current value at grid leads voltage value at grid in order to achieve VR at Point of Common Coupling. This condition of current value leading voltage value is suitable for loads with lagging power factor. Not

only this but in order to bring the value of PF to 1, current value at grid also has to be in ϕ with voltage value at the grid. As indicated above, simultaneous implementation of these two modes, namely, VR at Point of Common Coupling and control of PF to unity is impossible. Hence, by respectively modifying the CC technique of the SAPF, VR or correction of PF to unity or balancing of unbalanced loads, either of the 3 can be successfully implemented one after the other. In the previous section, that is 2.3.1, Unity Power Factor method for the implementation of SAPF has already been laid out. Equation 2.5 depicts estimated quantities of the three in ϕ elements of current values at grid.

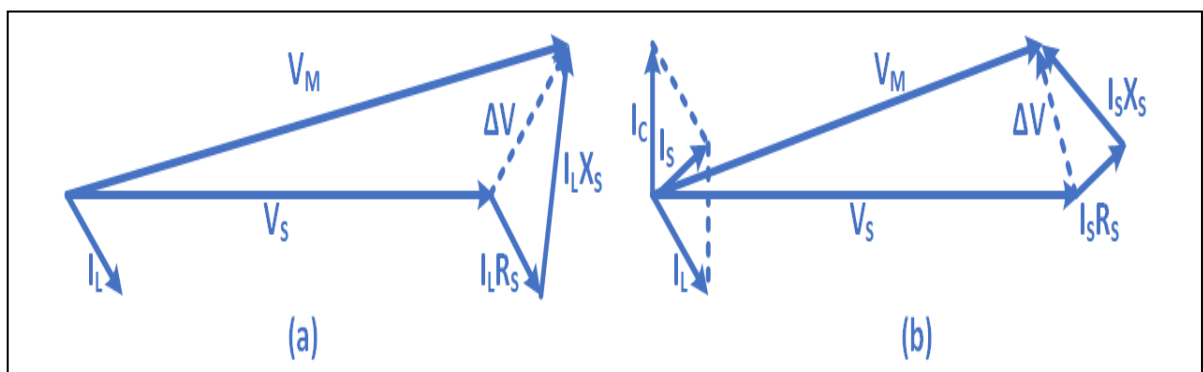


Fig. 14. Phasor diagrams for ZVR mode of operation: (a) without a SAPF and (b) with a SAPF.

2nd controller (Proportional Integral type) is employed over the V_{sp} & V_{sp}^* in order to estimate the I_{spq}^* .

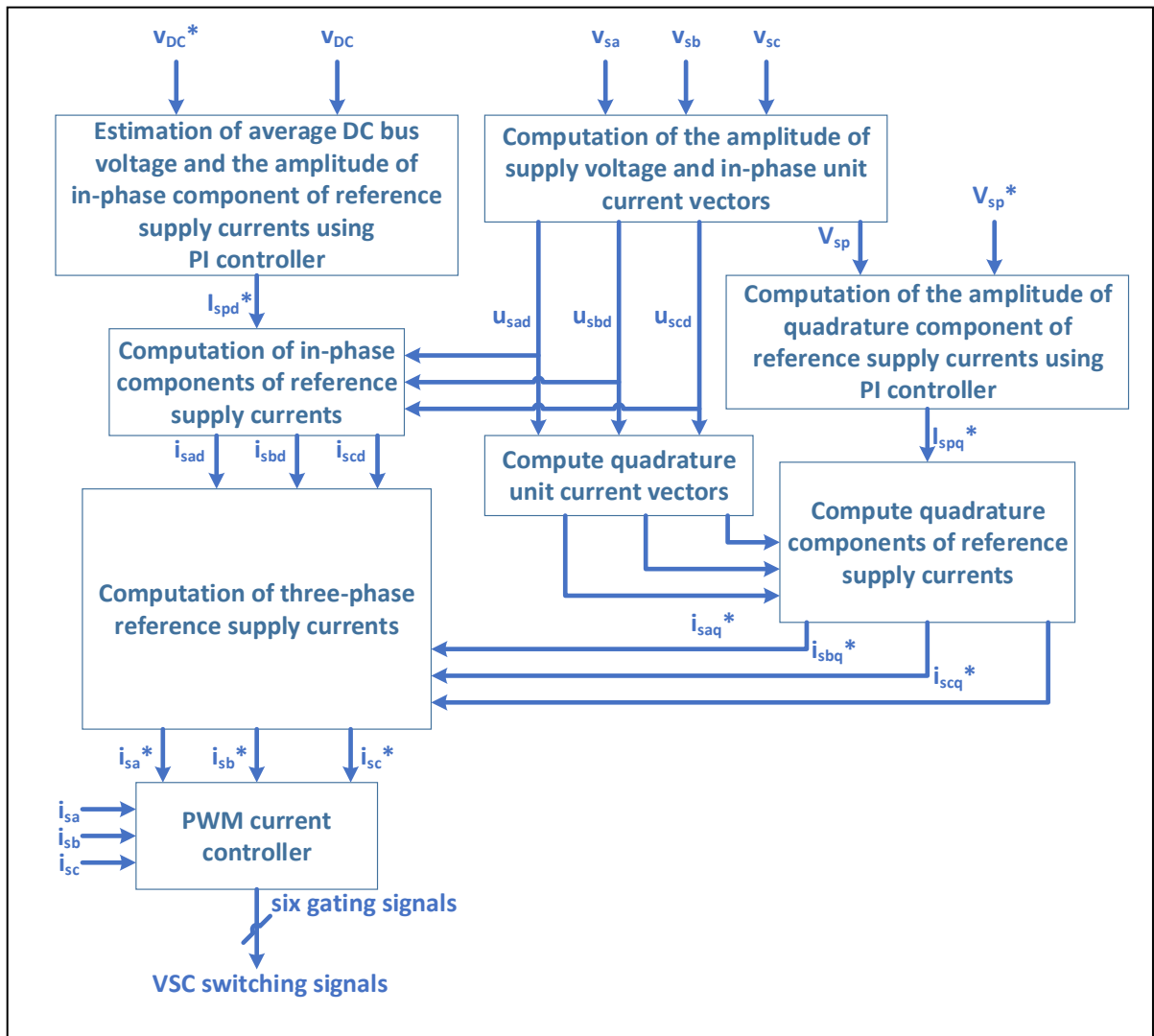


Fig. 15. SAPF control technique based on UT in Zero Voltage Regulation operating method.

A V_{sp_e} value is obtained with a comparison of the magnitude of voltage across the Point of Common Coupling with its reference value. Processing of the above error voltage signal is further achieved in a controller (Proportional Integral type). Equation 2.6 that demonstrates the $I_{sp_q^*}(n)$ at the instant of sampling, viz., n for maintaining a constant value of voltage across the Point of Common Coupling is depicted as:

$$I_{sp_q^*}(n) = I_{sp_q^*}(n-1) + K_{pt} \{v_{sp_e}(n) - v_{sp_e}(n-1)\} + K_{it} v_{sp_e}(n), \quad (2.6)$$

where K_{pt} and K_{it} are the proportional and integral gain constants of the ac bus voltage PI controller, respectively, $v_{sp_e}(n)$ and $v_{sp_e}(n-1)$ are the voltage errors at the n^{th} and $(n-1)^{\text{th}}$ instants, respectively, and $I_{sp_q^*}(n-1)$ is the desired Q (reactive power) at the instant $(n-1)$. The term $I_{sp_q^*}(n)$ is taken as the magnitude ($I_{sp_q^*}$) of the quadrature component of grid reference current values. Quadrature current UT and magnitude of $I_{sp_q^*}$ are used

which result in the estimation of grid reference current values (quadrature components, 3 ϕ). This is expressed in equation 2.7 below:

$$\begin{aligned} i_{saq}^* &= I_{sp\ q}^* u_{saq}, \\ i_{sbq}^* &= I_{sp\ q}^* u_{sbq}, \\ i_{scq}^* &= I_{sp\ q}^* u_{scq}, \end{aligned} \quad (2.7)$$

where u_{saq} , u_{sbq} and u_{scq} are current UTs (quadrature components) and are calculated as:

$$\begin{aligned} u_{saq} &= (-u_{sbd} + u_{scd}) / \sqrt{3}, \\ u_{sbq} &= (3u_{sad} + u_{sbd} - u_{scd}) / 2\sqrt{3}, \\ u_{scq} &= (-3u_{sad} + u_{sbd} - u_{scd}) / 2\sqrt{3}, \end{aligned} \quad (2.8)$$

Here, $u_{sad} = u_{sa}$, $u_{sbd} = u_{sb}$ & $u_{scd} = u_{sc}$ are in ϕ phase voltage UTs.

Equations 2.5 & 2.7 demonstrate that summation of quadrature and in ϕ components results in the estimation of instantaneous values of grid reference currents (3 ϕ). Magnitude of the quadrature component is nullified to achieve correction of PF and balancing of unbalanced loads and in this condition the in ϕ components of grid reference currents. Switches of the Voltage Source Converter of the SAPF are fed the switching pulses that are produced when the PWM or HCC is injected with sensed current values at the grid and these estimated values of grid reference currents (3 ϕ).

2.3.2.1 Control of SAPF with the use of Unit Template – based theory (ZVR) with use of normal/undistorted source

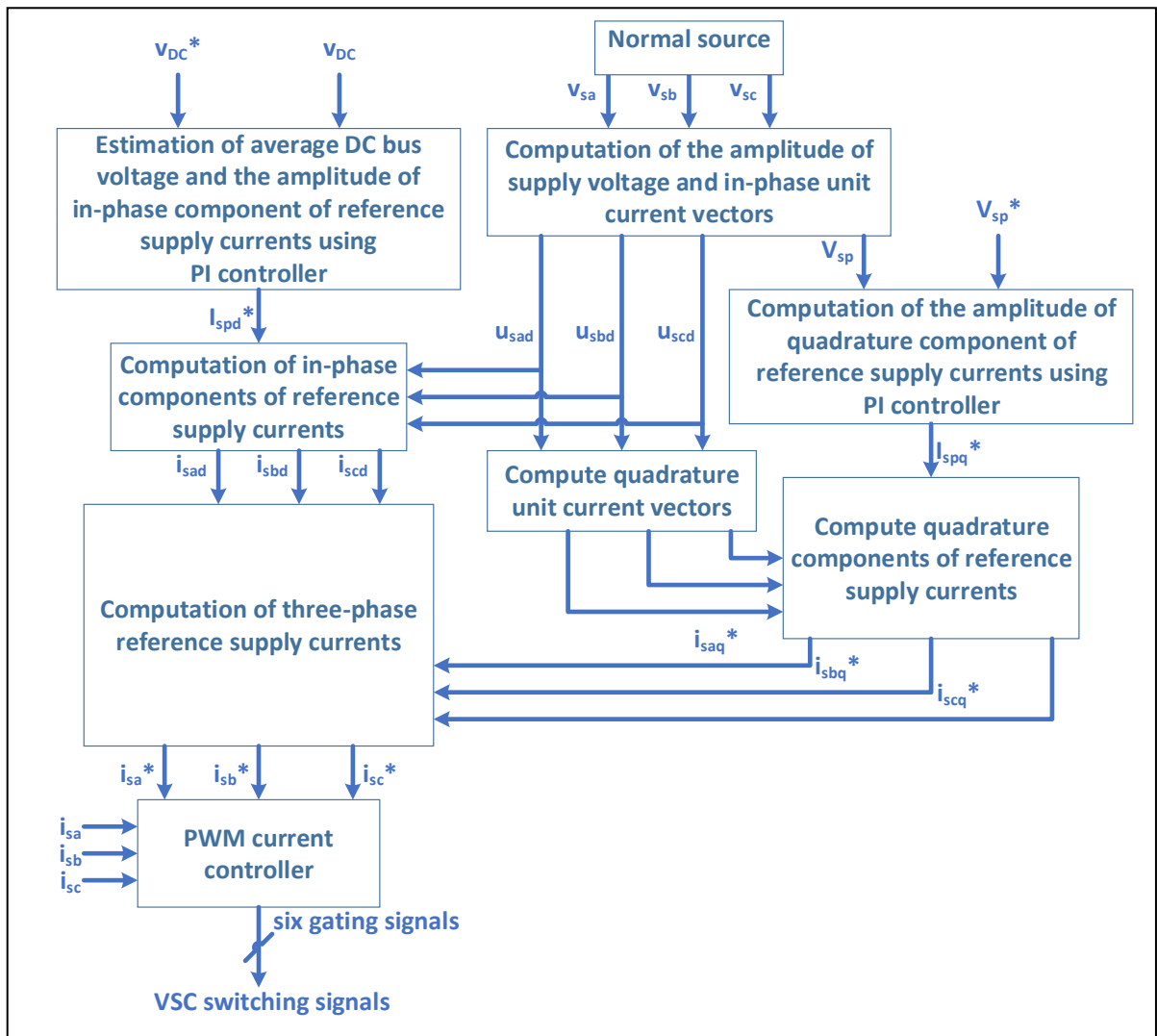


Fig. 16. UT – based control technique of SAPFs (ZVR) with normal source.

2.3.2.1.1 Voltage and current outputs

Fig. 17 demonstrates the dynamic performance of a SAPF with the unit template theory – based current extractor (ZVR) without using DSOGI technique.

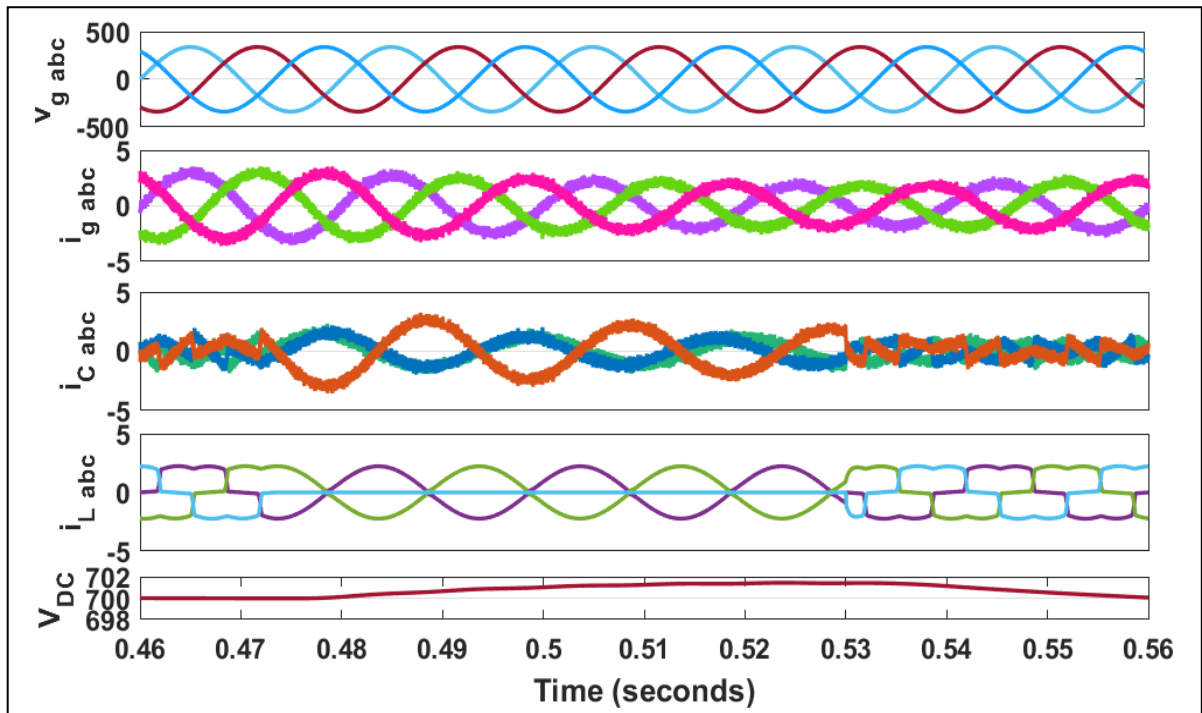


Fig. 17. UT – based control algorithm (ZVR) outcome (without DSOGI technique).

Fig. 17 shows the plots of grid voltage $v_{g, abc}$, grid current $i_{g, abc}$, compensator current $i_{C, abc}$, load current $i_{L, abc}$ and DC link voltage V_{DC} without DSOGI technique. Voltage and current inputs are undistorted/normal. An unbalance, in system, is created at 0.47 seconds by open circuiting one of the three phases at the load terminal. This leads to an unbalance in waveforms as shown in figure 17 above. Then, at 0.53 seconds all the three phases are connected normally, the effect of which can be seen through waveforms above. It is seen that V_{DC} settles to the 700 V value at 0.56 seconds. During model simulation, the reference value is taken as 700 V.

2.3.2.1.2 v_g , i_g and i_L THD values

Fig. 18 shows the corresponding THD values for v_g , i_g , and i_L . The THD value for i_g is 12.12 % which does not meet IEEE 519 standard. Hence, this technique does not work with undistorted/normal source.

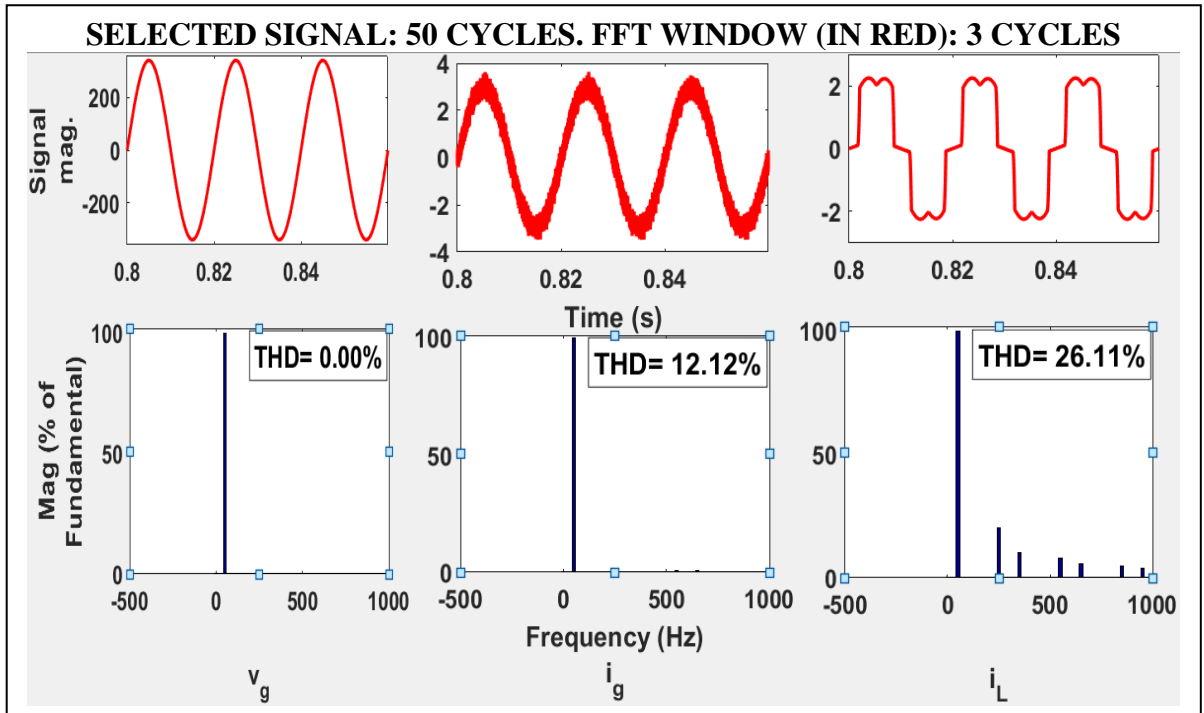


Fig. 18. THD values for UT – based control algorithm (ZVR) without DSOGI technique.

2.3.2.1.3 Quadrature – axis current (i_q) output

Fig. 19 shows the corresponding quadrature – axis current (i_q) output value of the control of SAPF in UPF mode of operation (ZVR) without the use of DSOGI technique.

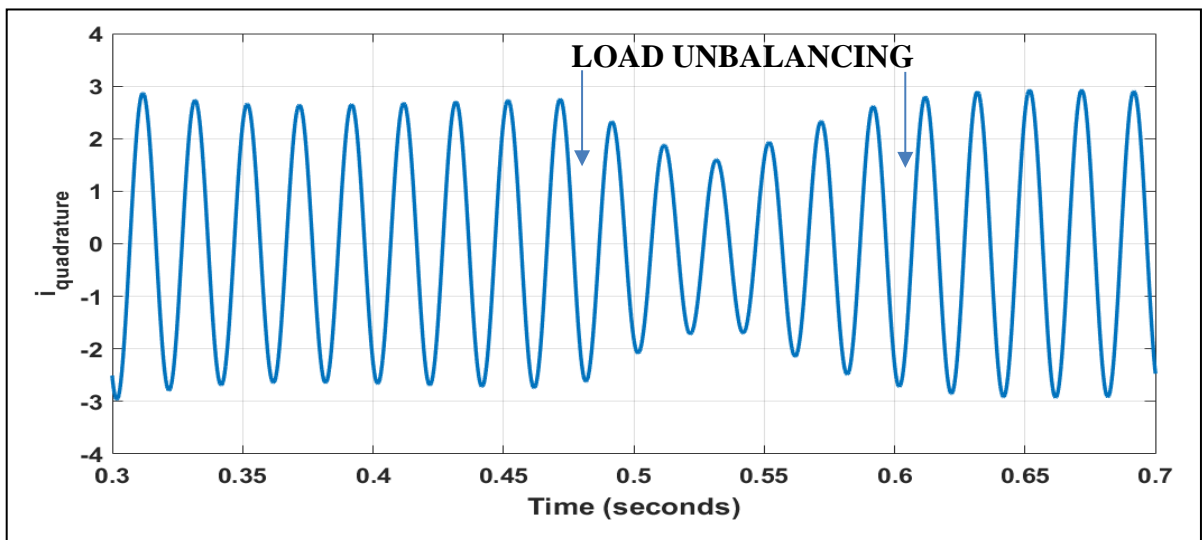


Fig. 19. Quadrature – axis current (i_q) output for the ZVR mode of operation without the use of DSOGI technique.

2.3.2.2 Control of SAPF with the use of Unit Template – based theory (ZVR) with use of distorted source

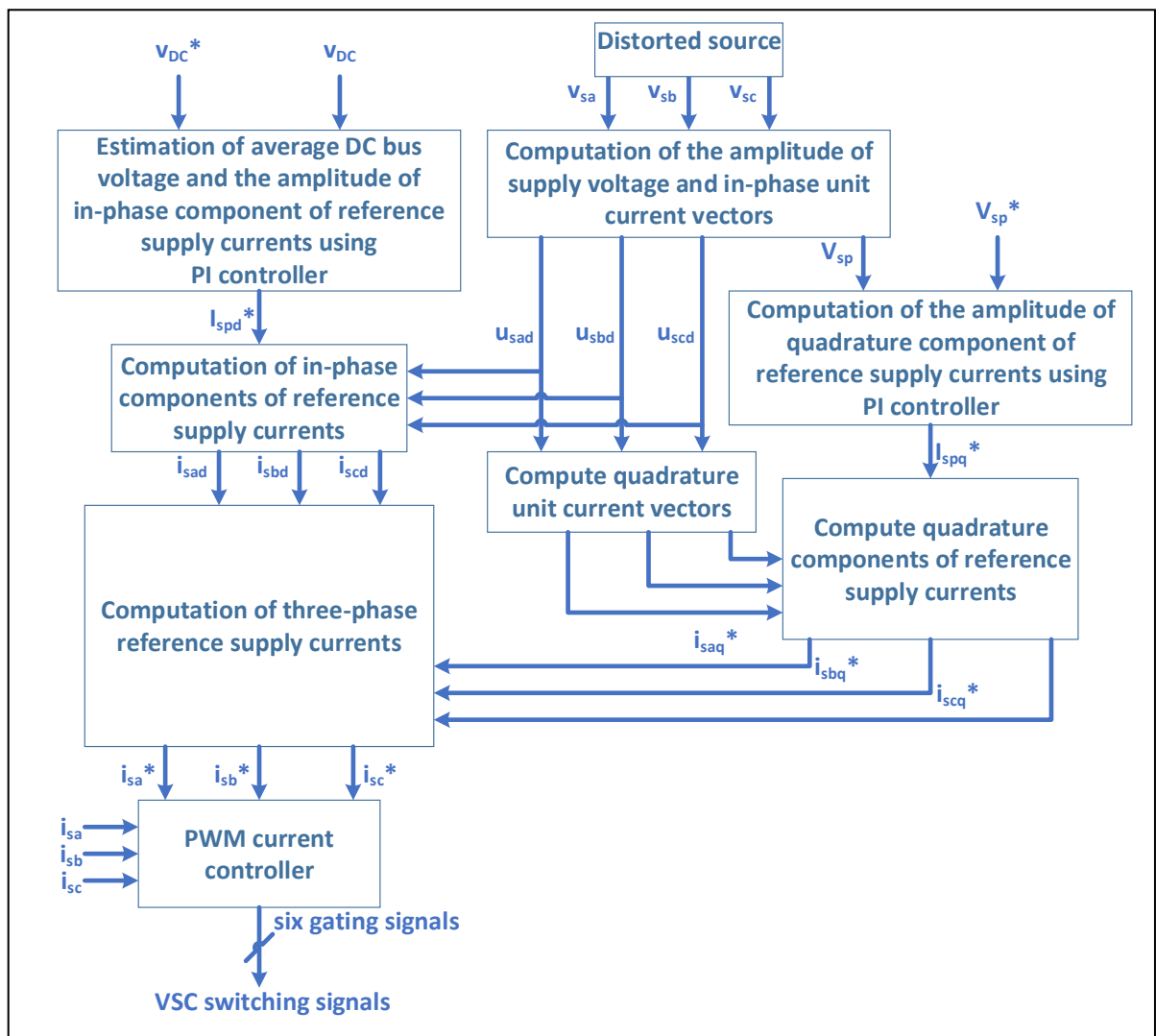


Fig. 20. UT – based control technique (ZVR) of SAPFs with distorted source.

2.4 Synchronous Reference Frame control algorithm of SAPF with results

SRF model is developed from the transformation of currents in a d – q frame with synchronous rotation; is the principle on which the SRF model is developed. Fig. 25 demonstrates the elementary block diagram on which this concept is based. As shown in Fig. 21, the input to the controller has three – ϕ voltages viz. v_a , v_b in addition to v_c and

also three – ϕ load currents viz. i_{La} , i_{Lb} in addition to i_{Lc} along with DC link voltage V_{Da} given as an input to the controller.

The normalized grid voltage signals are fed as inputs, in per unit, to a PLL, which produces the unit voltage templates viz. cosine and sine waveforms. By employing SRF theory, the 3 – ϕ current signals on the other hand are changed to direct – quadrature frame current pulses.

These current signals are, now, filtered by employing Low Pass Filter, since these are DC signals. Here, I_{LOSS} element generated using the voltage controller at DC link is summed up with the d element present in the current signal. Thereafter the signals are reconverted to again get i_{ga} , i_{gb} and i_{gc} . These a – b – c frame current signals are the reference grid signals and given as input to the Hysteresis Current Controller (HCC) which is used in order to produce final switching signals which have to be injected in SAPF for its controlling.

A detailed explanation of the SRFT technique is as follows. As current components are calculated in the pq model, in the same way current components have been calculated in $\alpha \beta$ frame. Moreover, by ways of Park's transformation, current values that have been mentioned above are changed from the $\alpha \beta$ model – dq model i.e. by using a transformation angle viz. θ as shown in matrix equation (2.9):

$$\begin{bmatrix} i_d \\ i_q \end{bmatrix} = \begin{bmatrix} \cos \theta & \sin \theta \\ -\sin \theta & \cos \theta \end{bmatrix} \begin{bmatrix} i_\alpha \\ i_\beta \end{bmatrix} \quad (2.9)$$

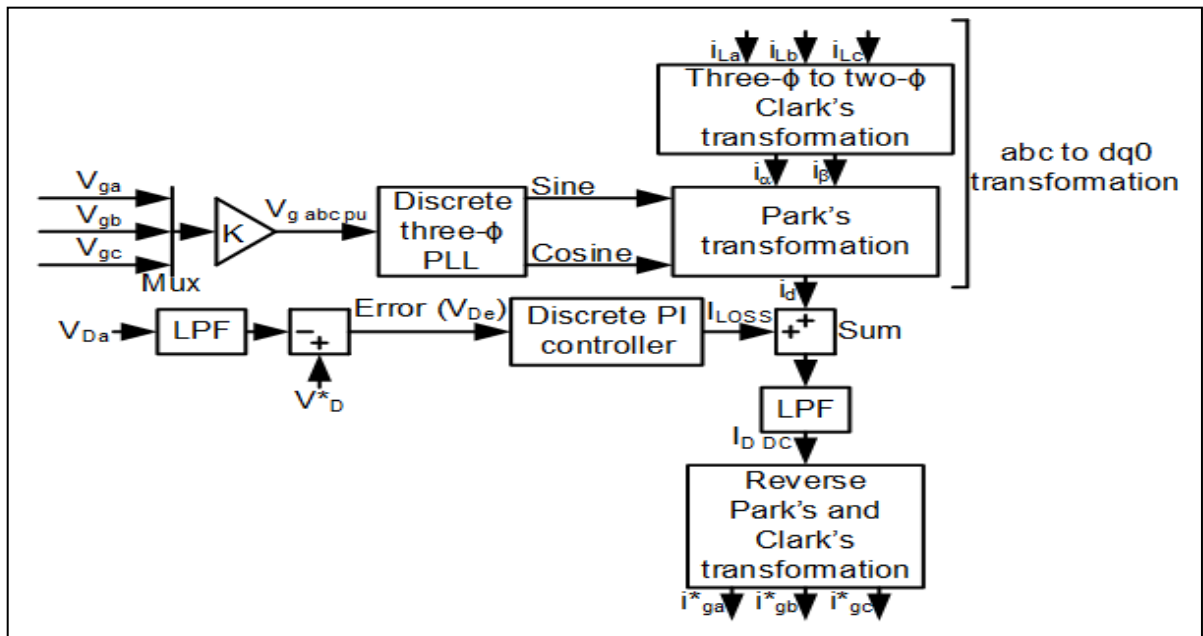


Fig. 21. SRFT – based control algorithm (without DSOGI technique).

In general, an LPF is employed to eliminate the ripple produced across the DC link voltage. Now, with the help of reverse Park's transformation the calculated DC current components $i_{d,dc}$ and $i_{q,dc}$ is changed back into $\alpha - \beta$ frame signals as illustrated in matrix equation (2.10):

$$\begin{bmatrix} i_{\alpha,DC} \\ i_{\beta,DC} \end{bmatrix} = \begin{bmatrix} \cos \theta & -\sin \theta \\ \sin \theta & \cos \theta \end{bmatrix} \begin{bmatrix} i_{d,DC} \\ i_{q,DC} \end{bmatrix} \quad (2.10)$$

By using the above derived $\alpha - \beta$ frame current signals, the conversion is made for deriving three - ϕ reference grid currents in a - b - c frame by means of matrix equation (2.11):

$$\begin{bmatrix} i_{ga}^* \\ i_{gb}^* \\ i_{gc}^* \end{bmatrix} = \sqrt{\frac{2}{3}} \begin{bmatrix} \frac{1}{\sqrt{2}} & 1 & 0 \\ \frac{1}{\sqrt{2}} & -\frac{1}{2} & \frac{\sqrt{3}}{2} \\ \frac{1}{\sqrt{2}} & -\frac{1}{2} & -\frac{\sqrt{3}}{2} \end{bmatrix} \begin{bmatrix} i_0^* \\ i_{g\alpha}^* \\ i_{g\beta}^* \end{bmatrix} \quad (2.11)$$

By keeping the i_q current component nil the supply reference current components can be calculated, the reactive power compensation can as well be provided.

2.4.1 Control of SAPF by means of SRFT based algorithm without use of DSOGI (normal source)

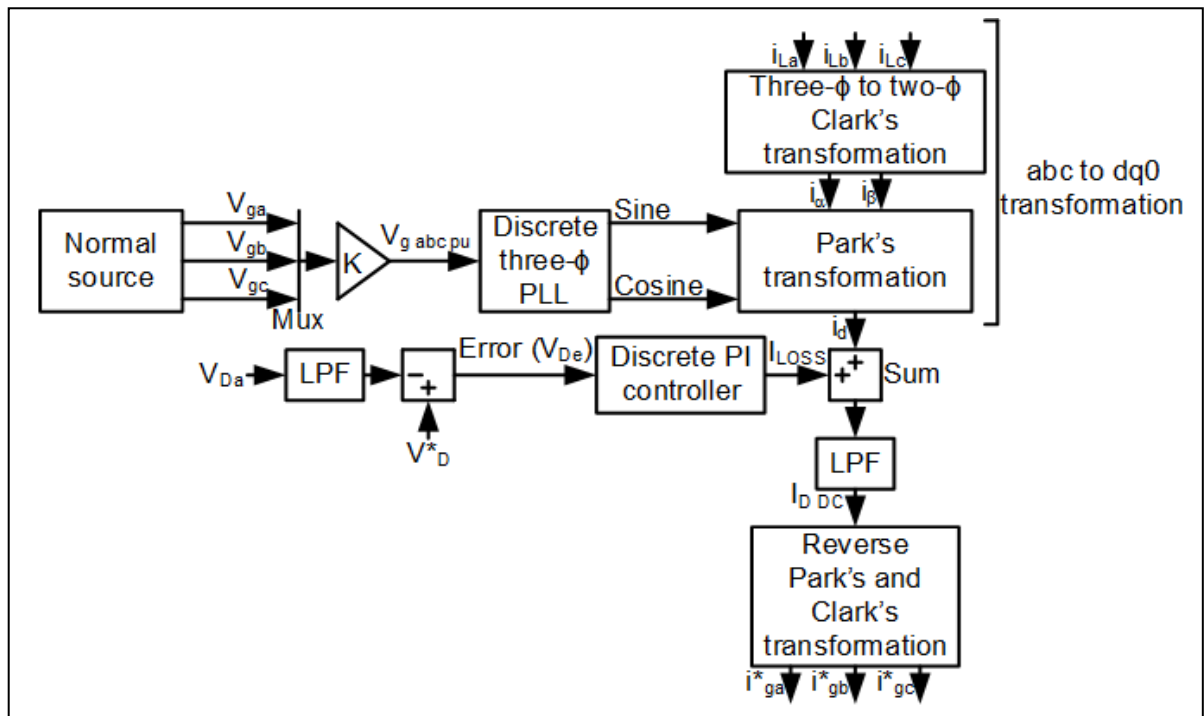


Fig. 22. SRFT – based control technique of SAPFs with normal source.

2.4.1.1 Voltage and current outputs

Fig. 23 shows the SAPF performance, controlled with the help of SRFT – based scheme without using DSOGI technique (normal source).

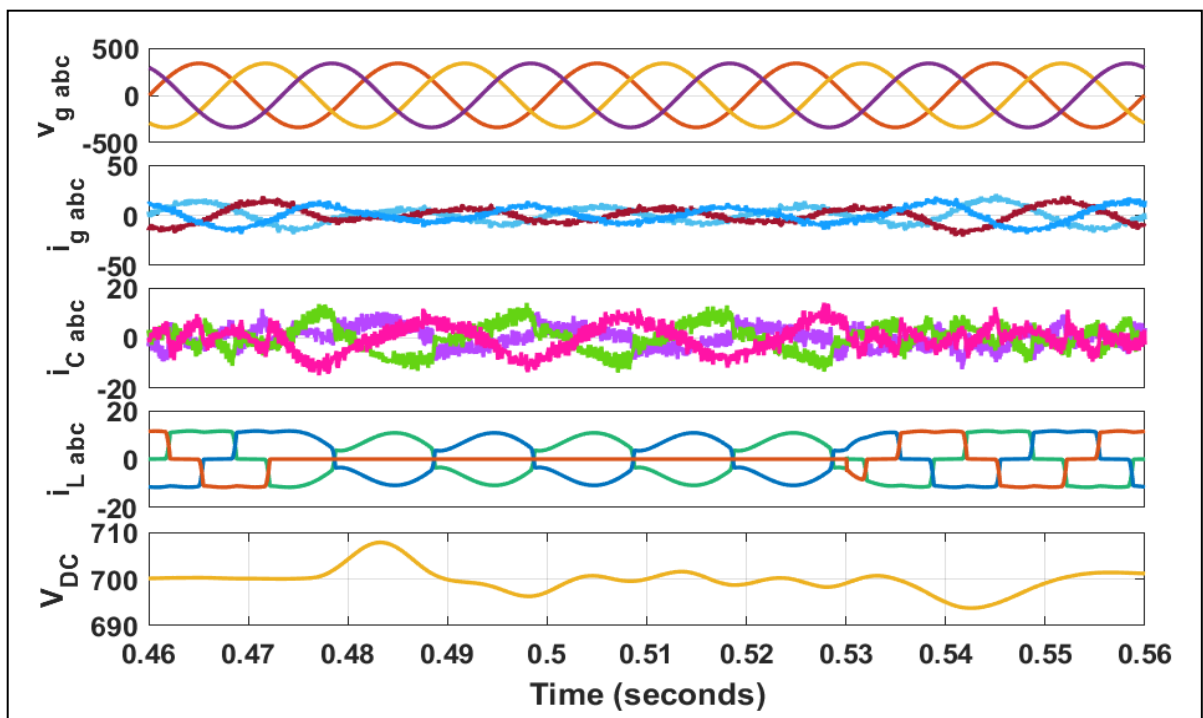


Fig. 23. SRFT – based control algorithm outcome (without DSOGI technique) using normal source

Simulation is carried out for alike unstable situation as of the preceding situation in the next section. Fig. 24 shows the plots of grid voltage $v_{g, abc}$, grid current $i_{g, abc}$, compensator current $i_{C, abc}$, load current $i_{L, abc}$ and DC link voltage V_{DC} without DSOGI technique (normal source). Voltage and current inputs are normal.

Model is tested for similar balance condition as in case I. During model simulation, the reference value is taken as 700 V. It is seen that V_{DC} settles to the 700 V value at 0.56 seconds. This shows that SRFT based technique is better as compared to UT – based control theory as far as settling of the V_{DC} back to the set V^*_D is concerned.

2.4.1.2 v_g , i_g and i_L THD values

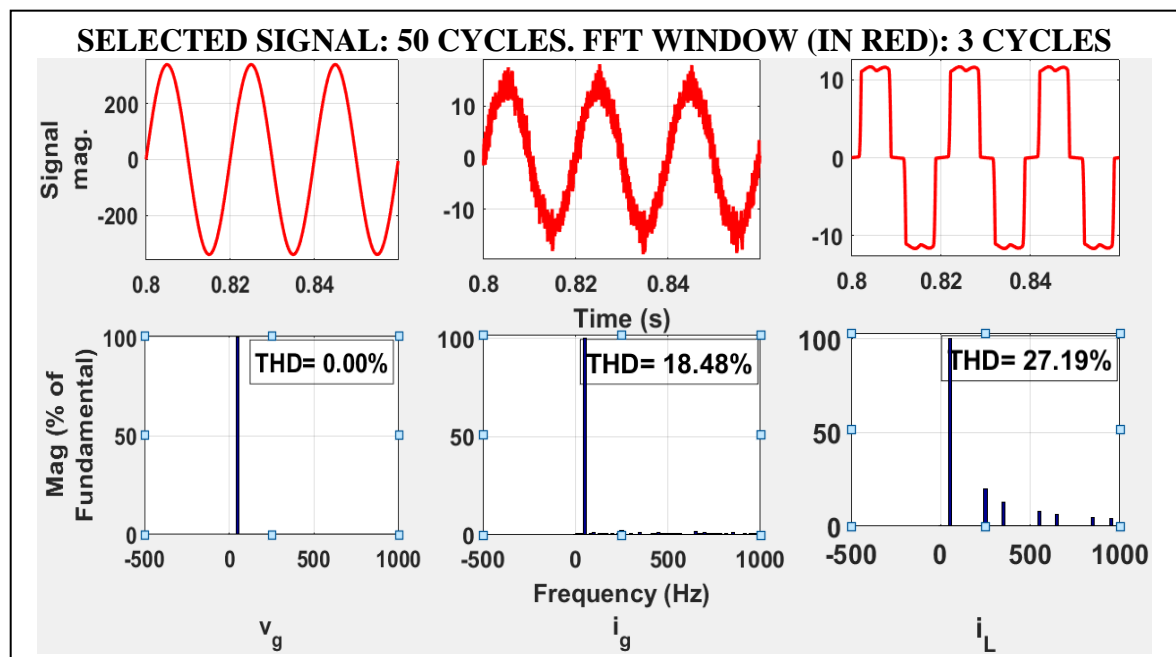


Fig. 24. THD values for SRFT – based control algorithm (without DSOGI technique) using normal source

Fig. 24 shows the corresponding THD values for v_g , i_g and i_L . The THD value for i_g is 18.48 % which does not meet the IEEE 519 standard. Hence, this technique also fails with normal source. The templates are created by means of PLL and when the grid is normal, the references are not affected. Perfect sinusoidal reference currents can be generated under normal grid conditions.

2.4.1.3 Direct – axis current ($i_{d(new)}$) and quadrature – axis current (i_q) outputs

Fig. 25 shows the corresponding direct – axis current ($i_{d(new)}$) and quadrature – axis current (i_q) output values of the control of SAPF performance controlled with the help of SRFT – based scheme without the use of DSOGI technique (normal source).

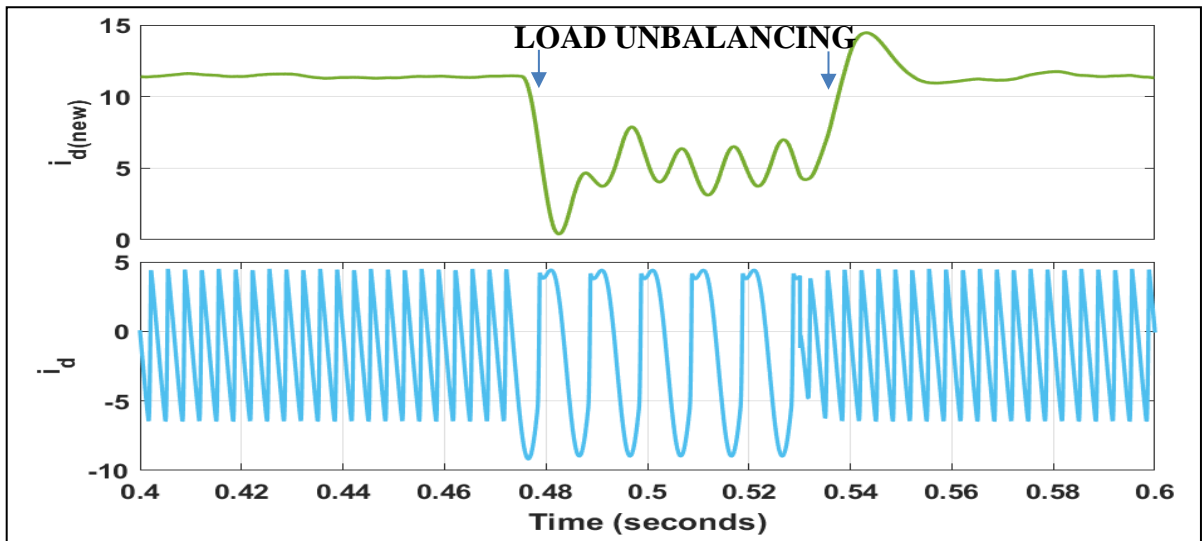


Fig. 25. Direct – axis current ($i_{d(new)}$) and quadrature – axis current (i_q) output for the SRFT – based scheme without the use of DSOGI technique (normal source).

2.4.2 Control of SAPF by means of SRFT based algorithm without use of DSOGI (distorted source)

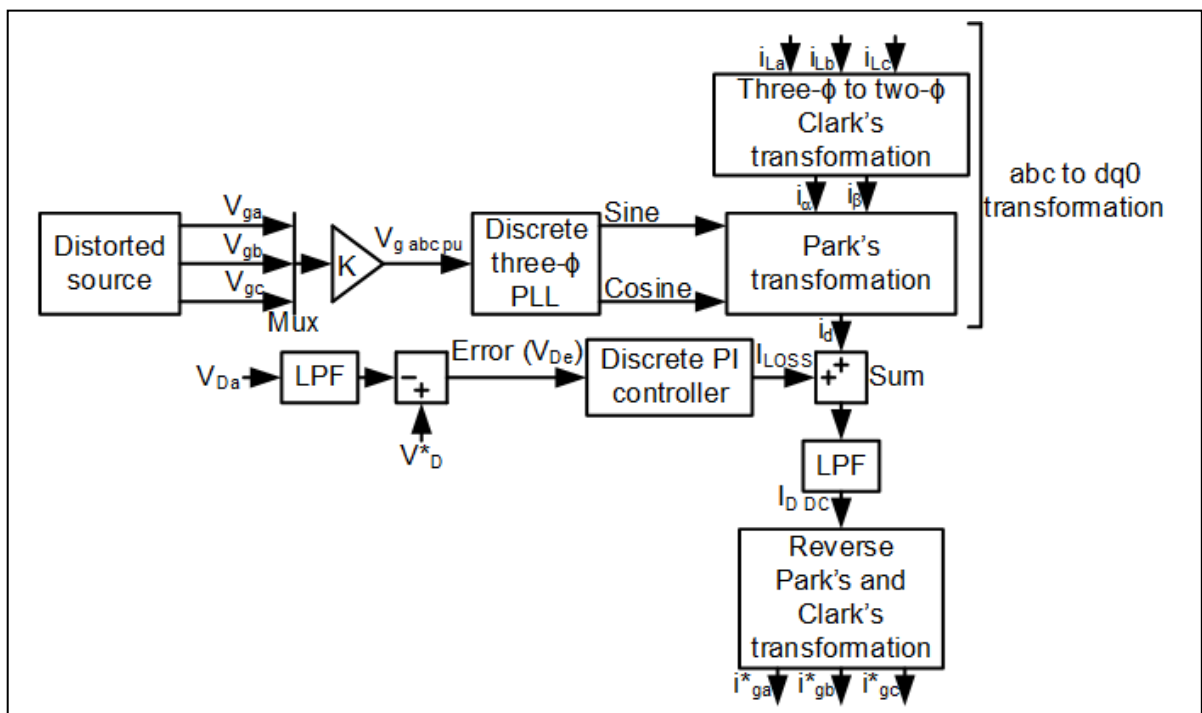


Fig. 26. SRFT – based control technique of SAPFs with distorted source.

2.4.2.1 Voltage and current outputs

Fig. 27 shows the SAPF performance controlled with the help of SRFT – based scheme without using DSOGI technique (distorted source).

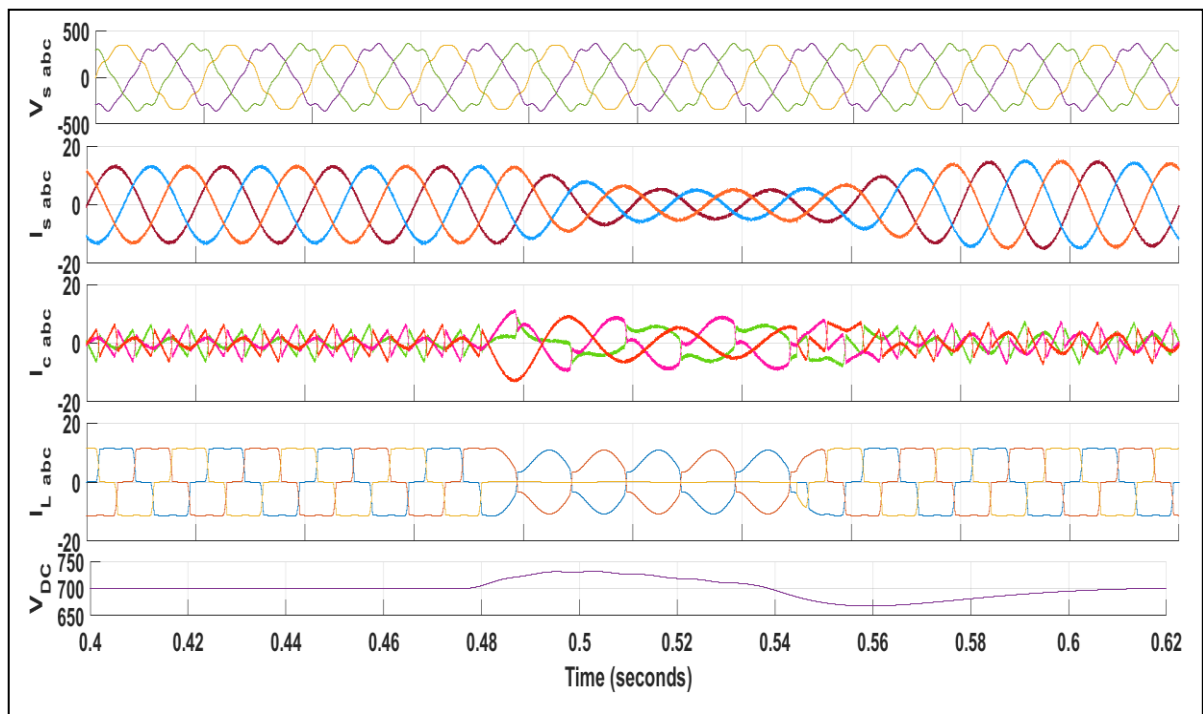


Fig. 27. SRFT – based control algorithm outcome (without DSOGI technique) in adverse grid conditions

Simulation is carried out for alike unstable situation as of the situation described in 2.3.2.1. Fig. 27 shows the plots of grid voltage $v_{s, abc}$, grid current $i_{s, abc}$, compensator current $i_{c, abc}$, load current $I_{L, abc}$ and DC link voltage V_{DC} without DSOGI technique (distorted source). Current and voltage inputs at the grid are distorted.

Model in this case, also, is tested for similar kind of phase unbalance condition as is described in case I. During model simulation, the reference value is taken as 700 V. It is seen that V_{DC} settles to the 700 V value at 0.58 seconds. This shows that SRFT based technique is better as compared to UT – based control theory (UPF) as far as settling of the V_{DC} back to the set V^*_D is concerned.

2.4.2.2 v_s , i_s and i_L THD values

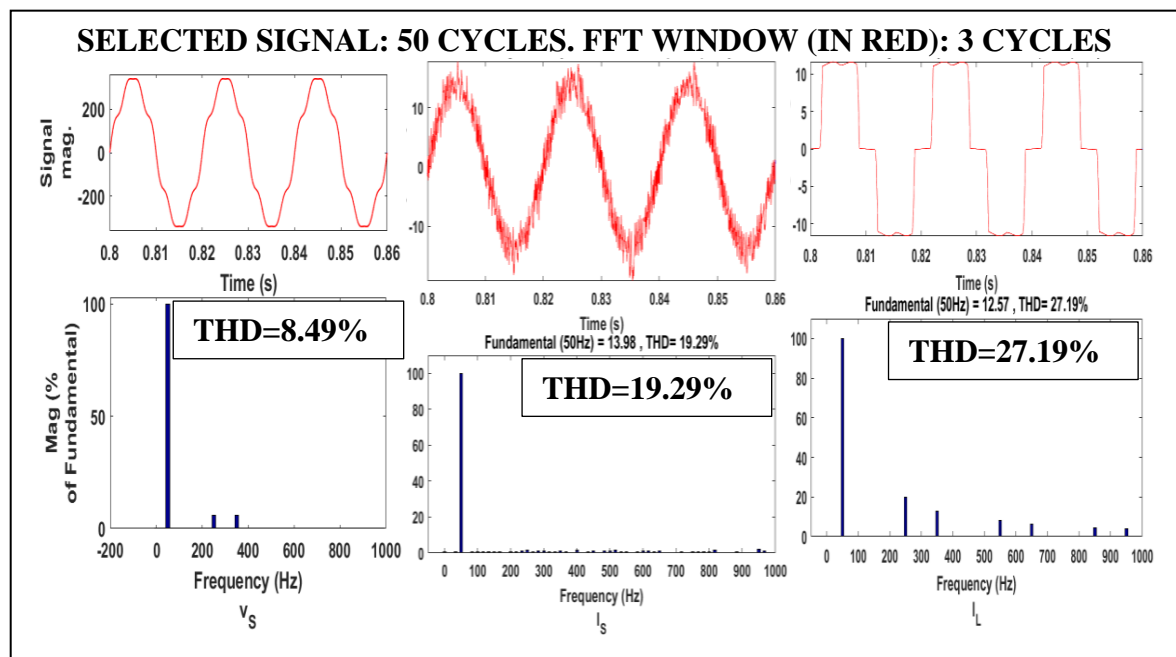


Fig. 28. THD values for SRFT – based control algorithm (without DSOGI technique) in adverse grid conditions

Fig. 28 shows the corresponding THD values for v_s , i_s and i_L . The THD value for i_s is 19.29 % which does not meet the IEEE 519 standard. Therefore, it can be inferred that this technique, also, fails when supply from the grid is distorted. The generated reference values are affected when the supply is distorted because the templates are created by using PLL. Perfect sinusoidal reference currents cannot be generated under adverse grid conditions.

2.4.2.3 Direct – axis current ($i_{d(new)}$) and quadrature– axis current (i_q) outputs

Fig. 29 shows the corresponding direct – axis current ($i_{d(new)}$) and quadrature– axis current (i_q) output values of the control of SAPF performance controlled with the help of SRFT – based scheme without the use of DSOGI technique (distorted source).

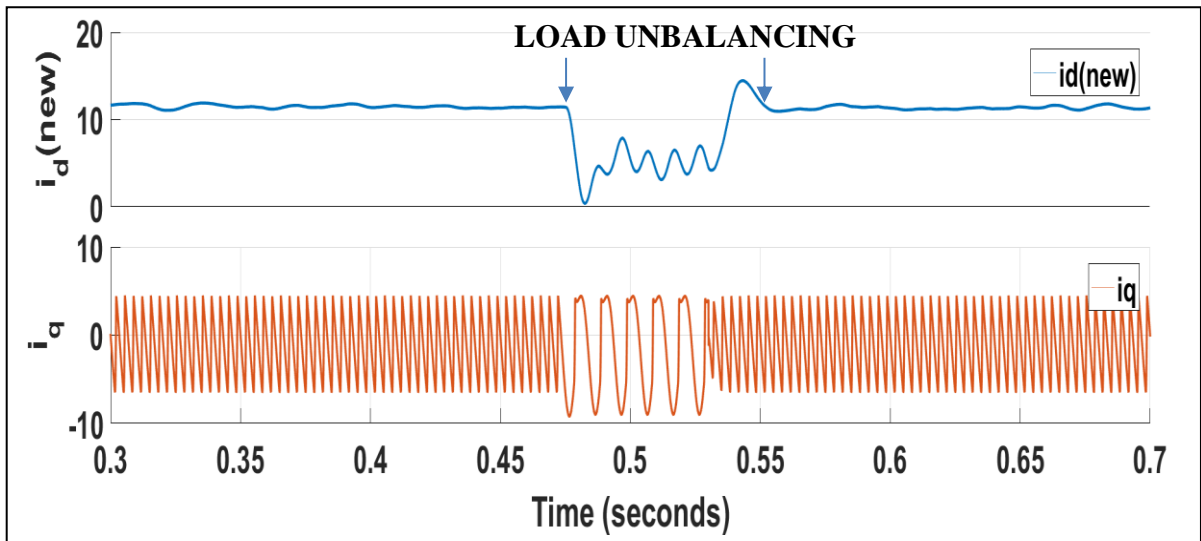


Fig. 29. Direct – axis current ($i_{d(new)}$) and quadrature – axis current (i_q) output for the SRFT – based scheme without the use of DSOGI technique (distorted source).

Table II. Comparison of all schemes used in this chapter.

Scheme name	Source type	Signal name	THD%
UT (UPF)	Normal/undistorted	v_g	0.00
		i_g	2.96
		i_L	25.95
	Distorted	v_g	8.49
		i_g	8.74
		i_L	25.95
UT (ZVR)	Normal/undistorted	v_g	0.00
		i_g	12.12
		i_L	26.11
SRF	Normal/undistorted	v_g	0.00
		i_g	18.48
		i_L	27.19
	Distorted	v_g	8.49
		i_g	19.29
		i_L	27.19

CHAPTER 3

DESIGN OF DUAL SOGI BASED ALGORITHM FOR 3 – ϕ SYSTEM

3.1 Introduction

There many methods to filter coordinates α β , the positive – sequence, frequency – adaptive detection, which is known as Dual Second Order Generalized Integrator (i.e. DSOGI) can be categorized. It uses 3 – ϕ Second Order Generalized Integrator (SOGI) type filters [16], the generalized block diagram of which is shown in Fig. 32 (i). Their second order transfer functions are what three – ϕ SOGI type filters are mainly noted for.

The proposed control algorithm has unit template and SRFT generation using Dual SOGI PLL which is described below.

The Generation of Reference Current is a main step to control a shunt active power filter (APF). In various transaction papers, several RCG techniques are put forward. It has been deduced that the synchronous reference frame theory is the most popular technique in use. The SRF theory provides satisfactory steady – state as well as dynamic performance and simultaneous simple digital implementation, where its application can only be used over three – ϕ systems. A simple and effective example of the three – phase SRF theory for three – phase shunt active power filters has been put forward in this dissertation. This proposed model is based on employing Second Order Generalized Integrators (SOGI) and Phase Locked Loop. To fine tune the control parameters, a systematic design procedure based on the pole – zero cancellation, and the extended symmetrical optimum theory is proposed. During the designing, the effects of distortions in the grid voltage and the same in the grid frequency have been taken into account. At the end of this chapter, in order to prove the efficiency of the proposed approach, results of the simulation have been shown in detail.

Nowadays, with ever increasing use of power electronic – based devices / equipment, the harmonic contamination in electrical networks is growing rapidly. Harmonics:

1. increase the losses in electrical equipment,
2. cause malfunction of protective devices,
3. create interference with communication circuits,
4. damage sensitive loads and
5. result in perturbing torque and vibration in electrical motors. [26]

Therefore, the compensation of harmonics has become a serious concern for both electricity suppliers and consumers [27].

To deal with harmonic problems, as well as to provide reactive power compensation, passive filters have been employed traditionally. These filters have a relatively low cost and high reliability, but they suffer from many disadvantages, such as:

1. large size,
2. resonance susceptibility with the load and line impedances,
3. de-tuning caused by aging,
4. fixed compensating characteristics etc. [28]

Thus, in order to avoid these shortcomings, the Active Power Filters (APFs) have attracted considerable attentions.

An APF is a power electronic converter – based device which is intended to mitigate the power quality problems caused by nonlinear loads. Several topologies for APFs have been proposed, with the most widely used being the shunt APFs (SAPFs). [2], [3] As shown in Fig. 30, a SAPF is connected in parallel with the nonlinear load and controlled to inject (draw) a compensating current, i_C , to (from) the grid such that, the source current, i_S , is an in – phase sinusoidal signal with the grid voltage, v_g , at the point of common coupling (PCC).

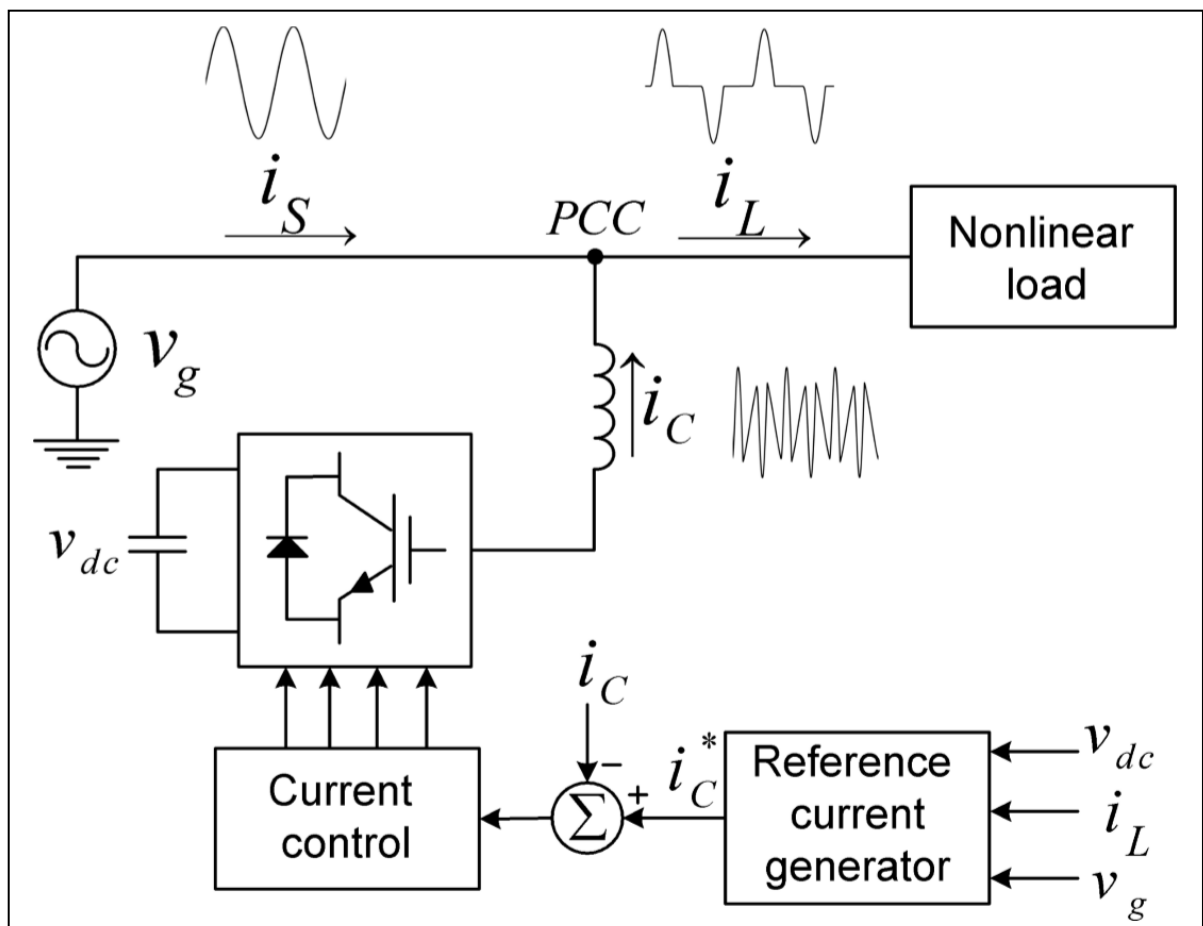


Fig. 30. SAPF connected in parallel with nonlinear load.

For the operation of a Shunt Active Power Filter, drawing reference compensating current happens to be the step of highest importance. [29] Different types of Reference Current Generation (RCG) models have been proposed by authors in some papers. The methodologies in concern can be mainly categorized into two techniques that is, the frequency domain and the time domain.

The majorly used techniques for the frequency domain are Sliding DFT (SDFT), the Digital Fourier Transform (DFT) as well as Fast Fourier Transform (FFT) that have been given in literature. [30] – [32] One is able to use them for both single – phase and three – phase Active Power Filters and they also give a satisfactory accuracy in the detection of the harmonics. The techniques based on the Fourier transform, in spite of these commendable benefits, present the usual shortcomings; these are, requirement of higher banks of memory and large values of computational burden. [31] Also, because of the relatively longer duration of time period (usually >2 cycles of the fundamental frequency of the time period)

required for evaluation of Fourier coefficients, the aforementioned techniques are better, when paired with conditions where there are no variations in load. [33]

In the time domain format, the most popular approach for RCG is the synchronous reference theory. This model was initially designed for three – wire, three – phase systems and has been majorly expanded, in the following years. The synchronous reference frame theory presents quick dynamic response and low evaluation complexity when put against the techniques in the frequency domain, but its usage was only possible over 3 – ϕ systems.

Making it possible to denote the single – phase systems as a kind of pseudo two – phase ($\alpha \beta$) systems, in the synchronous reference frame model, the voltage across the grid and the current through the load experience a shift in phase of ninety degrees. On the same grounds, the three – phase synchronous reference frame model can be used in accordance with a single – phase system. The voltage signal at the grid is read purely as a sinusoidal waveform; this is a significant shortcoming with respect to this theory. Therefore, the retrieval of reference current gets majorly degraded due to availability of any distortion in the voltage across the grid. Moreover, due to the dependence on frequency of the methods employed to obtain a shift in phase of ninety degrees, whilst the approximation of the reference current value, changes in the grid frequency cause errors.

In the report, a simple and efficient application of the 3 – ϕ synchronous reference frame theory for 3 – ϕ Shunt Active Power Filters is put forth. At the end, the efficiency of the proposed approach is proven through data returned by the simulation results.

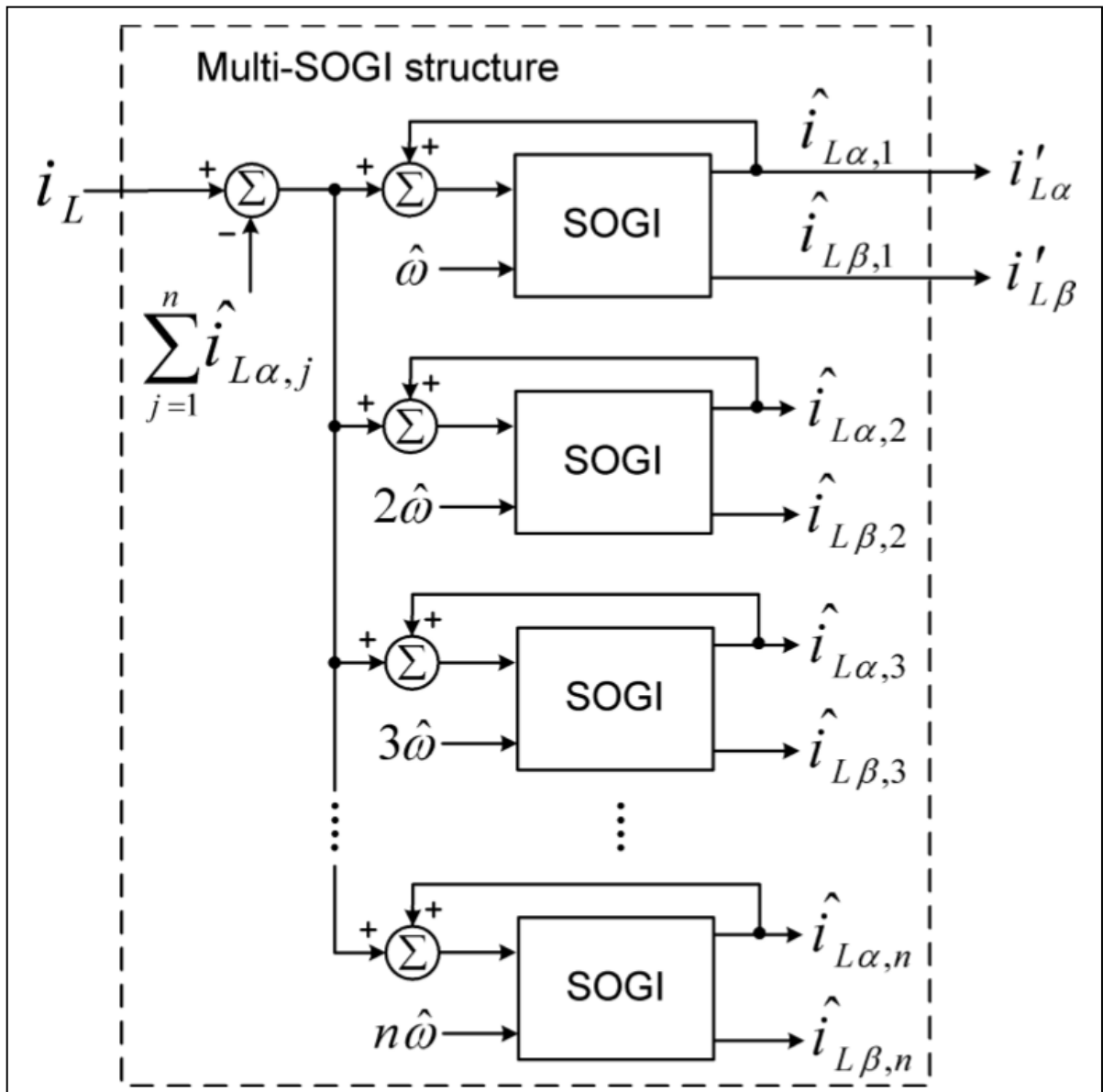


Fig. 31. Multi – SOGI structure. [45]

3.2 Algorithm Employed for Reference Current Generation

A generalized algorithm employed for Reference Current Generation scheme has been demonstrated in Fig. 33 (i). In order to produce i'_{ga} , i'_{gb} , v'_{ga} as well as v'_{gb} Second Order Generalized Integrator model has been used. Fig. 33 (ii) demonstrates the technique of a Second Order Generalized Integrator model. As shown in this Fig., the damping factor has been denoted by k . [45] In order to achieve a balanced group of in quadrature output signals which have correct magnitudes, it becomes quite mandatory that the center frequency value and the input pulse frequency value of the Second Order

Generalized Integrator model are equivalent in value. To achieve this goal, the center frequency is adjusted by an estimation of the grid voltage frequency. The estimated frequency is obtained by using a synchronous reference frame PLL (SRF – PLL). SRF – PLLs have a long history of use in three – phase systems, however in single – phase applications, their implementation is more complicated, because of the lack of multiple independent input signals. [46], [47] To overcome this problem, the generation of a secondary orthogonal phase from the original single – phase grid voltage is necessary. In the suggested approach, as shown, the same in – phase and quadrature – phase versions of the grid voltage (i.e., $v'_{g\alpha}$ and $v'_{g\beta}$) that are used to extract the reference compensating current, are employed in the SRF – PLL. Thus, the need for generating a secondary orthogonal phase for the SRF – PLL is eliminated. At first glance, one may argue that, the precise extraction of the reference compensating current requires considering a high level of filtering (small value of the damping factor k) for SOGI structures, which results in a relatively long settling time for $v'_{g\alpha\beta}$ and $i'_{L\alpha\beta}$. Therefore, considering $v'_{g\alpha\beta}$ as the input signals of the SRF – PLL will result in a very poor dynamic response in estimation of the grid voltage frequency, and may degrade the stability of the PLL. This deduction is true when a PI compensator is used as the loop filter in the SRF – PLL.

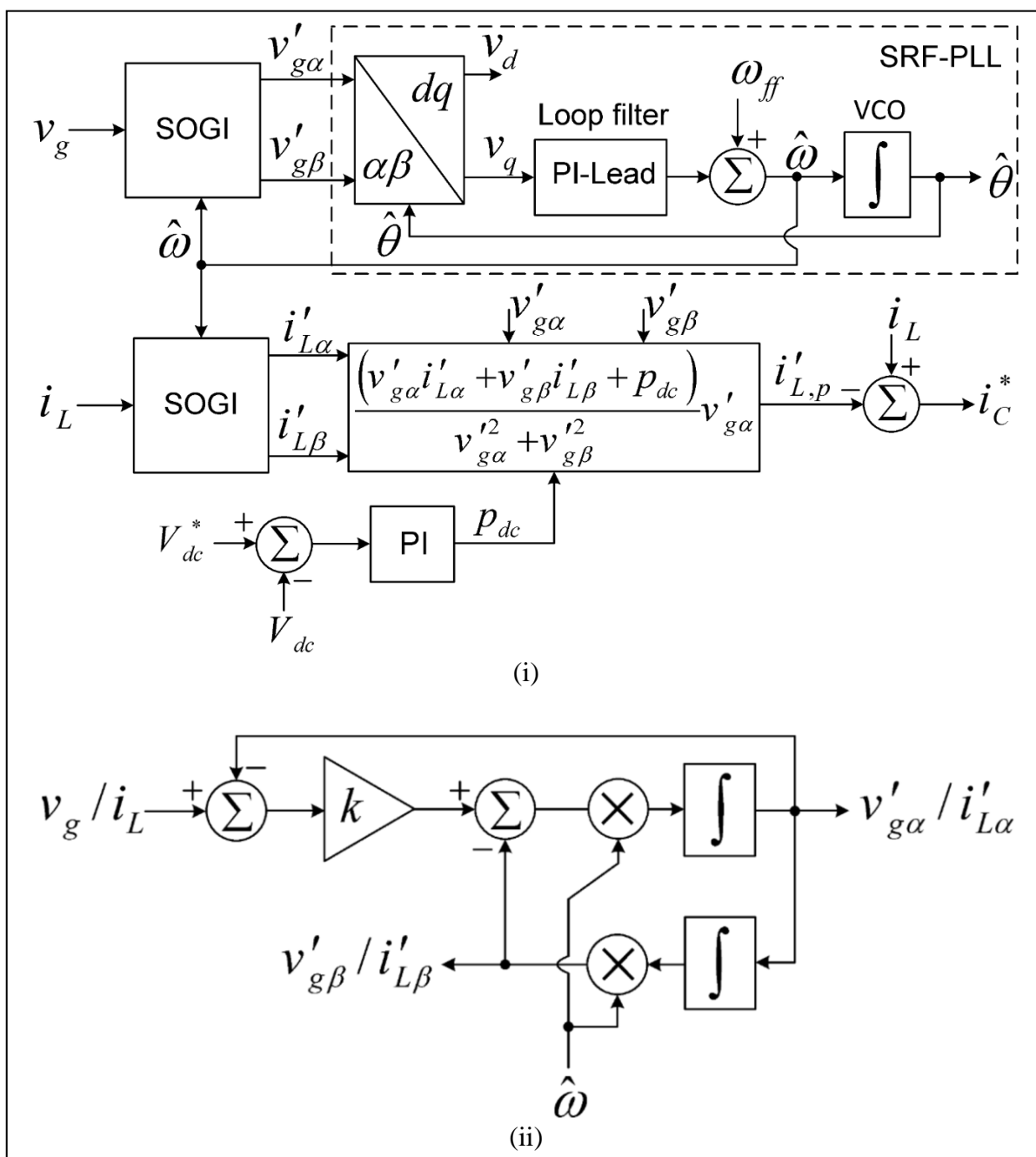


Fig. 32. Algorithm employed for Reference Current Generation: (i) general technique and (ii) inside Second Order Generalized Integrator subsystem block.

3.3 Design Guidelines

The characteristic transfer functions obtained from Fig. 32 (ii) of the Second Order Generalized Integrator subsystem block are as follows:

$$D(s) = \frac{v'_{g\alpha}}{v_g} = \frac{i'_{L\alpha}}{i_L} = \frac{k \hat{\omega} s}{s^2 + k \hat{\omega} s + \hat{\omega}^2} \quad (3.1 \text{ (a)})$$

$$Q(s) = \frac{v'_{g\beta}}{v_g} = \frac{i'_{L\beta}}{i_L} = \frac{k \hat{w}^2}{s^2 + k \hat{w} s + \hat{w}^2} \quad (3.1 (b))$$

The transfer functions are given in equations 3.1 (a) & 3.1 (b). A small value of damping factor leads to a narrower bandwidth and hence filtering capability gets enhanced. Still, a significantly small value of damping factor has a disadvantage attached to it. Which is, that it degrades the dynamic performance of the Second Order Generalized Integrator. This further leads to a great amount of time delay in the generation of the compensating current (reference value). It is well known that, during the load transients, the delay in extraction of the reference current increases the duration for which APF must sink / source the fundamental current, hence increases the required APF rating. [29], [48] It can therefore be concluded that an optimum value of k has to be found out so that none between the speed of response and harmonic rejection is compromised.

It can be easily shown that, under the frequency locked condition (i.e., $w = \hat{w}$), the outputs of the SOGI for a given input voltage $v_g = V \cos(w t + \phi)$ and for $k < 2$ are:

$$v_{g\alpha}'(t) = V \cos(w t + \phi) + A_\alpha \cos(w \sqrt{1 - (\frac{k}{2})^2} t + \phi_\alpha) e^{-\frac{k \hat{w}}{2} t} \quad (3.2)$$

$$v_{g\beta}'(t) = V \sin(w t + \phi) + A_\beta \sin(w \sqrt{1 - (\frac{k}{2})^2} t + \phi_\beta) e^{-\frac{k \hat{w}}{2} t} \quad (3.3)$$

where A_α , A_β , ϕ_α and ϕ_β are functions of V , ϕ and k . The similar results can be obtained for the load current i_L .

From (3.2) and (3.3), it is observed that, the transient terms decay to zero with a time constant of $T = 2 / k \hat{w}$. Thus, by considering a same damping factor k for both SOGI structures in Fig. 32, for the extraction of the reference current, the settling time can be approximated as:

$$t_S = 4 T = \frac{8}{k \hat{w}}. \quad (3.4)$$

Based on (3.4), the damping factor k can be simply determined by deciding a value for the settling time t_S .

When looking from the case of rejection in the harmonics, the figure used as the damping factor is sufficient for low distorted currents in the load. Whereas, there is the possibility of the condition not being satisfied, if there is quite a large harmonic content at

load. The concerned shortcoming is possible to be addressed by introducing more Second Order Generalized Integrator blocks in parallel with the single Second Order Generalized Integrator structure of the load current; see Fig. 31 [45]. Every SOGI block acts to suppress a particular harmonic constituent in the load current and for which it is altered to resonate at a preset frequency of harmonics, therefore increasing the accuracy in the retrieval of the reference compensating current. Therefore, in order to attain faster / quicker dynamic performance, it is possible to enhance the bandwidth of the fundamental frequency Second Order Generalized Integrator.

Multiple Second Order Generalized Integrator design is displayed in Fig. 31. The extra Second Order Generalized Integrator blocks result in increments in the curve of the gain at their specific frequencies of resonance. Hence, notable reductions are seen in the error in extraction, if there is high distortion in the current at the load. The dynamics of fundamental Second Order Generalized Integrator block are not significantly affected by the number of extra Second Order Generalized Integrator blocks. This is because, unless large factors of damping are used in these blocks, their effect is only seen to the frequencies in the vicinity of their frequencies of resonance.

The amount of Second Order Generalized Integrator blocks needed to be put in is variable upon the level of distortion (in current at the load). Although, a middle ground that is optimum has to be found between the effort required in computation and precision of the computed values. This is because, it is observed that the load is a large limiting factor. In this project report, addition of two Second Order Generalized Integrator blocks is proposed.

It is noted that, by using added harmonic component by using more Second Order Generalized Integrator blocks for the currents at the load, the required value of in – quadrature outputs of the grid voltage Second Order Generalized Integrator block can be increased, this is in case of grid values wherein distortions are large.

3.4 Configuration and control algorithm

In order to get a good dynamic response, faultlessly detect and further also separate the angle of the phase of positive and negative components of the sequence, the SOGI based PLL is brought to use. The Second Order Generalized Integrator block open loop transfer function is shown as in eq. (3.5):

$$T(s) = \frac{K w_r s}{s^2 + w_r^2} \quad (3.5)$$

The transfer functions of the closed loop of v'_α and $q v'_\alpha$ of the Second Order Generalized Integrators block shown in Fig. 34 with error signal (V^*_{De}) is given as follows:

$$\frac{q v'_\alpha(s)}{v} = \frac{w_r}{s} * \frac{v'_\alpha(s)}{v} = \frac{K w_r s}{s^2 + K w_r s + w_r^2} \quad (3.6)$$

It is essential to have a proper tuning of the gain or damping factor – K that influence the bandwidth of the system in the closed loop and the grid voltage angular frequency, w . k , the damping factor decides the level of filtering and response. Tuning of k is required to be in such a way that filtering response should be properly effective under distorted grid conditions too. Damping of the higher harmonics is inversely proportional to the value of k . This further means that the lesser the value of k the better the damping of higher harmonics. Therefore, in this project simulation, ω and k values are chosen as 314 and 0.5 respectively. These values have been chosen according to the optimum operation of the model prepared.

Specific shifts in phase for nominal frequency and also gain are the highlighted features of a filter that allow their function and operation. There are two methods to determine the phase of signal output from the filter. It can either be determined by using Synchronous Reference Frame – Phase Locked Loop or by using *arcus tangens* function. Above described is the use of Synchronous Reference Frame – Phase Locked Loop. High quality of filtering of most of the distortions in the signal is characteristic for the Dual Second Order Generalized Integrators. Furthermore, higher frequency values are successfully damped too.

Dual QSGs with the use of SOGI are used to be able to get the components of d – q of the α axis voltages (which are denoted by v'_α and $q v'_\alpha$ correspondingly) in addition to β axis voltages (denoted by v'_β and $q v'_\beta$ correspondingly). Two sine waves v' and $q v'$ are produced with a phase Difference of 90° as shown in Fig. 33. The SOGI is also called an adaptive filter with an infinite gain and is defined as in equation (3.5).

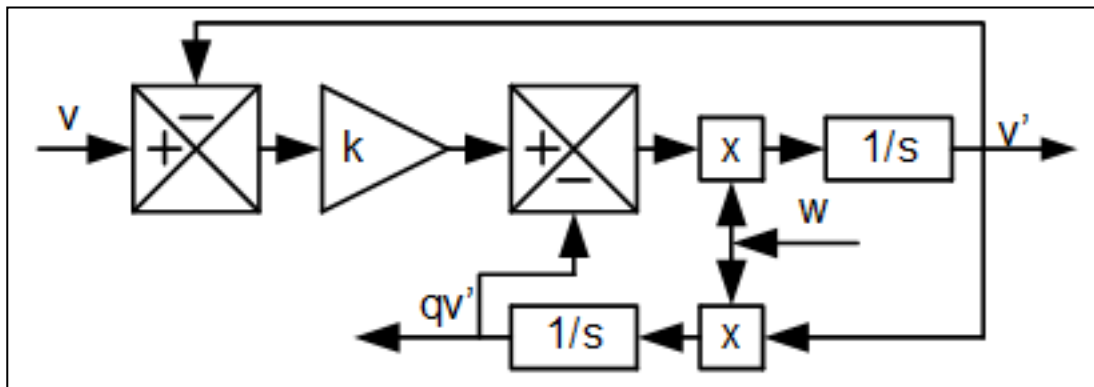


Fig. 33. QSG based on SOGI.

The subsequent comparisons shown in equations (3.7) and (3.8) are used to calculate the α and also β axis voltages for +ve and –ve sequence components:

$$\begin{cases} v_{\alpha+} = \frac{1}{2} * (v'_\alpha - q v'_\beta) \\ v_{\beta+} = \frac{1}{2} * (q v'_\alpha + v'_\beta) \end{cases} \quad (3.7)$$

$$\begin{cases} v_{\alpha-} = \frac{1}{2} * (v'_\alpha - q v'_\beta) \\ v_{\beta-} = \frac{1}{2} * (-q v'_\alpha + v'_\beta) \end{cases} \quad (3.8)$$

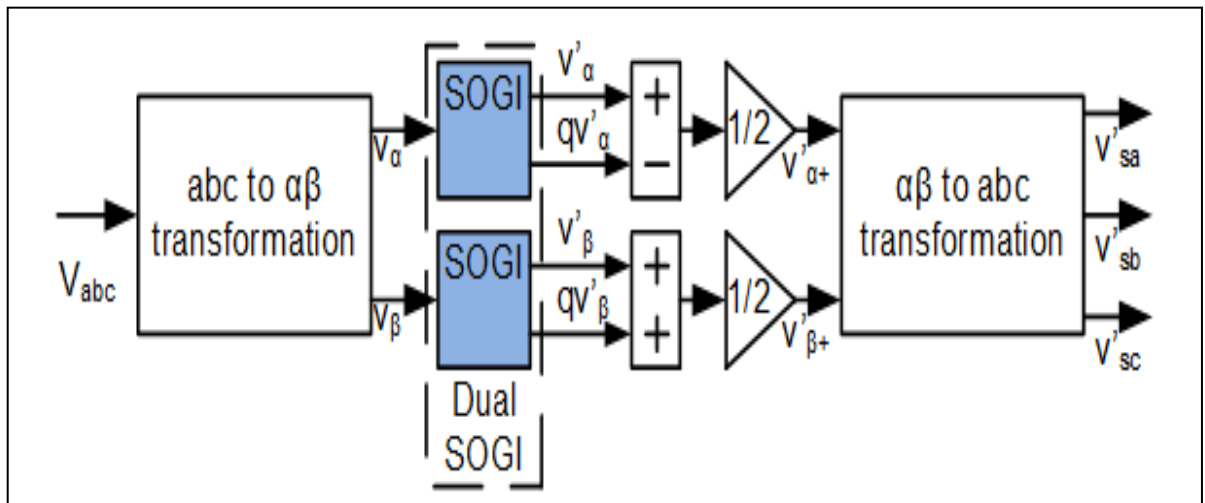


Fig. 34. Basic scheme of suggested Reference Current Generation (RCG) technique (3 – ϕ).

3.5 SAPF Controlling technique in Unity Power Factor Operating Method with the use of DSOGI

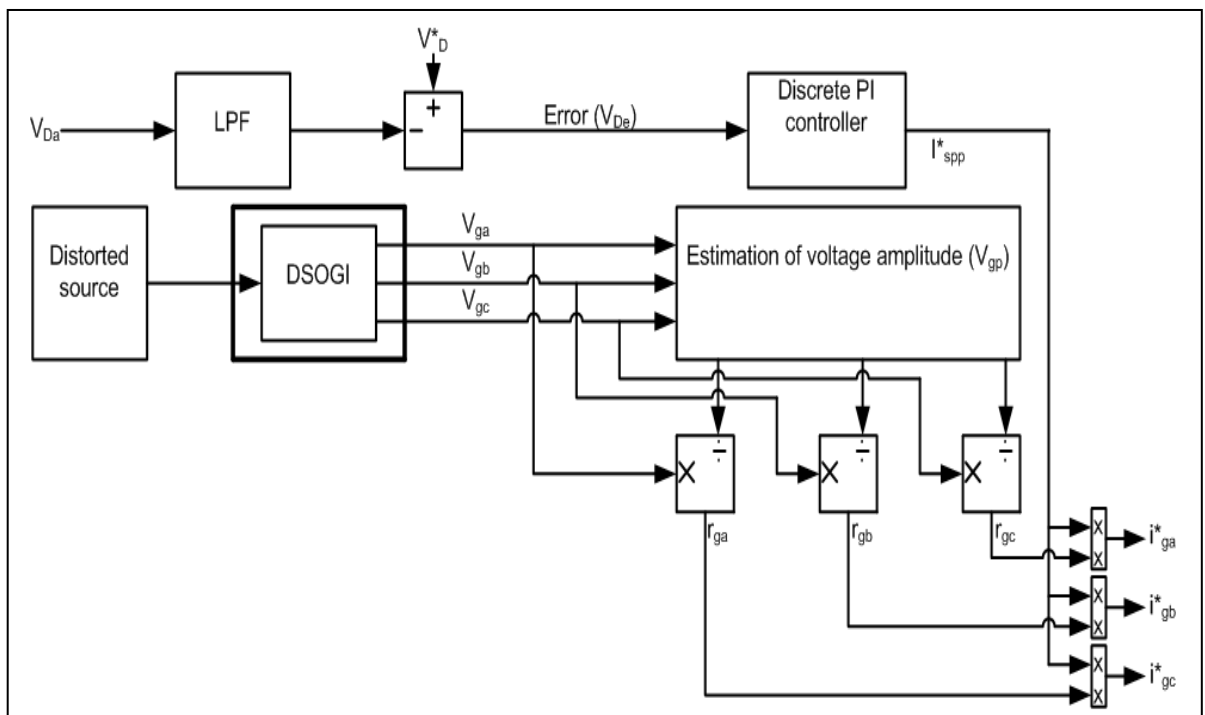


Fig. 35. UT – based control technique of SAPFs (with DSOGI technique).

3.5.1 Voltage and current outputs

Fig. 36 shows the plots of grid voltage $v_{s, abc}$, grid current $i_{s, abc}$, compensator current $i_{c, abc}$, load current $i_{L, abc}$ and DC link voltage V_{DC} with DSOGI technique. By use of DSOGI technique, current and voltage input signals have been made perfectly sinusoidal and hence are no more distorted. The model is tested for the same unbalanced conditions as in chapter 2. It is observed that V_{Da} settles to the 700 V value at 0.59 seconds.

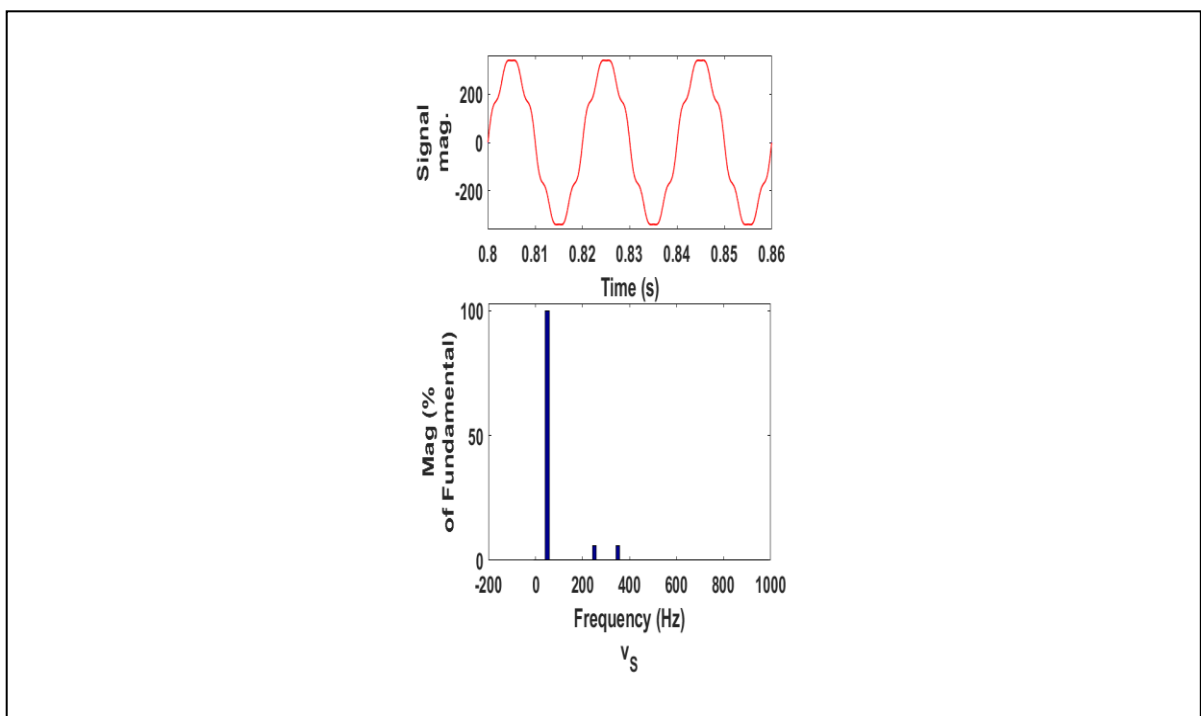


Fig. 36. UT – based control algorithm outcome (with DSOGI technique).

3.5.2 v_s , i_s and i_L THD values

Fig. 37 shows the corresponding THD values for v_s , i_s and i_L . The THD value for i_s now is 2.94 % which meets the IEEE 519 standard. Therefore, it is proved that the proposed DSOGI technique produces the desired results. The considered load, in the model, is reactive – resistive type, which is connected at the end of a diode rectifier block. The unbalance is introduced at 0.47 s by using a circuit breaker in one of the three phases.

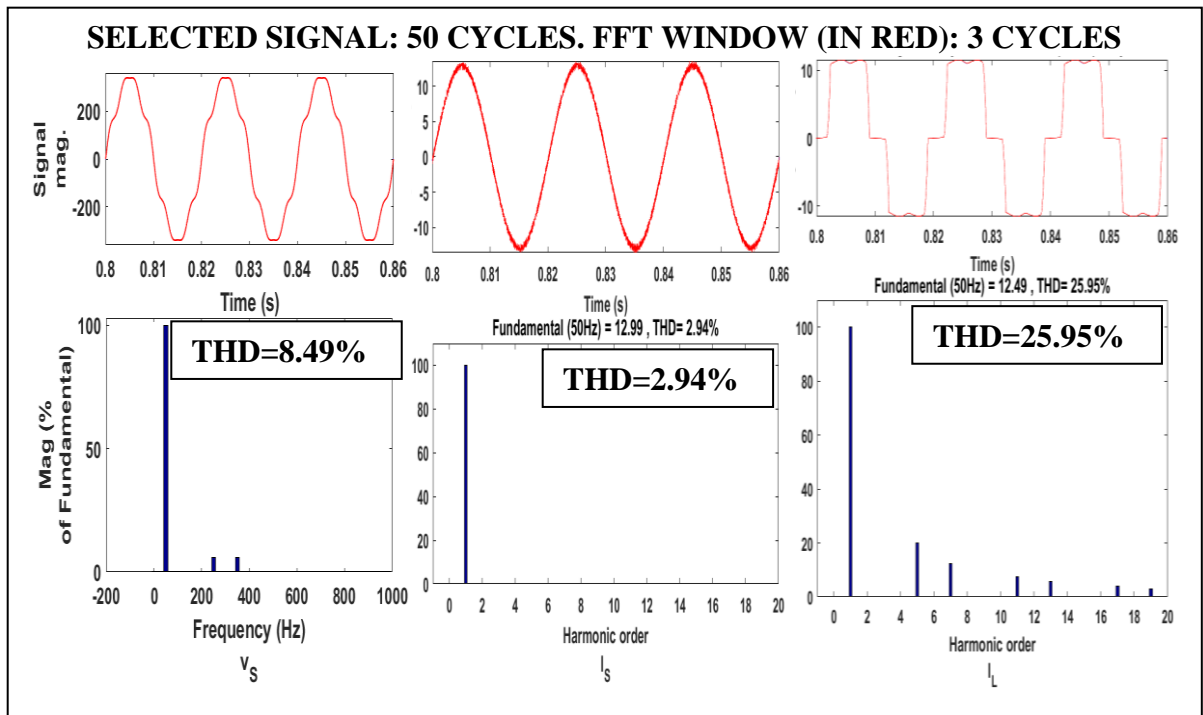


Fig. 37. THD values for UT – based control algorithm (with DSOGI technique).

3.5.3 Quadrature – axis current (i_q) output

Fig. 38 shows the corresponding quadrature – axis current (i_q) output value of the control of SAPF in UPF mode of operation with the use of DSOGI technique.

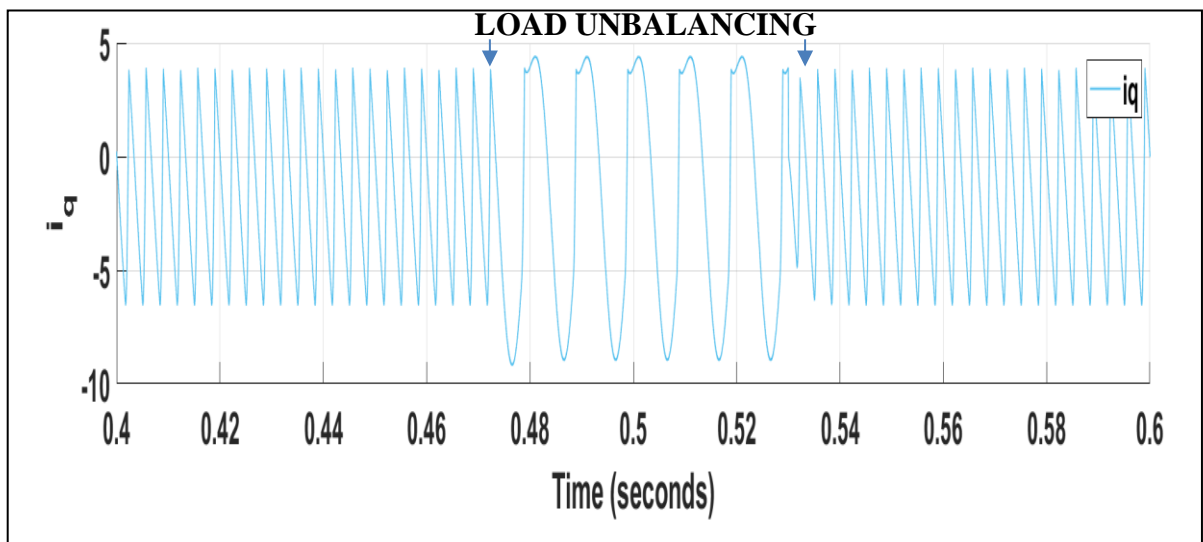


Fig. 38. Quadrature – axis current (i_q) output for the UPF mode of operation with the use of DSOGI technique.

3.6 Synchronous Reference Frame control algorithm of SAPF with the use of DSOGI

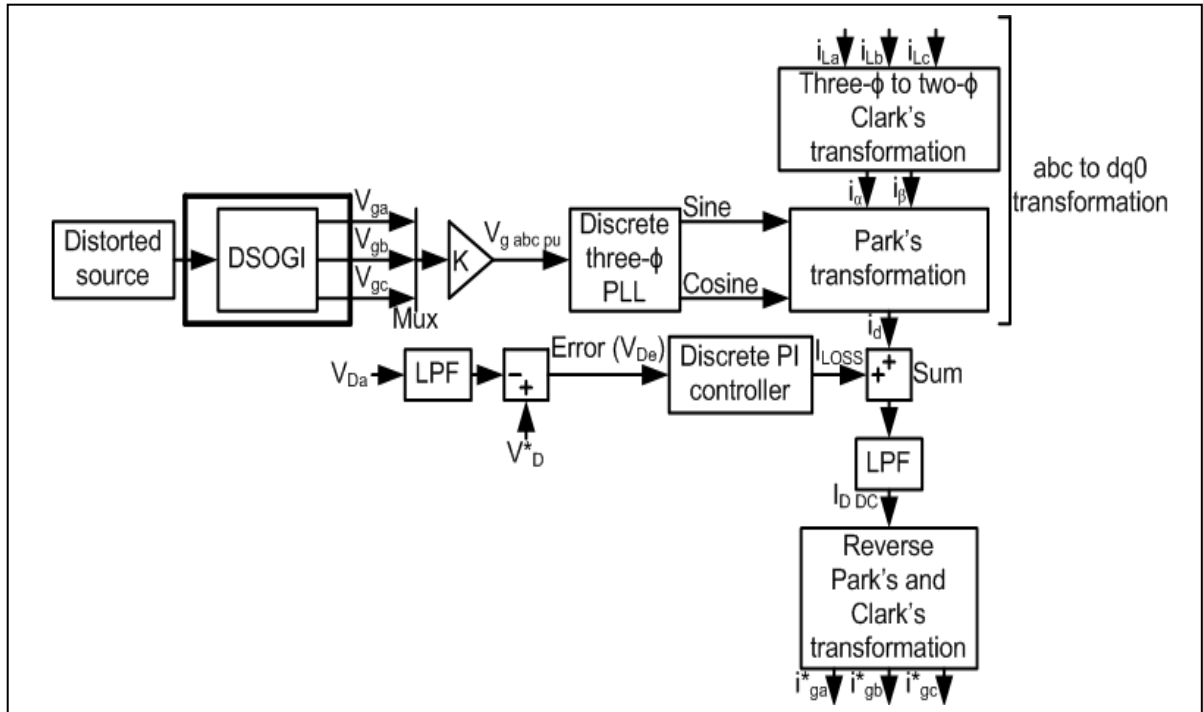


Fig. 39. SRFT – based control algorithm (with DSOGI technique).

3.6.1 Voltage and current outputs

Fig. 40 shows the plots of grid voltage $v_{s, abc}$, grid current $i_{s, abc}$, compensator current $i_{c, abc}$, load current $i_{L, abc}$ and DC link voltage V_{DC} with DSOGI technique. By use of DSOGI technique, current and voltage input signals have been made perfectly sinusoidal and hence are no more distorted. The model is tested for the same unbalanced conditions as in chapter 2. It is observed that V_{Da} settles to the 700 V value at 0.57 seconds.

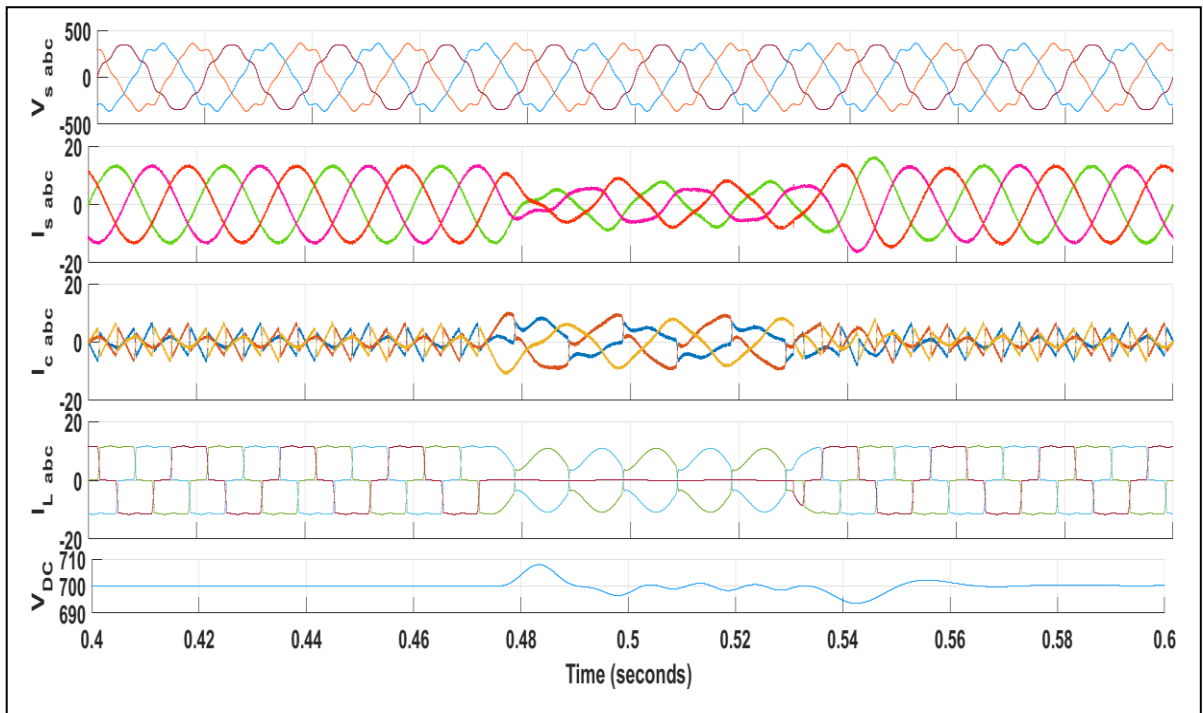


Fig. 40. SRFT – based control algorithm outcome (with DSOGI technique).

3.6.2 v_s , i_g and i_L THD values

Fig. 41 shows the corresponding THD values for v_s , i_g and i_L . The THD value for i_s now is 2.84 % which meets the IEEE 519 standard. Therefore, it is proved that the proposed DSOGI technique produces the desired results. The considered load, in the model, is reactive – resistive type, which is connected at the end of a diode rectifier block. The unbalance is introduced at 0.47 s by using a circuit breaker in one of the three phases.

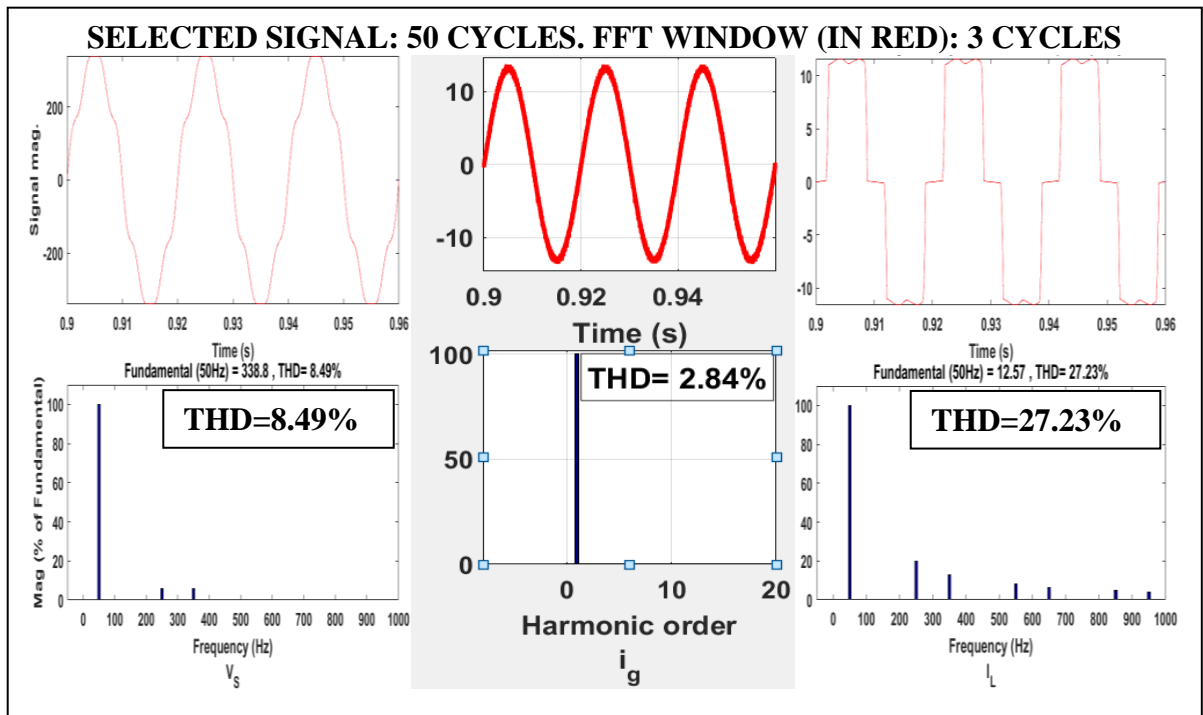


Fig. 41. THD values for SRFT – based control algorithm (with DSOGI technique).

3.6.3 Direct ($i_{d(new)}$) and quadrature – axis current (i_q) outputs

Fig. 42 shows the corresponding direct ($i_{d(new)}$) and quadrature – axis current (i_q) output values of the control of SAPF in SRFT mode of operation with the use of DSOGI technique.

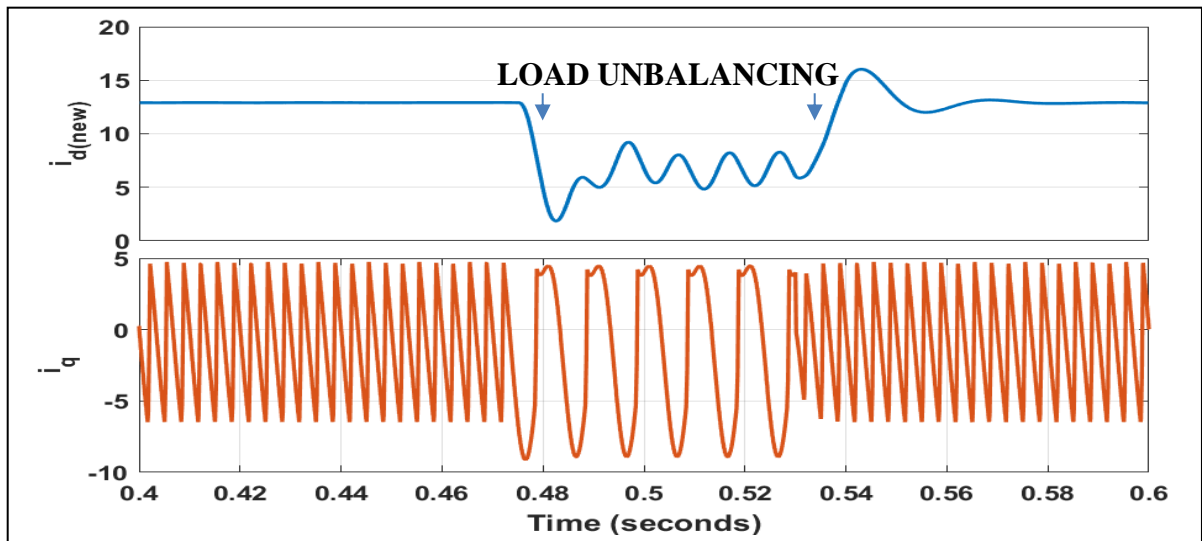


Fig. 42. Direct ($i_{d(new)}$) and quadrature – axis current (i_q) output for the SRFT mode of operation with the use of DSOGI technique.

3.7 Conclusion

Three simple and effective algorithms based on UT based and SRF theory for controlling the SAPF have been studied in this chapter under distorted grid conditions. It was inferred from simulation test results that all of the control schemes used, all of them failed to achieve < 5 percent THD in grid currents; that too even under moderately distorted grid conditions.

A DSOGI block has been used in simulation in order to produce perfect sinusoidal voltage templates from distorted source and filter the distortions. The two approaches used in simulation yielded perfectly sinusoidal grid currents, with a slight modification / change in control algorithms, under adverse grid conditions too. Simulation results show that under unbalanced load conditions and changes in load gave satisfactory results.

TABLE III. COMPARISON OF RESULTING TOTAL HARMONIC DISTORTION (THD) VALUES.

Case			THD %
Algorithm based on Unit template / Proportional – Integral controller	With distorted grid	v_g	8.49
		i_g	8.74
		i_L	25.95
	Using DSOGI technique	v_g	8.49
		i_g	2.94
		i_L	25.95
SRFT based control algorithm	With distorted grid	v_g	8.49
		i_g	19.29
		i_L	27.19
	Using DSOGI technique	v_g	8.49
		i_g	2.84
		i_L	27.23

A comparison of the THD values shows a significant drop in the distortion values of the grid current (i_g) i.e. now within 5% when using DSOGI. It has been observed that without the use of DSOGI block, the two algorithms fail to achieve less than 5 percent THD in grid current values. The reason behind this is simple, it is that since the voltage is itself distorted, reference currents are not perfectly generated. Therefore, it can be said that DSOGI helps to compute the positive sequence component of supply voltages and achieves perfect source synchronization.

CHAPTER 4

A SYNCHRONOUS REFERENCE FRAME BASED PLL CONTROL FOR A GRID – TIED PHOTOVOLTAIC SYSTEM (SINGLE – PHASE)

Some crucial requirements must be met in order to achieve a Photovoltaic system interconnection. One of such vital methods in a PV system that is interconnected is the synchronization of the Grid. When putting together the utility system, Phase Locked Loops are a must, in order to correctly achieve identification of the phase. As we will see below, in this chapter, for the (Grid tied) PV system, a control technique (Phase Locked Loop) with a reference frame (in sync) has been used. Design and analysis of the Phase Locked Loop is so done in order to achieve two goals; first is the introduction of the source with minimum power, moreover to do this in conjunction with correct usage and control of the inverter in dq frame. In order to prove working of a model including Photovoltaic application which is grid tied, component design of such a model has been undertaken using Simulink in MathWorks MATLAB. Moreover, the model design has been properly tested after simulation with the help of MathWorks SIMULINK (simulation software). Consisting of x (variable) number of PV panels and modules, a pv array can be defined as the complete power – generating unit as shown in Fig. 43.

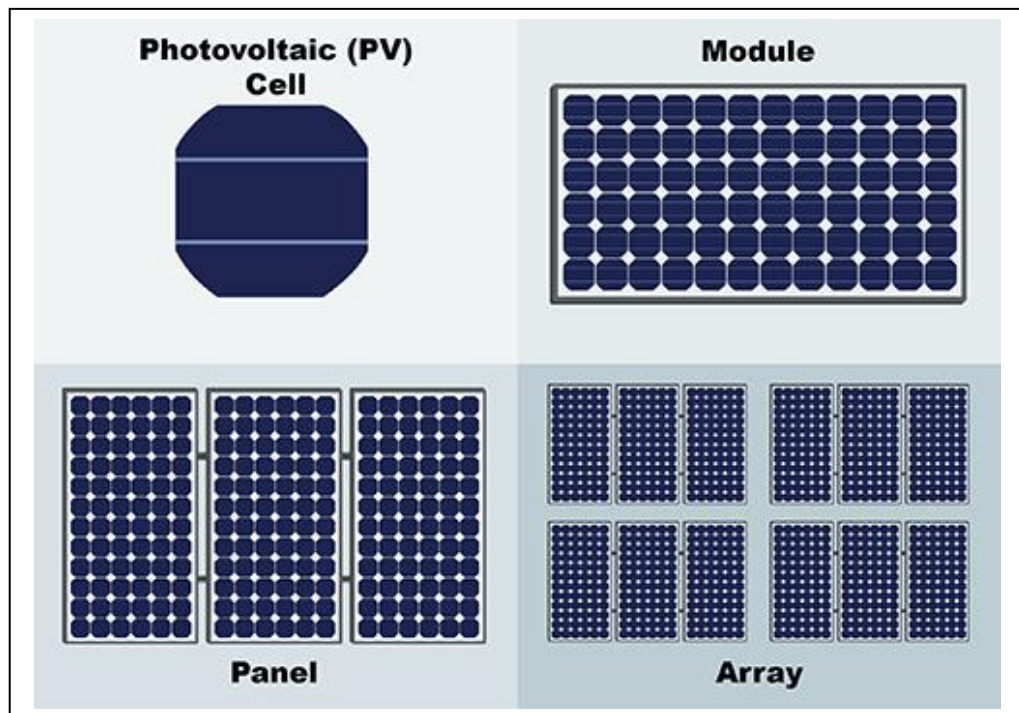


Fig. 43. PV cell, module, panel and array.

Here, in the simulated model, a PV array consisting of 60 panels was used. The 60 Photovoltaic Panels were arranged in 6 rows connected in parallel with each row containing 10 panels connected in series. As a background for testing of the proposed design for the PV array, variations in the values of the local environment of the system have been introduced, in order to provide proof of proper functioning. For ascertaining the right functioning of the Maximum Power Point Tracker (MPPT), the output from the Photovoltaic panels has been recorded. In order to prove the correct functioning of the synchronized PV array employed in a single – phase grid model, several evaluators and markers of the performance of the proposed design have been provided by the end of this dissertation report. The plots of the single – phase inverter output voltage, plots of values of the ac currents introduced in the model, analysis of the system based on THD values and more such results have been included at the end of this thesis report.

4.1 Introduction

The world is seeing a radical and revolutionary rise in the demand as well as usability of solar power generated using Photovoltaic panels. Without any need for the

requirement of pre – power generation infrastructure, solar power generated with the help of PV panels, does not present any hazards / dangers in disposal and processing of the required equipment. In addition to this, solar power generated with the help of PV panels can be made readily available to large parts of the population around the world. Moreover, solar power generated with the help of PV panels does not harbor any worries for having an ecological footprint, it is because it is simply energy irradiated from the Sun. There is, therefore, no wonder that PV energy from the sun can generate power in orders of magnitudes way more than other traditional sources of power, especially, conventional fossil fuels. Until now, prevalence of the usage of PV energy majorly tended to stay off – the – grid of a country’s core power network and was comparatively small scale. It was being confined to small scale applications for example those on the terrace of buildings. Today, there has been an increase in worldwide demands and interests in order to advance power generation through solar energy. Moreover, there has been a relatively higher prevalence of large – scale PV systems manufacturing. It is because of this that the scenario is that cost / investments required per panel / for each unit have gone dramatically spiraling downwards which has increased the usage of PV power generated systems in the major grid networks. [55]

The model of the Photovoltaic system infused with the grid is shown in Fig. 44, where a parallel connection between the utility main grid and Photovoltaic panels have been made. The necessary job of proper stabilization of the power is done by the inverter, which acts as a PCU (Power Conditioning Unit). The PCU converts the output of the PV module array into a suitable grade of ac power source, under normal conditions. If a fault occurs in any one of the two systems; PV system / utility grid, the PV array system dislodges itself from the supply.

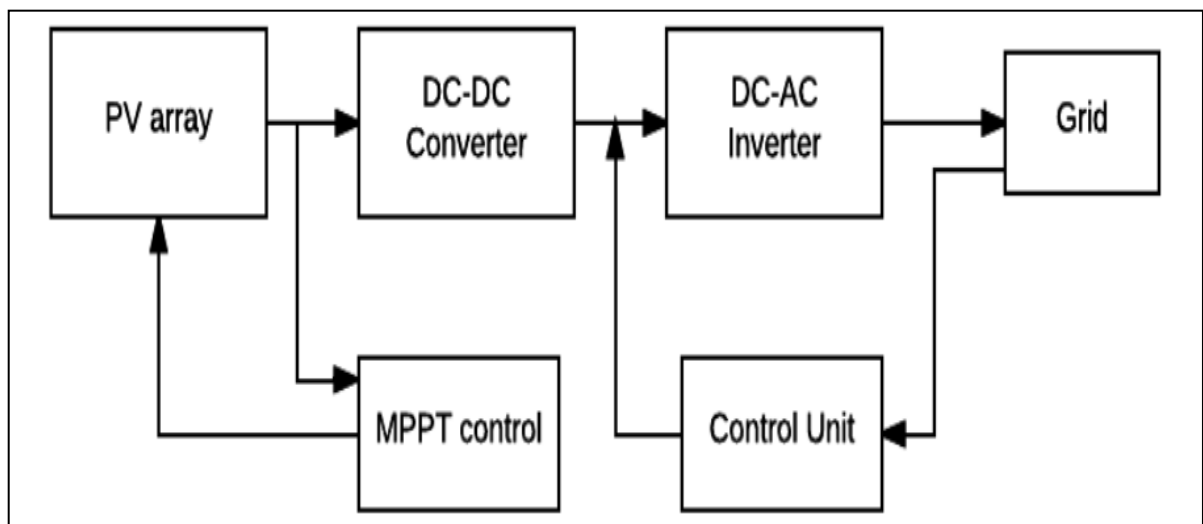


Fig. 44. Layout of grid connected PV system.

The common interface between the main utility grid and PV array subsystem works bilaterally, thanks to the power distribution panel. As a result, power can be delivered to the loads connected to the system network by using both the PV array subsystem and also, the main utility grid. Therefore, depending upon the requirement of the load at the time, relative to the production of PV array power, the load would be supplied power from the utility grid when in case of shortage in the power supplied by PV array system, and on the other hand, the utility grid will receive power from the PV array system in case PV array system produces a sufficient amount of power.

A number of publications have been published on the topic PV array systems connected to the main utility grid. One such example of a publication on the topic array of PV Panels has been presented in [56]. An MPPT based on gradient and an interface for the PE devices has been presented in this publication.

It is clear that irrespective of the configuration of a grid – tied PV system there are some vital requirements for its successful grid integration. Out of them, grid synchronization is very important. A PLL system can be used for this purpose. Therefore, this chapter presents an SRF based PLL control for a grid – tied PV system.

4.2 Grid tied Photovoltaic system

In Fig. 45, a general model for a Photovoltaic system in connection with the grid has been displayed. This model consists of a DC – DC boost converter, synchronization of three – phase de – coupling transformer, a capacitor at the input, an inverter for driving the system along with a PV panel array with a MPPT controller. In addition to the components mentioned, a capacitor at the DC – link, an inductor that acts as a filter and voltage at main Grid are also present. In order to meet the required ratings for power generation and voltage (at the input), the PV cell modules are connected in series – parallel grid. The DC – DC boost converter is responsible for enabling the MPPT mode. The capacitor connected at the DC – link helps for the DC – link voltage mode. The PV voltage value at the MPPT mode is enabled by the capacitor connected at the input. The inductor alters the output voltage value coming out of the DC – DC boost converter because the UPF must be present between the voltage and current values at the main grid. The significance / use of the MPPT controller is that it detects the point of maximum power generation from the PV panel array current and voltage values, which further provides a voltage reference value.

4.2.1 PV array

Photovoltaic modules contain a singular diode. Despite the presence of multiple diode systems (2, 3, etc.), the 1 diode model provides a simpler and more accurate result. [56]

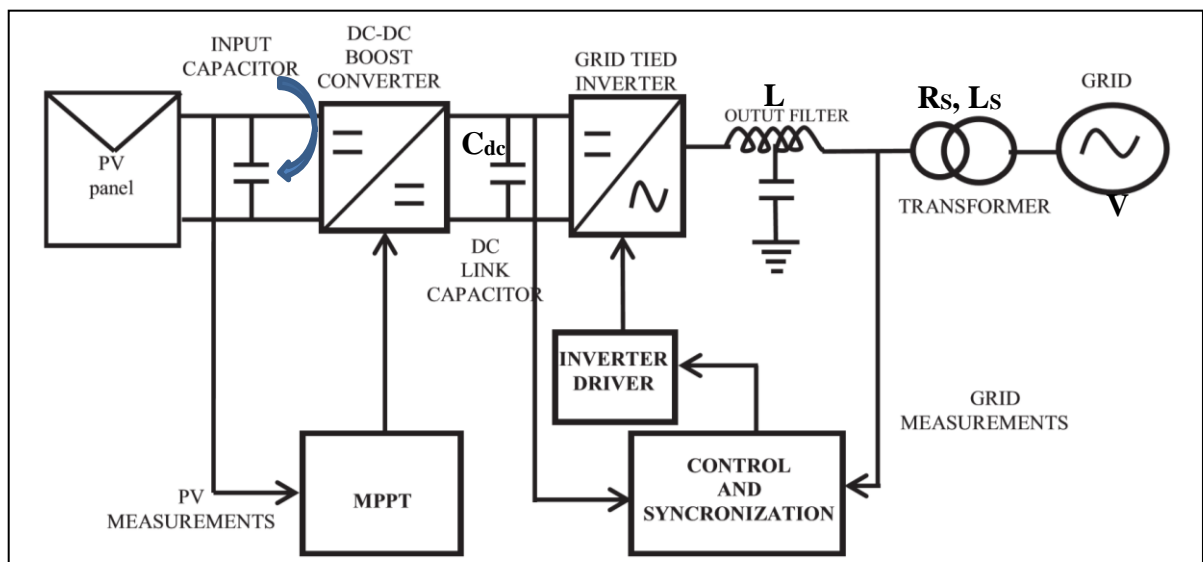


Fig. 45. Grid connected Photovoltaic system layout.

A photovoltaic panel module has several preset variables: I_{ph} , I_o , R_s and R_{sh} which denote clean current source, diode current, resistances; series and shunt. The equation below shows the current – voltage characteristics of a Photovoltaic module with 5 parameters and 1 diode:

$$I = I_{ph} - I_o \left[\exp \left(\frac{V + I R_s}{n_s V_t} \right) - 1 \right] - \frac{V + I R_s}{R_{sh}} \quad (4.1)$$

where I_{ph} and I_o are currents produced by the incident light and dark – saturation current accordingly.

4.2.2 Maximum Power Point Tracker

A Photovoltaic model commonly returns max. power when the point of operation aligns at Maximum Power Point. A tracker is required in order to obtain maximum power value. An algorithm recognizes the point of operation at the Maximum Power Point; Fig. 46 (a). This is the result of the MPPT. Further, the PCU, that is DC – DC boost converter is responsible for aligning the point of operation returned by the MPPT algorithm with that which is the actual point of operation. The MPPT technique used in the model here is known as Perturbation & Observation (P & O) technique. It is a famous operation point tracker which is because of its ease of implementation and simple nature. At each of the sampling times, in this technique, the algorithm evaluates the PV array power sample and the

corresponding change that is dP/dV is then derived. At each periodic perturbation of PV voltage value, the MPPT operates. The P and O MPPT algorithm has been explained by a flow – chart in Fig. 46 (b).

4.2.3 Modeling of Three Phase Grid – Tied PV System

By applying KCL to the DC link capacitor node, the following state – space equation for capacitor voltage is obtained

$$v_{pv} = \frac{1}{C} (i_{pv} - i_{dc}) \quad (4.2)$$

In the inverter, the output current is equal to the injected current when conduction losses as well as the switching losses of the inverter are assumed to be almost nil.

It can be considered to be a system that is non – linear as well as dependent on time because of its varying gate signal and current signal. A few useful strategies and modifications that can be used to ease the control process of this non – linear time varying system have been discussed in the section to come.

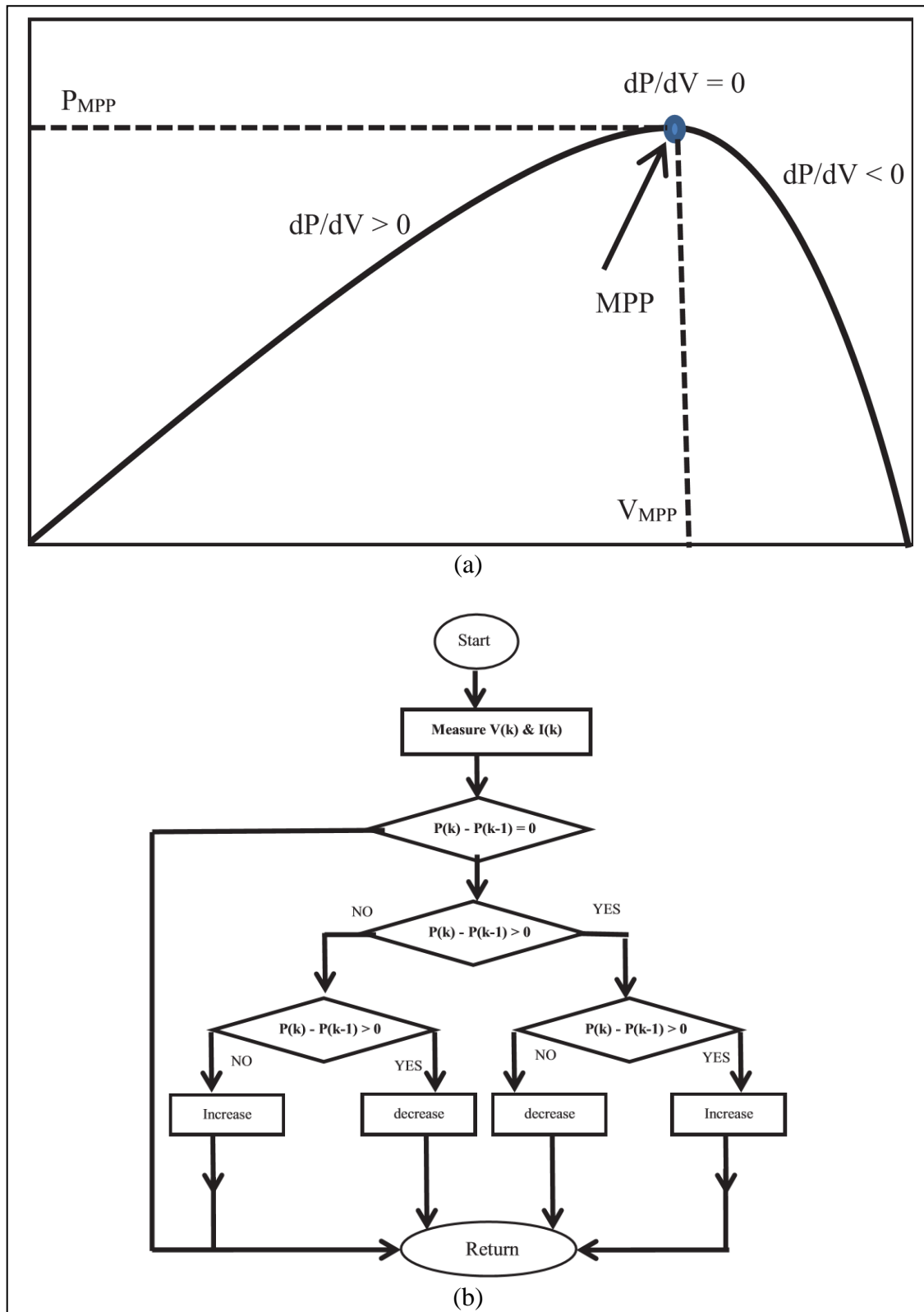


Fig. 46. (a) Power Voltage plot of Photovoltaic array and (b) Flowchart for Maximum Power Point Tracker technique based on Perturb and Observe algorithm.

4.2.4 Phase Locked Loop grid synchronization algorithm

The current at the supply terminal and from Photovoltaic unit should be in full synchronization with each other. Therefore, PLL which is a grid synchronization technique is hence necessarily required. A reference phase value of the source voltage is mainly produced in this algorithm. This reference phase value is put to use as it is required to be synchronized when $ABC \rightarrow dq$ (*Park transformation*) transformation steps take place. Phase Detector (with input signal V_i), Loop Filter (with input signal V_e) and VCO (with input signal V_{CO}) are the components of Phase Locked Loop. A representation in the form of block diagram has been shown in Fig. 47. Table IV explains significance of above mentioned 3 components and the input and output signal denotations in tabular form.

Table IV. Functions of PLL components

Serial number	Component	Function	Input signal	Output signal
1.	Phase Detector	Compares the reference or input signal with the output signal	V_i	V_e
2.	Loop Filter	Gets rid of harmonic components in the phase detector output that are not required	V_e	V_{CO}
3.	VCO	Generates an output signal that has a frequency which oscillates around a main frequency liable to the loop filter	V_{CO}	V_o

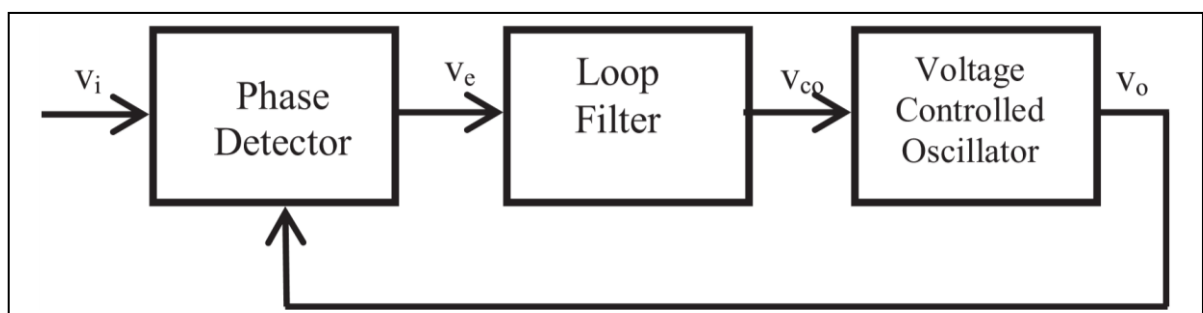


Fig. 47. Basic block diagram for a Phase Locked Loop technique.

4.3 Employing of Synchronous Reference Frame PLL Algorithm

$ABC \rightarrow dq$ reference frame transformation step is used in Synchronous Reference Frame algorithm. This transformation is employed to change the control variables to their corresponding dc signals. DC signals are thus easier to be filtered and controlled. A layout of the dq – controlled reference frame transformation technique is shown in Fig. 54. In order to control the dc bus voltage, the active power (denoted by P) output is brought to use here. For the current controller, in case of constant value of reactive power (denoted by Q), the above – mentioned active power (P) is taken to be used for the current controller and also the reactive current is assumed to be zero. Otherwise, if it becomes necessary to control the reactive power (Q) then a reactive power (Q) reference value should be added to the SRFT – PLL controller.

In this section of the chapter, a control algorithm based on *direct quadrature (dq) method* designed with the help of a controller which is based on PI mode is implemented. Matrix equation (4.3) demonstrates the basic structure of a controller (Proportional Integral type) with *direct quadrature* co – ordinates as follows:

$$G_{PI}^{(dq)}(s) = \begin{bmatrix} K_P + \frac{K_I}{s} & 0 \\ 0 & K_P + \frac{K_I}{s} \end{bmatrix} \quad (4.3)$$

Here, the integral and proportional gains of the PI controller are denoted as K_I & K_P respectively. The current that is controlled has to be in phase with voltage at the source is a mandatory condition that has to be fulfilled. But, even before that, it is a compulsory pre – requisite that unwanted harmonic signals should be filtered from voltages at the source.

The attainable maximum value of input power (P_{in}) has to be injected into the dc bus. Now, this required maximum value of P_{in} is extracted by using the MPPT and employing DC – DC type converter. Design of the CS of the inverter has to be such that voltage at the dc bus should be maintained constant by P_{out} during all conditions. Equation (4.4) demonstrates the function of the controller (Proportional Integral type). Error difference between the output power from the capacitor and peak PhotoVoltaic array power is used to estimate the $I_{d,ref}$ value as shown below:

$$I_{d,ref} = \frac{1}{V_d} (K_P (P_{in} - P_{out}) + K_I \int (P_{in} - P_{out}) dt) \quad (4.4)$$

Here, voltage at PCC is denoted as V_d . Now, $V_{q,ref}$ and $V_{d,ref}$ are further calculated (as shown in equations (4.5)) using the value of the reference current obtained from equation (4.4). Equation (4.5) output is then fed to a generator (pulse width modulation type) which generates gate pulses that are injected in the inverter.

$$V_{d,ref} = K_P (I_{d,ref} - I_d) + K_I \int (I_{d,ref} - I_d) dt - w L I_q + V_d \quad (4.5)$$

$$V_{q,ref} = K_P (I_{q,ref} - I_q) + K_I \int (I_{q,ref} - I_q) dt - w L I_d + V_q$$

These dq components of voltage are then reverse transformed to the ABC frame signals. Modulating signals are required by the PWM generators. For this purpose, a voltage signal at the dc bus is used. In addition to this, a filter, which is built using an inductor, is used to make the error in each *direct quadrature (dq) signal* equal to nil. The results obtained in this chapter have been shown below in the next section that is Section 4.4.

4.4 Results and Discussions

In this work, BP – MSX120 PV panel is taken into consideration. Table IV shows the Information about the studied PV system. Fig. 45 shows the studied 3 – ϕ grid connected PV system. This system has a generating station. A SRF PI controller with SPWM generator model is designed to provide gate signals to the inverter.

Table V. System Specification of The GRID – Tied PV System

<i>Parameters</i>	<i>Values</i>	<i>Parameters</i>	<i>Values</i>
I_{sc}	1.44 A	K_I	1.33×10^{-3}
V_{oc}	3.75 V		

The code of the studied PV array is constructed in MATLAB / SIMULINK domain as given:

function I = I_{pv} (V, G, T)

% I – Output current (Ampere (s))

% V – Output voltage (Volt (s))

% G – Operating solar irradiation (KW (s) m⁻²)

% T – Operating temperature (C)

% k – Boltzmann's constant (J (s)/ K or m (s)² kg (s) s⁻² K⁻¹)

% q – Electron charge (Coulomb (s))

% n – Ideal factor dependent of the PV characteristics

% k_i – Short – circuit current temperature coefficient (A (s) / K)

% E_g – Band gap energy of semiconductor used in a cell (eV (s))

% N_S – Number of cell (s) in series

% N_P - Number of cell (s) in parallel

% T_r – Reference temperature at STC (K)

% V_{OC} – Open circuit voltage (Volt (s))

% I_{ph} – Photo current (Ampere (s))

% I_{SC} – Short circuit current (Ampere (s))

% I_S – Cell saturation current (Ampere (s))

% I_r – Cell reverse saturation current (Ampere (s))

% R_S – Series Resistance (Ohm (s))

% R_{sh} – Shunt Resistance (Ohm (s)),

k = 1.3806488 e⁻²³;

q = 1.6021766 e⁻¹⁹;

n = 1.3; % 1.3 for poly crystalline solar cell (1 < n < 2)

k_i = 1.33 e⁻³; % 0.065 A (s) / C

E_g = 1.12; % Si – 1.12, GaAs – 1.42

N_S = 10;

N_P = 6;

T_r = 273.15 + 25; % 25 ° C 0 ° C = 273.15 K

V_{OC} = 37.51 / N_S;

I_{SC} = 8.63 / N_P;

T_k = 273.15 + T;

V_C = V / N_S;

V_t = (n * k * T_r) / q;

V_{ta} = (n * k * T_k) / q;

b = (E_g * q) / (n * k);


```

% Photo current at operating temperature
Iss = Isc * (1 + (ki * (Tk - Tr)));
% Photo current at operating irradiation
Iph = G * Iss;

% Total calculation
Ir = Isc / (exp (Voc / Vt) - 1);
Is = Ir * (Tk / Tr) ^ (3 / n) * exp (b * (1 / Tr - 1 / Tk));

% Calculation for Rs using slope of I - V curve
dV dI = - 2.0 / Ns; % Take dV / dI at Voc from I - V curve of datasheet
Xv = Ir / Vt * exp (Voc / Vt);
Rs = - dV dI - 1 / Xv;

% I = Iph - Is * (exp ((Vc + I * Rs) / Vta) - 1)
% f (I) = Iph - I - Is * (exp ((Vc + I * Rs) / Vta) - 1) = 0
% Solve for I by Newton's method: Ia2 = Ia1 - f (Ia1) / f' (Ia1)
% Initialize I with zeros
I = zeros (size (Vc));
for j = 1:5;
    I = I - (Iph - I - Is .* (exp ((Vc + I .* Rs) ./ Vta) - 1)) ...
        ./ (- 1 - Is * (Rs ./ Vta) .* exp ((Vc + I .* Rs) ./ Vta));
end
I = I * Np;
end

```

The Power – Voltage and Current – Voltage curves plotted for various solar – irradiance values are in Fig. 48 (a) and (b). Ascertaining from these plots, it is evident that the two plots, intersect three crucial vertices; “open circuit”, “short circuit” point and the MPP. The single – phase o/p voltage as well as current plots have been shown in Fig. 48.

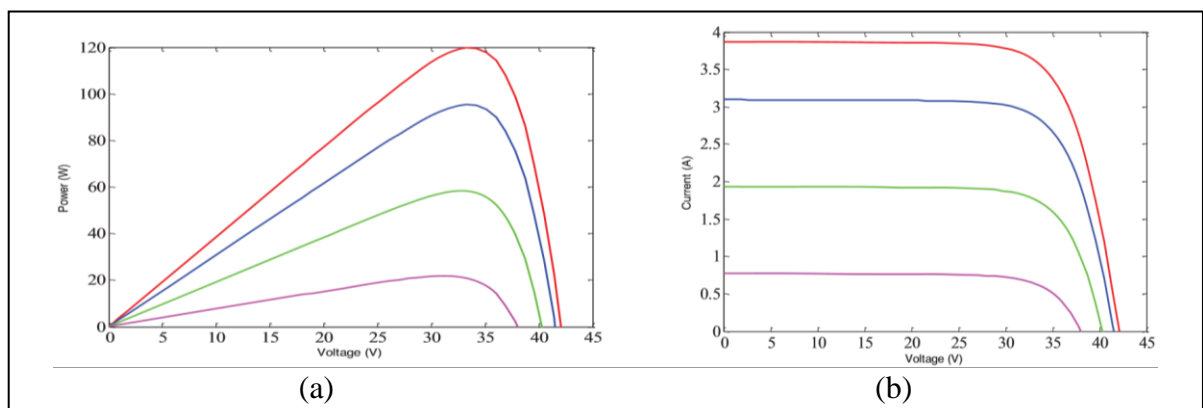


Fig. 48. (a) Power – Voltage Characteristics and (b) Current – Voltage characteristics of each Photovoltaic cell of the concerned Photovoltaic array at various values of solar irradiance.

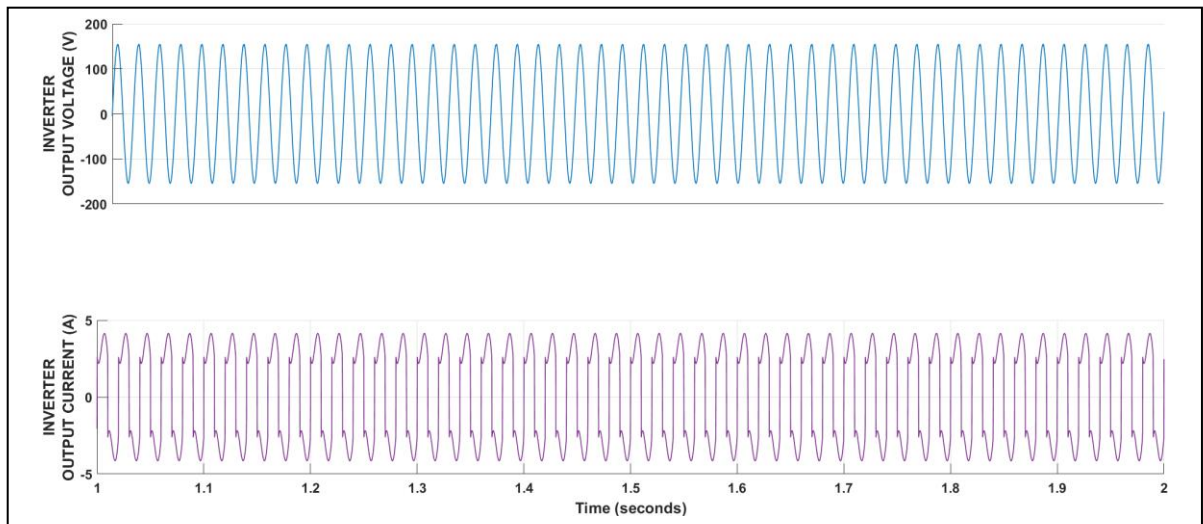


Fig. 49. Voltage and current waveforms at inverter output.

Output current signal of the inverter has a sinusoidal waveform. Moreover, the filter, which has inductance present in it, is employed to suppress THD value. Fast Fourier Transform analysis provides proof for the same, shown in Fig. 51. Ascertaining through these figures, it is evident that the THD for the inverter voltage was 0.00 %. Hence, the value of THD was brought below the five percent IEEE standard limit.

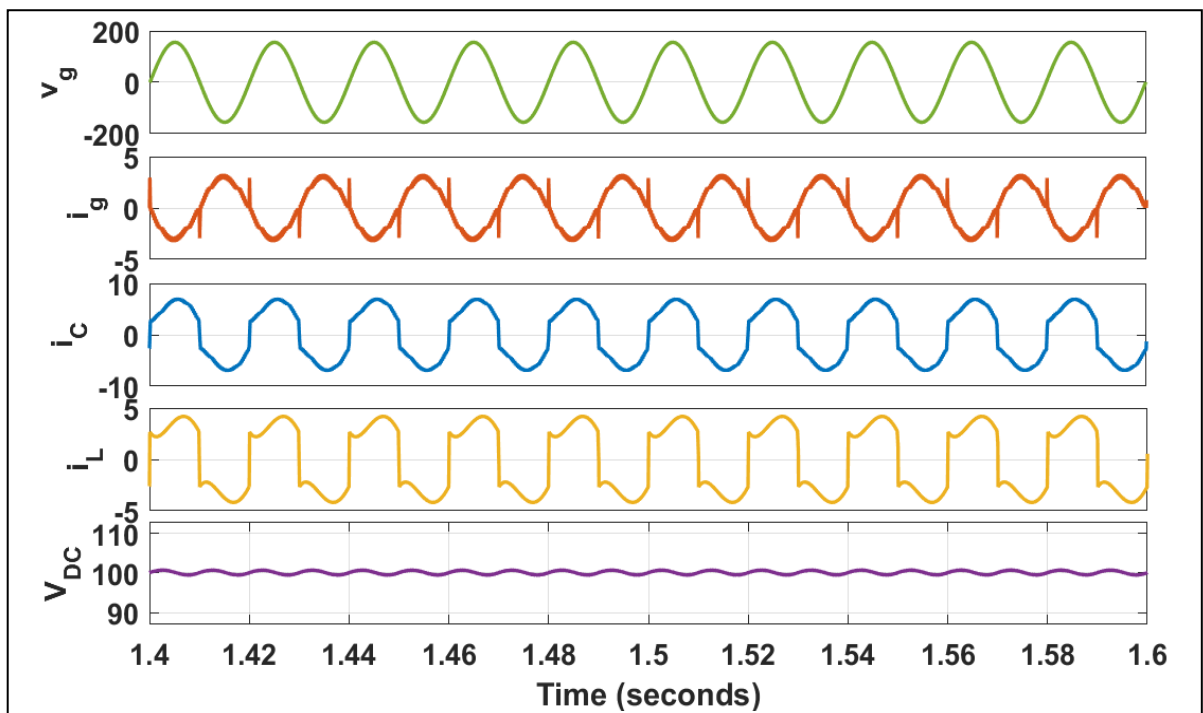


Fig. 50. Voltage and current waveforms at grid, converter current, load current and dc voltage.

The Photo – Voltaic system under consideration contains a capacitor at the DC Link (Fig. 52). Over here, the output voltage of the dc – dc converter is made constant value

using the capacitor, it also has another significance wherein it also provides isolation between the dc – dc boost – converter output port and the inverter input terminal.

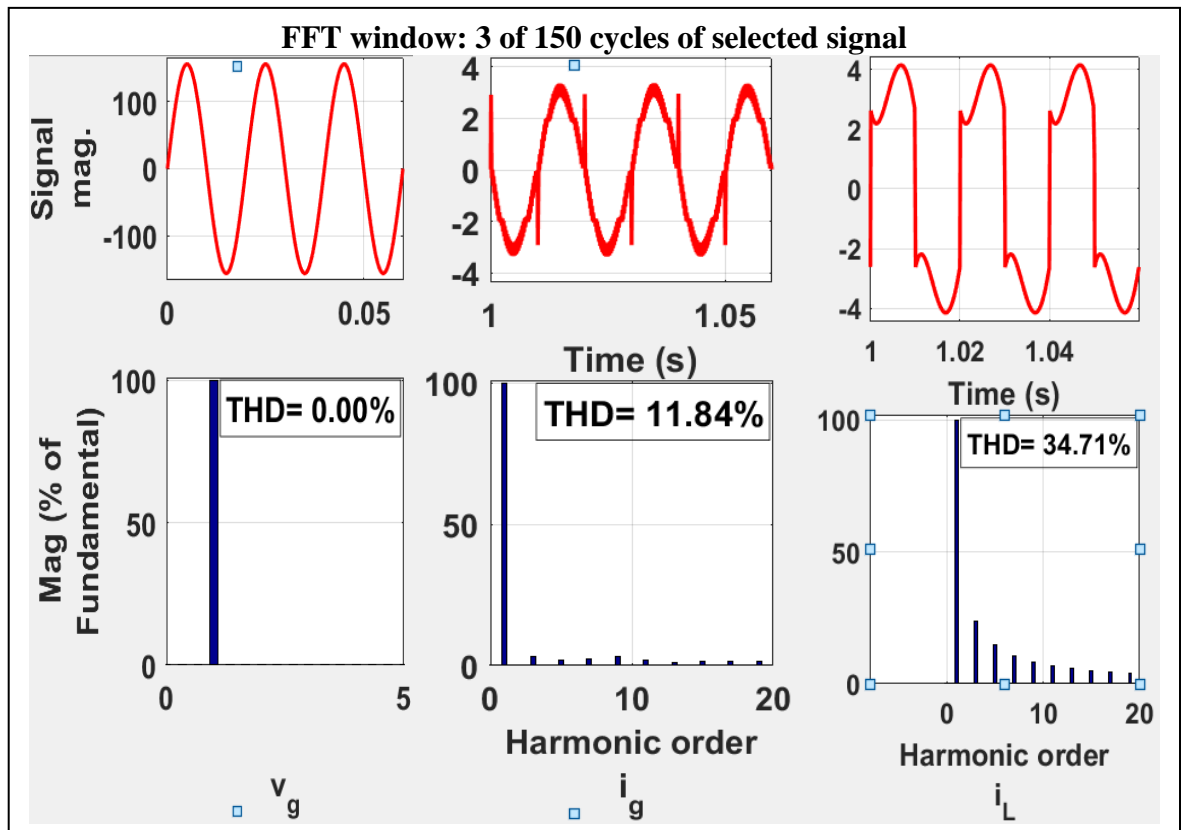


Fig. 51. Total Harmonic Distortion at o/p grid current and voltage and load current using FFT.

This system provides the active power (P) required in case when there is an abrupt change in the load, moreover, delivering the required active power in case of losses in the inverter due to switching. In order to obtain the correct conversion (DC to AC), the voltage across the capacitor must remain a constant value, which is demonstrated in Fig. 53.

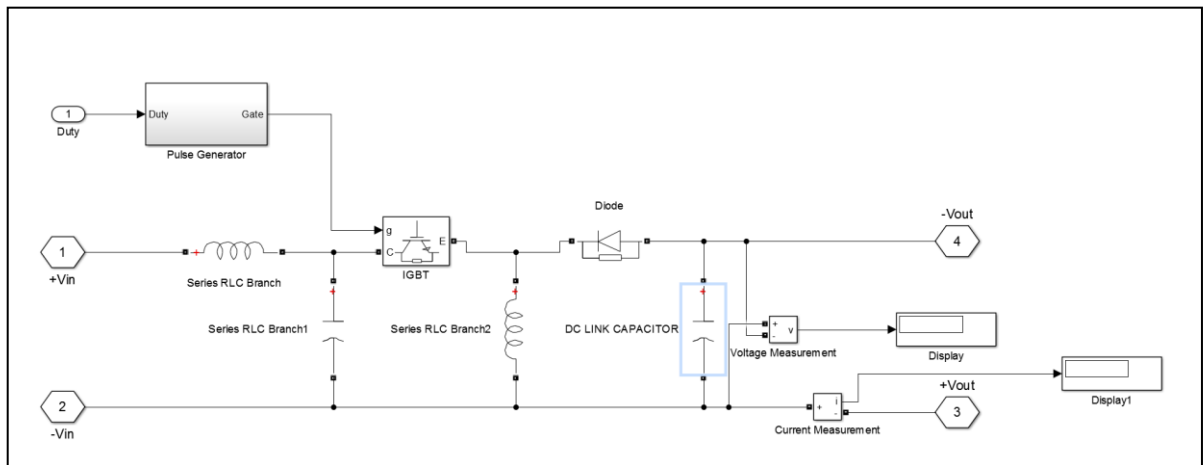


Fig. 52. Capacitor at DC – link.

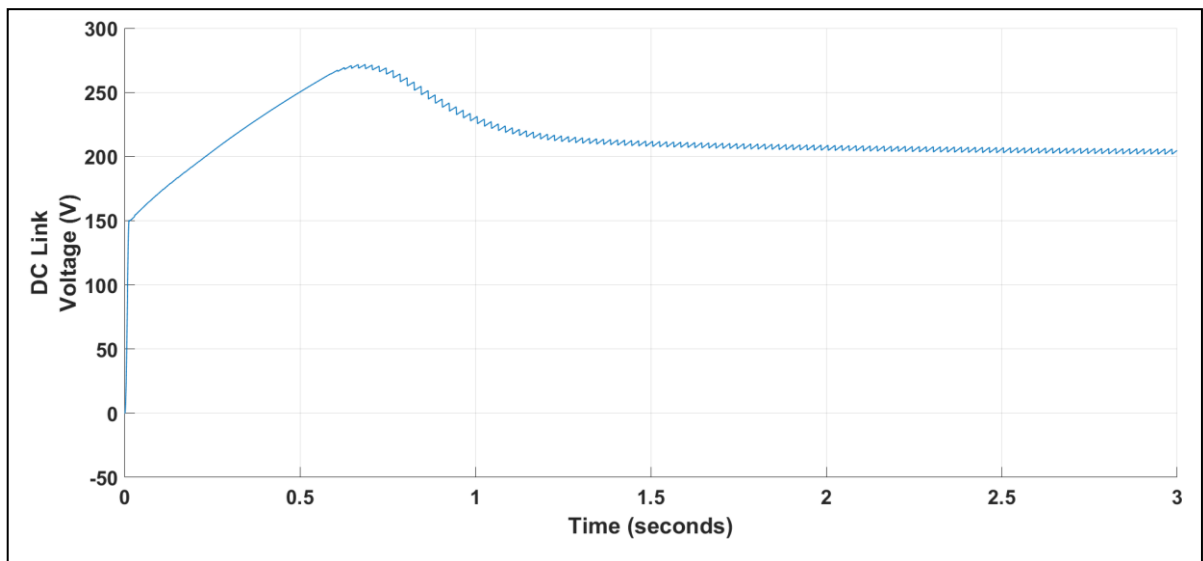


Fig. 53. Voltage across capacitor at DC – link.

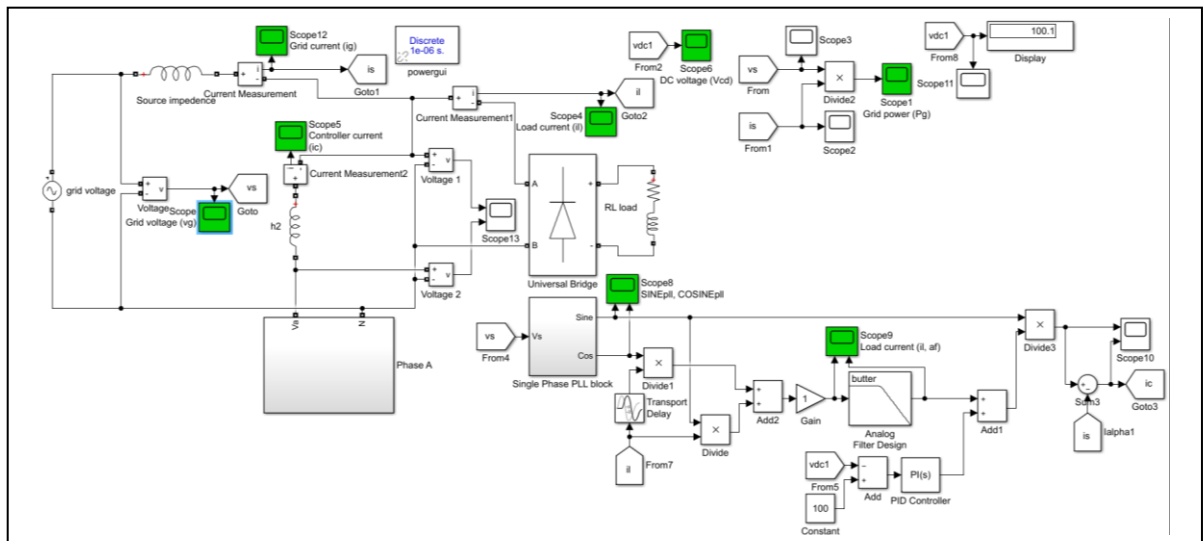


Fig. 54. SRF based closed loop model with PV.

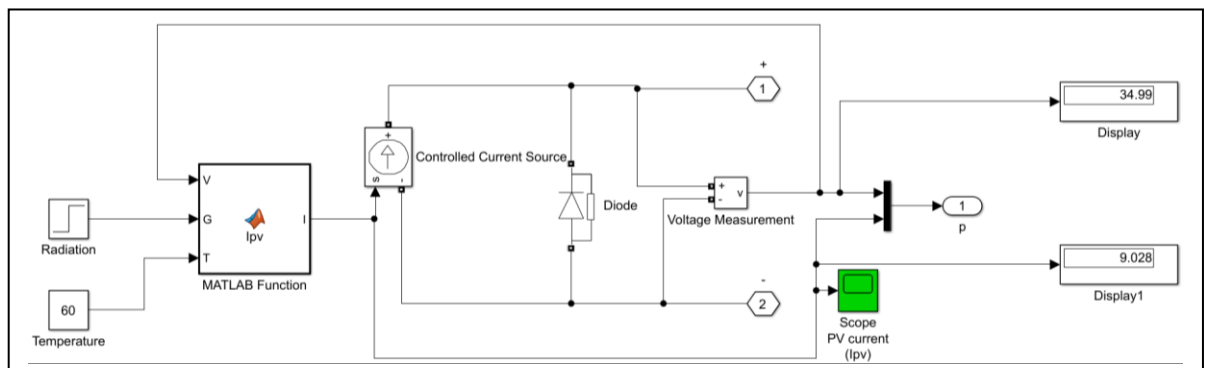


Fig. 55. PV current generation.

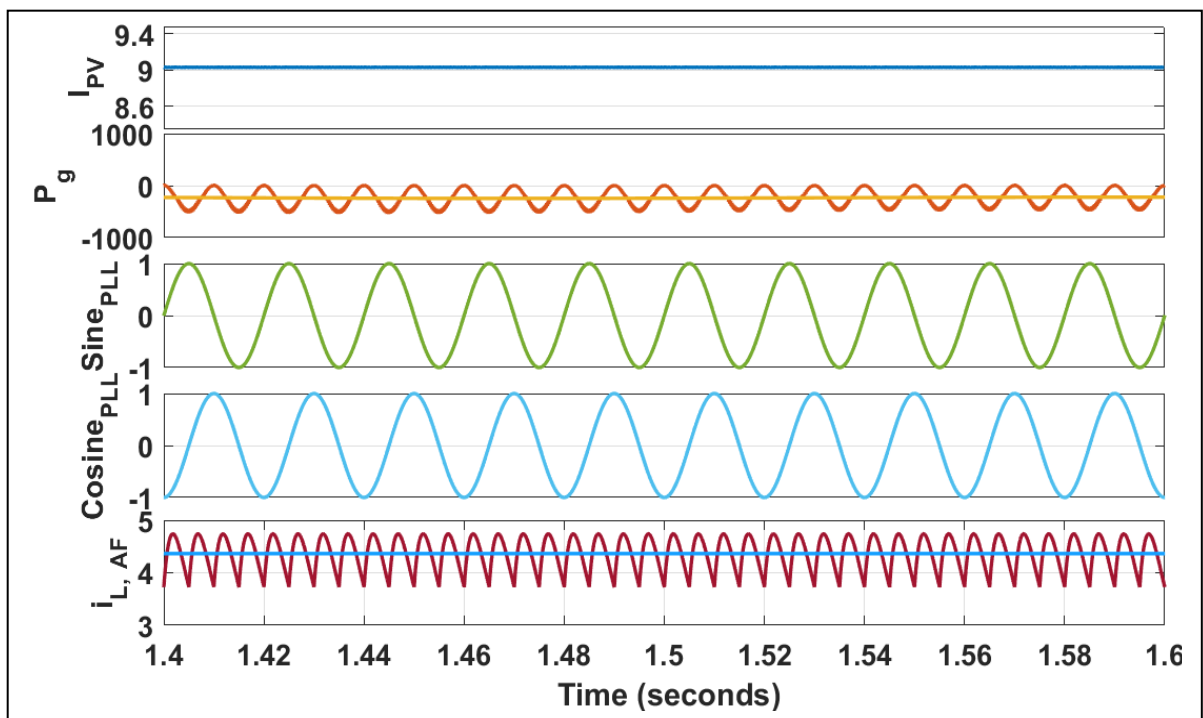


Fig. 56. PV current, grid power signals, PLL outputs and analog filter signals.

Simulation model is shown in fig.s 52, 54 and 55 with scope blocks marked in green background color which are used to gather results. In simulation, PV array provides a pv current (I_{PV}) equal to 9.028 A as shown in Fig. 56. Generated grid power (P_g) is around 250 W which is depicted by filtered value in yellow color.

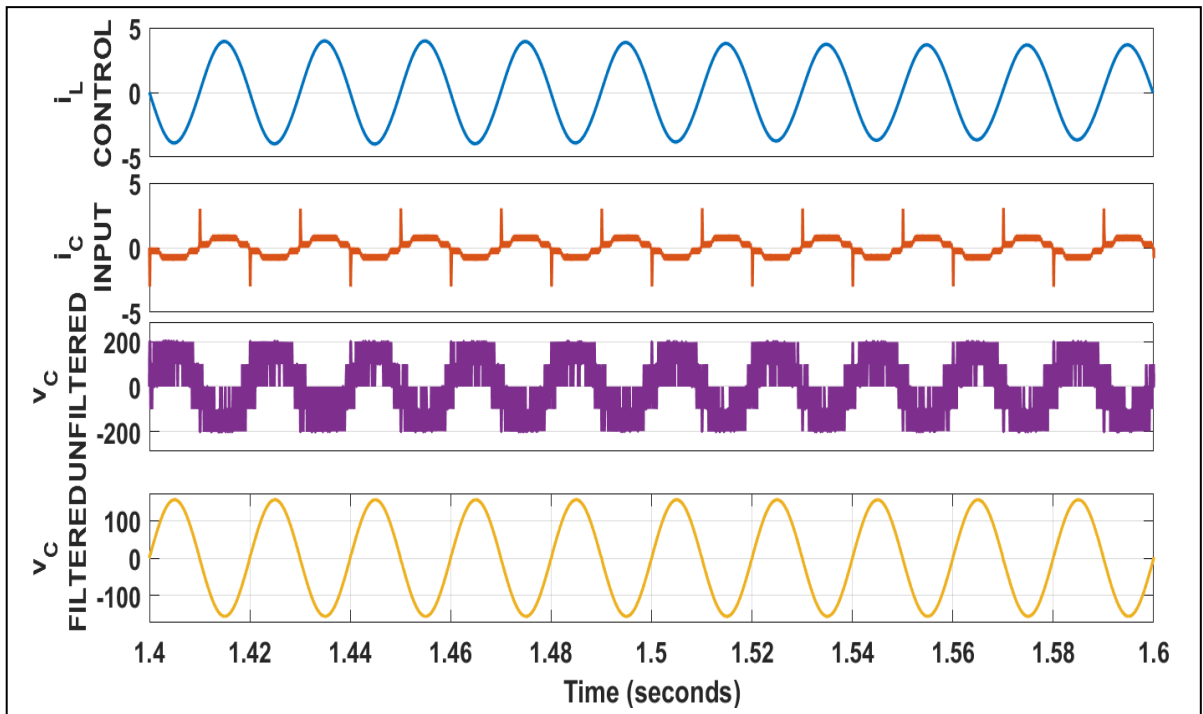


Fig. 57. Controlled load current, input current, unfiltered and filtered voltage signals.

Distributed generation permits the consumer who is generating heat or electricity for their own needs to send their surplus electrical power back into the power grid. The negative value of grid power may be correct if the reference +ve direction of active power of the grid is from the grid to the local generation side. In case of fig. 56, the active power produced from the local generators appears as a negative value with respect to the reference direction of the active power of the grid. Phase-locked loop (PLL) is a key technology in grid connected converters. Single phase PLL subsystem generates sine and cosine waveforms. A Butterworth (design method), lowpass analog filter design block (state-space form) with filter order equal to 8 and passband edge frequency equal to $2 \cdot \pi \cdot 30$ rad/s has been used to filter load current.

$$i_{L, CONTROL} = (i_L \times (\sin \theta + \cos \theta) \times K) + ((100 - V_{DC}) \times (P + (I \times (1/s)))) \times \sin \theta \quad (4.6)$$

$$K = 1 \quad (4.7)$$

$$P = 0.1 \quad (4.8)$$

$$I = 10 \quad (4.9)$$

Equation 4.6 waveform is depicted in fig. 57. Then, source current is subtracted from equation 4.6, output of which is depicted by $i_{C, INPUT}$:

$$i_{C, INPUT} = i_{L, CONTROL} - i_{C, INPUT} \quad (4.10)$$

This signal is used to generate pulses which are injected to controller input.

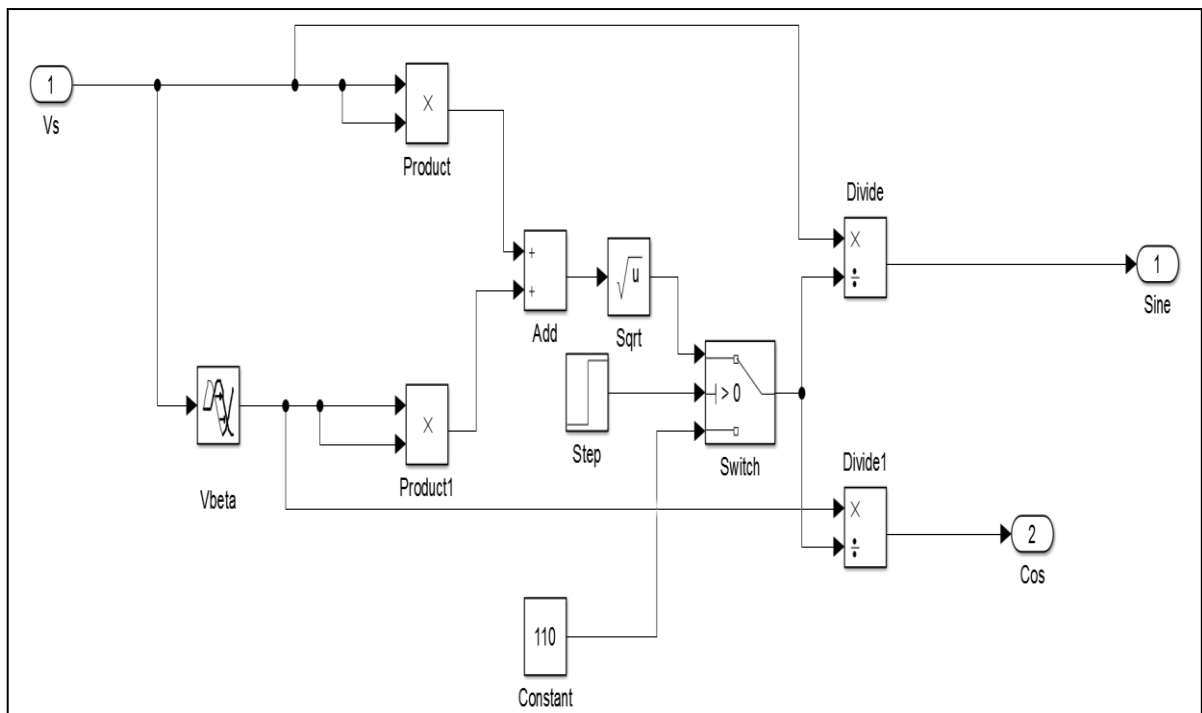


Fig. 58. Single Phase PLL subsystem

In grid connected applications the synchronization of output signals of the converters to be connected with grid parameters – frequency and phase is of great importance. Different methods based on Fourier transforms, zero – crossing detection, Kalman filters, phase – locked loops (PLL) and others are used for this synchronization. Fig. 58 presents a PLL, for synchronization of the output current of single – phase grid connected inverters with the utility grid voltage, used in control scheme.

4.5 Conclusion

A 1 - ϕ PV subsystem (grid – connected type) is put forward in this chapter. In this model, dc – dc boost converter helps the MPPT method. A 1 – ϕ Voltage Source Inverter (VSI) which is using the synchronous dq control technique was employed to provide the required active – power (P) to the 1 – ϕ DC supply. A capacitor was used to store power present at the DC – Link. In order to obtain a satisfactory simulation model which acts as a

proof for the working as well as the proposed design, a MATLAB model in addition to SIMULINK software was employed in 2016a version of the said software.

CONCLUSION OF THE THESIS

Chapter 1 gives general introduction of DG systems which include small and micro hydro, wind turbine, PV arrays, biomass gasification, geothermal and ocean energy, its impacts, highlights, problems, repercussions on electric power system, control, operation and stability. Further, SAPF system is explained with help of circuit diagram based on MathWorks MATLAB / Simulink model. At the end of this chapter a literature review of references is summarized which includes information on DG systems, SAPF system, passive filters, CC systems, its control and features.

Chapter 2 includes controlling techniques and operating principle and basic function of SAPFs for three – phase system. Three different SAPF configurations with circuit diagram for each configuration, passive devices required for it and time and frequency domain CC techniques have been explained wherein equations and simulation results for v_g , i_g , i_c , i_L , V_{DC} , i_d , i_q and THD v_g , i_g and i_L signals are derived for three techniques viz. UT – based UPF and ZVR and SRFT with normal / undistorted and distorted grid conditions. A comparison table at the end of this chapter shows the THD value increases with distorted grid condition.

Chapter 3 proposes a solution for this problem. This chapter includes design and fig. of QSG based on single, dual and multi – SOGI structure for three – phase system. Equations and derived simulation results for signals same as in previous chapter further explain the algorithm. It can be concluded that performance improves and THD decreases with use of above – mentioned harmonics filtering algorithm as demonstrated in tabular form at the end of this chapter.

Chapter 4 analyses a synchronous reference frame based PLL control for a grid – tied PV system (single – phase) with help of block and circuit diagrams. Initially PV concept is introduced also specifying that a 6 x 10 PV panel grid is used in simulation coding for which MATLAB Function block is used. Each component viz. PV array, MPPT, grid – connected PV system modeling, PV and VI plots at different values of solar irradiance, P & O algorithm, SRF single – phase PLL grid synchronization algorithm and its components have been explained with circuit diagrams, plots, flowcharts equations and simulation models wherever necessary. System parameter specifications have been tabled. Results and conclusion show v_c , voltage across capacitor at dc link, I_{PV} , P_g , sine_{PLL} , cosine_{PLL} and $i_{L, AF}$.

FUTURE SCOPE OF WORK

‘Our imagination is the only limit to what we can hope to have in the future.’

Charles F. Kettering

Many different adaptations, tests and experiments have been left for the future due to lack of time (i.e. the experiments with real data are usually very time consuming, requiring even days to finish a single run). Future work concerns deeper analysis of particular mechanisms, new proposals to try different methods or simple curiosity.

In this thesis performance investigations of time domain techniques, when operating under non – ideal grid – voltage conditions, is studied and an improved technique DSOGI, capable of effectively operating with most of the non – ideal grid voltage conditions, is presented. Some suggestions for further investigations in this field are as follows:

1. The proposed DSOGI structure is limited to estimate the fundamental positive and negative sequence components along with the dc – offset from the distorted input signal. It can be further restructured to multiple SOGI structures by connecting n number of SOGIs in parallel to extract n number harmonic components including fundamental.
2. The inclusion of n SOGI can offer one or more of the following advantages in harmonic compensation and / or some other control applications:
 - i). Selective harmonic elimination capability which helps to attend the most problematic harmonics.
 - ii). Avoids unnecessary investment / computation on excessive converter ratings.
3. The performance improvement of other grid – connected converter applications like series APF, hybrid APF, FACTS devices, PV or wind based DGs by modifying their control scheme using the multi SOGI can be studied.
4. The presented work has opened the following area of further research work: extension of the proposed current controller technique for general n – level multi – level converter based SAPF for high power applications and its implementation.

REFERENCES

- [1] A. Moreno - Munoz, *Power Quality: Mitigation Technologies in a Distributed Environment*. London, U.K.: Springer - Verlag, 2007.
- [2] J. Matas, L. G. de Vicuna, J. Miret, J. M. Guerrero, and M. Castilla, "Feedback linearization of a single – phase active power filter via sliding mode control," *IEEE Trans. Power Electron.*, vol. 23, no. 1, pp. 116 - 125, Jan. 2008.
- [3] J. M. Maza - Ortega, J. A. Rosendo - Macias, A. Gomez - Exposito, S. Ceballos - Mannozi, and M. Barragan - Villarejo, "Reference current computation for active power filters by running DFT techniques," *IEEE Trans. Power Del.*, vol. 25, no. 3, pp. 446 - 456, Jul. 2010.
- [4] B. - S. Chen and Y. - Y. Hsu, "A minimal harmonic controller for a STATCOM," *IEEE Trans. Ind. Electron.*, vol. 55, no. 2, pp. 655 – 664, Feb. 2008.
- [5] H. Akagi, E. H. Watanabe, and M. Aredes, *Instantaneous Power Theory and Applications to Power Conditioning*. Hoboken, NJ: Wiley, 2007.
- [6] R. S. Herrera, P. Salmeron, and H. Kim, "Instantaneous reactive power theory applied to active power filter compensation: Different approaches, assessment, and experimental results," *IEEE Trans. Ind. Electron.*, vol. 55, no. 1, pp. 184 – 196, Jan. 2008.
- [7] D. M. Divan, S. Bhattacharya, and B. Banerjee, "Synchronous frame harmonic isolator using active series filter," in *Proc. Eur. Power Electron. Conf.*, 1991, pp. 3030 – 3035.
- [8] B. Singh and V. Verma, "Selective compensation of power-quality problems through active power filter by current decomposition," *IEEE Trans. Power Del.*, vol. 23, no. 2, pp. 792 – 799, Apr. 2008.
- [9] C. Lascu, L. Asiminoaei, I. Boldea, and F. Blaabjerg, "Frequency response analysis of current controllers for selective harmonic compensation in active power filters," *IEEE Trans. Ind. Electron.*, vol. 56, no. 2, pp. 337 – 347, Feb. 2009.

- [10] A. Luo, Z. Shuai, W. Zhu, and Z. J. Shen, “Combined system for harmonic suppression and reactive power compensation,” *IEEE Trans. Ind. Electron.*, vol. 56, no. 2, pp. 418 – 428, Feb. 2009.
- [11] K. - K. Shyu, M. - J. Yang, Y. - M. Chen, and Y. - F. Lin, “Model reference adaptive control design for a shunt active – power - filter system,” *IEEE Trans. Ind. Electron.*, vol. 55, no. 1, pp. 97 – 106, Jan. 2008.
- [12] S. Mohagheghi, Y. Valle, G. K. Venayagamoorthy, and R. G. Harley, “A proportional – integrator type adaptive critic design – based neuro controller for a static compensator in a multimachine power system,” *IEEE Trans. Ind. Electron.*, vol. 54, no. 1, pp. 86 – 96, Feb. 2007.
- [13] Z. Shu, Y. Guo, and J. Lian, “Steady – state and dynamic study of active power filter with efficient FPGA – based control algorithm,” *IEEE Trans. Ind. Electron.*, vol. 55, no. 4, pp. 1527 – 1536, Apr. 2008.
- [14] Ackermann T., et al. Distributed generation: a definition, *Electric Power Systems Research*, 2001; 57. Google Scholar.
- [15] Begović M., et al. Impact of Renewable Distributed Generation on Power Systems, 34th Hawaii International Conference on System Sciences, 2001. Google Scholar.
- [16] Bloem J. Producerea distribuită și regenerabilă – Integrare și interconectare, Calitatea și utilizarea energiei electrice – Ghid de aplicare (Distributed Generation and Renewables – Integration and interconnection, quality and use of electricity – Application Guide), www.sier.ro, 2007. Google Scholar.
- [17] Dulău L. J. Hybrid Wind and Solar Power System, 2nd IFAC Workshop on Convergence of Information Technologies and Control Methods with Power Systems, Poster Session, 2013. Google Scholar.
- [18] Ochoa L. F., et al. – Minimizing Energy Losses: Optimal Accommodation and Smart Operation of Renewable Distributed Generation, *IEEE Transactions on Power Systems*, 2011; 26 (1). Google Scholar.

- [19] Padhi P., et al. – Distributed Generation: Impacts and Cost Analysis, Special Issue of International Journal of Power System Operation and Energy Management, 1 (3). Google Scholar.
- [20] Pepermans G., et al. – Distributed generation: definition, benefits and issues, Energy Policy 2005; 33. Google Scholar.
- [21] Sheikhi A., et al. – Distributed Generation Penetration Impact on Distribution Networks Loss, International Conference on Renewable Energies and Power Quality, 2013. Google Scholar.
- [22] Singh S. N., et al. – Distributed Generation in Power Systems: An Overview and Key Issues, Indian Engineering Congress, 2009. Google Scholar.
- [23] Wasiak I., et al. – Integration of distributed energy sources with electrical power grid, Bulletin of The Polish Academy of Sciences, Technical Sciences, 2009; 57 (4). Google Scholar.
- [24] www.neplan.ch. Google Scholar.
- [25] C. Lascu, L. Asiminoaei, I. Boldea, and F. Blaabjerg, "High performance current controller for selective harmonic compensation in active power filters," *IEEE Trans. Power Electron.*, vol. 22, no. 5, pp. 1826 - 1835, Sep. 2007. (Pubitemid 47423057).
- [26] D. Yazdani, A. Bakhshai, G. Joos, and M. Mojiri, "A real – time three – phase selective – harmonic – extraction approach for grid-connected converters," *IEEE Trans. Ind. Electron.*, vol. 56, no. 10, pp. 4097 - 4106, Oct. 2009.
- [27] F. D. Freijedo, J. Doval - Gandoy, O. Lopez, P. Fernandez - Comesana, and C. Martinez - Penalver, "A signal – processing adaptive algorithm for selective current harmonic cancellation in active power filters," *IEEE Trans. Ind. Electron.*, vol. 56, no. 8, pp. 2829 - 2840, Aug. 2009.

- [28] A. Varschavsky, J. Dixon, M. Rotella, and L. Moran, "Cascaded nine – level inverter for hybrid – series active power filter, using industrial controller," *IEEE Trans. Ind. Electron.*, vol. 57, no. 8, pp. 2761 - 2767, Aug. 2010.
- [29] R. Chudamani, K. Vasudevan, and C. S. Ramalingam, "Non – linear least – squares – based harmonic estimation algorithm for a shunt active power filter," *IET Power Electron.*, vol. 2, no. 2, pp. 134 - 146, Mar. 2009.
- [30] B. P. McGrath, D. G. Holmes, and J. J. H. Galloway, "Power converter line synchronization using a discrete Fourier transform (DFT) based on variable sampling rate," *IEEE Trans. Power Electron.*, vol. 20, no. 4, pp. 877 - 884, Jul. 2005.
- [31] L. Asiminoaei, F. Blaabjerg, and S. Hansen, "Detection is key – Harmonic detection methods for active power filter applications," *IEEE Ind. Appl. Mag.*, vol. 13, no. 4, pp. 22 - 33, Jul. / Aug. 2007.
- [32] E. Jacobsen, and R. Lyons, "The sliding DFT," *IEEE signal Process. Mag.*, vol. 20, no. 2, pp. 74 - 80, Mar. 2003.
- [33] H. Li, F. Zhuo, Z. Wang, W. Lei, and L. Wu, "A novel time – domain current – detection algorithm for shunt active power filters," *IEEE Trans. Power Syst.*, vol. 20, no. 2, pp. 644 - 651, May 2005.
- [34] H. Wang, Q. Li, and M. Wu, "Investigation on a new algorithm for instantaneous reactive and harmonic currents detection applied to intensive nonlinear loads," *IEEE Trans. Power Del.*, vol. 22, no. 4, pp. 2312 - 2318, Oct. 2007.
- [35] H. Akagi, Y. Kanazawa, and A. Nabae, "Instantaneous reactive power compensators comprising switching devices without energy storage components," *IEEE Trans. Ind. Appl.*, vol. IA - 20, no. 3, pp. 625 - 630, May / June 1984.
- [36] H. Akagi, Y. Kanazawa, and A. Nabae, "Generalized theory of the instantaneous reactive power in three – phase circuits," in *Proc. IPEC*, 1983, pp. 1375 - 1386.

- [37] M. Aredes, H. Akagi, E. H. Watanabe, S.E. Vergara, and L. F. Encarnacao, "Comparisons between the $p - q$ and $p - q - r$ theories in three - phase four wire systems," *IEEE Trans. Power Electron.*, vol. 24, no. 4, pp. 924 - 933, Apr. 2009.
- [38] J. C. Montano, "Reviewing concepts of instantaneous and average compensations in polyphase systems," *IEEE Trans. Ind. Electron.*, vol. 58, no. 1, pp. 213 - 220, Jan. 2011.
- [39] J. Liu, J. Yang, and Z. Wang "A new approach for single - phase harmonic current detecting and its application in a hybrid active power filter," in *Proc. Annu. Conf. IEEE Indust. Electron. Soc. (IECON99)*, 1999, vol. 2, pp. 849 - 854.
- [40] M. T. Haque, "Single phase PQ theory for active filters," in *Proc IEEE TENCON'02, 2002*, pp. 1941 - 1944.
- [41] H. Akagi, E. H. Watanabe, and M. Aredes, *Instantaneous power theory and applications to power conditioning*. Piscataway, NJ / New York: IEEE Press / Wiley - Interscience, 2007.
- [42] M. Saitou, and T. Shimizu, "Generalized theory of instantaneous active and reactive powers in single - phase circuits based on Hilbert transform," in *Proc. 33rd Annu. IEEE PESC*, Jun. 2002, pp. 1419 - 1424.
- [43] V. Khadkikar, M. Singh, A. Chandra, and B. Singh, "Implementation of single - phase synchronous dq reference frame controller for shunt active filter under distorted voltage condition," in *Proc. IEEE PEDES Conf.*, Dec. 2006, pp. 1 - 6.
- [44] V. Khadkikar, A. Chandra, and B. N. Singh, "Generalized single - phase $p - q$ theory for active power filtering: Simulation and DSP - based experimental investigation," *IET Power Electron.*, vol. 2, no. 1, pp. 67 - 78, Jan. 2009.
- [45] P. Rodriguez, A. Luna, I. Candela, R. Mujal, R. Teodorescu and F. Blaabjerg, "Multiresonant frequency - locked loop for grid synchronization of power converters under distorted grid conditions," *IEEE Trans. Ind. Electron.*, vol. 58, no. 1, pp. 127 - 138, Jan. 2011.

- [46] S. Golestan, M. Monfared, F.D. Freijedo, J. M. Guerrero, “Design and tuning of a modified power – based PLL for single – phase grid connected power conditioning systems,” *IEEE Trans. Power Electron.*, vol. 27, no. 8, pp. 3639 - 3650, Aug. 2012.
- [47] S. Golestan, M. Monfared, F. D. Freijedo, J. M. Guerrero, “Dynamics assessment of advanced single - phase PLL structures,” *IEEE Trans. Ind. Electron.* vol. PP, no. 99, pp. 1 - 11, Apr. 2012.
- [48] T. C. Green, and J. H. Marks, “Ratings of active power filters,” *IEE Proc. - Electr. Power Appl.*, vol. 150, no. 5, Sep. 2003.
- [49] *Voltage Characteristics of Electricity Supplied by Public Distribution Systems*, European Standard EN 50160, 2008.
- [50] S. Preitl and R. - E. Precup, “An extension of tuning relations after symmetrical optimum method for PI and PID controller,” *Automatica*, vol. 35, no. 10, pp. 1731-1736, Oct. 1999.
- [51] R. Teodorescu, M. Liserre, and P. Rodriguez, *Grid Converters for Photovoltaic and Wind Power Systems*. New York: IEEE - Wiley, 2011.
- [52] K. Shu and E. Sanchez - Sinencio, *CMOS PLL Synthesizers – Analysis and Design*. New York: Springer, 2005.
- [53] R. C. Dorf and R. H. Bishop, *Modern Control Systems*, 9th ed. Englewood Cliffs, NJ: Prentice - Hall, 2000.
- [54] P. Rodriguez, R. Teodorescu, I. Candela, A. Timbus, M. Liserre, and F. Blaabjerg, “New positive – sequence voltage detector for grid synchronization of power converters under faulty grid conditions”, *Proc. IEEE - PESC* 1, 1 - 7 (2006).
- [55] Z. B. Erdem, “The contribution of renewable resources in meeting Turkey’s energy – related challenges”, *Renewable and Sustainable Energy Reviews*, vol. 14, no. 9, pp. 2710 – 2722, 2010.

[56] M. E. Ropp and S. Gonzalez, “Development of a MATLAB / SIMULINK model of a single – phase grid – connected photovoltaic system”, *IEEE Trans. Energy Convers.*, vol. 24, no. 1, pp. 195 – 202, 2009.

[57] S. P. Kaur and A. Singh, “DSOGI based Grid Synchronization under Adverse Grid Conditions” *II IEEE International Conference on Power Electronics, Intelligent Control and Energy Systems*, 2018.